Universidade de São Paulo
Instituto de Física

Não-Gaussianidades Primordiais: Teoria e Perspectivas para Observações

Caroline Macedo Guandalin

Orientador: Prof. Dr. Luis Raul Weber Abramo

Dissertação de mestrado apresentada ao Instituto de Física da Universidade de São Paulo, como requisito parcial para a obtenção do título de Mestre em Ciências.

Banca Examinadora:
Prof. Dr. Luis Raul Weber Abramo (IF-USP)
Prof. Dr. Rogério Rosenfeld (IFT-UNESP)
Prof. Dr. Thiago dos Santos Pereira (UEL)

São Paulo
2018

FICHA CATALOGRÁFICA
Preparada pelo Serviço de Biblioteca e Informação
do Instituto de Física da Universidade de São Paulo

Guandalin, Caroline Macedo

Não-gaussianidades primordiais: teoria e perspectivas para observações. São Paulo, 2018.

Dissertação (Mestrado) – Universidade de São Paulo. Instituto de Física. Depto. de Física Matemática.

Orientador: Prof. Dr. Luis Raul Weber Abramo.
Área de Concentração: Física.

Unitermos: 1. Cosmologia; 2. Inflação (Cosmologia);
3. Cosmologia inflacionária; 4. Estrutura do universo; 5. Universo primordial.

USP/IF/SBI-079/2018

University of São Paulo
Institute of Physics

Primordial non-Gaussianities: Theory and Prospects for Observations

Caroline Macedo Guandalin

Advisor: Prof. Dr. Luis Raul Weber Abramo

Master's dissertation presented to the Institute of Physics of the University of São Paulo, as a partial fulfillment of the requirements for obtaining the degree of Master of Science.

Examination Committee:
Prof. Dr. Luis Raul Weber Abramo (IF-USP)
Prof. Dr. Rogério Rosenfeld (IFT-UNESP)
Prof. Dr. Thiago dos Santos Pereira (UEL)

São Paulo
2018

To Luiz and Mary,

the cornerstones of my education

Agradecimentos

Existem muitas pessoas que contribuíram com este trabalho, das mais diversas formas possíveis, e cuja ajuda permitiu que o projeto fosse realizado. A lista é longa, talvez algum nome me escape e por isso peço desculpas, mas omitir todos os nomes elimina o caráter de reconhecimento desta parte da dissertação.

Primeiramente, gostaria de agradecer ao Prof. Dr. Luis Raul Weber Abramo, quem aceitou me orientar e propôs este projeto, confiando na minha capacidade para realizar este trabalho. Gostaria de agradecer pela paciência e toda a ajuda provida ao longo dos dois anos em que realizei o trabalho aqui apresentado.

Agradeço Felipe Prado Corrêa Pereira pela companhia e apoio, ajuda e paciência; minha família que, mesmo longe, sempre me incentivou; e agradeço, principalmente, ao meu pai, Luiz, e a minha mãe, Mary, por nunca duvidarem de mim.

Por todos os comentários, sugestões, ajuda e solicitude, agradeço Antonino Troja, Carolina Queiroz, Catherine Watkinson, Gabriela Sato-Polito, Henrique Rubira, Hugo Camacho, Julian Bautista, Marcos Lima, Renan Boschetti e Williams Ribeiro. Em particular, agradeço Rodrigo Voivodic por toda a ajuda prestada, que não foi pouca, ao longo desses dois anos.

Para aqueles fora da Cosmologia, devo imenso reconhecimento a Antônio Bruno Morales e Carlos Bercini Vargas, cuja ajuda constante transcende este mestrado.

Pelo apoio financeiro, gostaria de agradecer à Fundação de Amparo à Pesquisa do Estado de São Paulo (FAPESP) e à Coordenação de Aperfeiçoamento de Pessoal de Nível Superior (CAPES) por conceder a bolsa de mestrado (processo número 2016/19909-7) essencial à realização do trabalho e ao Conselho Nacional de Desenvolvimento Científico e Tecnológico (CNPq). Agradeço à secretaria (em particular Amélia Genova, Cecília Blanco e Simone Shinomiya) e ao setor de apoio ao grupo de processamento numérico (João da Silva Borges) do Departamento de Física-Matemática da Universidade de São Paulo (USP), por toda sua assistência; ao pessoal da biblioteca e à equipe de limpeza do Instituto de Física da USP e a todos os

docentes que contribuíram com a minha formação ao longo da graduação e da pós-graduação.

Acknowledgments

There are many people who contributed to this work, in the most various ways, and whose help allowed the project to be carried out. The list is long, maybe some names slip my mind and for that I apologize, but omitting all the names takes out the gratitude character of this part of the dissertation.

First, I would like to thank Prof. Dr. Luis Raul Weber Abramo, who agreed to advise me and proposed this project, trusting in my ability to carry out this work. I would like to thank him for all the patience and guidance provided throughout these two years.

I thank Felipe Prado Corrêa Pereira for the companionship and support, help and patience; my family which always encouraged me, even far away; and, especially, I thank my father, Luiz, and my mother, Mary, for never doubting me.

For all the comments, suggestions, help and solicitude, I thank Antonino Troja, Carolina Queiroz, Catherine Watkinson, Gabriela Sato-Polito, Henrique Rubira, Hugo Camacho, Julian Bautista, Marcos Lima, Renan Boschetti and Williams Ribeiro. In particular, I would like to thank Rodrigo Voivodic for all the help, which has been a lot, given over the past two years.

For those outside of Cosmology, I owe immense gratitude to Antônio Bruno Morales and Carlos Bercini Vargas, whose constant help transcends this Master's degree.

For the financial support, I would like to thank the São Paulo Research Foundation (FAPESP) and the *Coordenação de Aperfeiçoamento de Pessoal de Nível Superior* (CAPES) for granting the Master's fellowship (grant 2016/19909-7) essential for this work, and the National Council for Scientific and Technological Development (CNPq). I also thank the secretariat (in particular Amélia Genova, Cecília Blanco and Simone Shinomiya) and to the support sector of the numerical processing group (João da Silva Borges) of the Mathematical Physics Department, for all their assistance; the library and cleaning staff of the Institute of Physics of the University of São Paulo and all the professors who contributed to my development during my undergraduate and postgraduate studies.

Resumo

A física do Universo primordial deixa sinais distintos na Radiação Cósmica de Fundo (CMB) e Estrutura em Larga Escala (LSS). O paradigma atual da cosmologia explica a origem das estruturas que vemos hoje (CMB e LSS) através da inflação, teoria que diz que o Universo passou por um período de expansão acelerada. As flutuações de densidade que eventualmente crescem, dando origem às flutuações de temperatura da CMB, às galáxias e outras estruturas que vemos na LSS, provém da quantização do campo escalar (inflaton) que provoca a tal expansão acelerada. O modelo inflacionário mais simples, o qual contém um único campo escalar nas condições de rolamento lento e termo cinético canônico da ação, possui o espectro de potências (transformada de Fourier da função de correlação de dois pontos) aproximadamente invariante de escala e o bispectro (transformada de Fourier da função de correlação de três pontos) aproximadamente nulo. Tal característica é conhecida por Gaussianidade, uma vez que campos aleatórios cuja distribuição é uma normal tem todas as funções de correlação de ordem ímpar nulas. Contudo, modelos inflacionários mais complexos (mais campos escalares, termos cinéticos não-triviais na ação, etc) e alternativas possíveis à inflação possuem um bispectro não nulo, o qual pode ser parametrizado através do parâmetro de não-linearidade $f_{\rm NL}$, cujo valor difere de modelo para modelo. Neste trabalho estudamos os ingredientes básicos para entender tais afirmações e focamos nas evidências observacionais desse parâmetro e como os levantamentos de galáxias atuais e futuros podem impor restrições ao valor de $f_{\rm NL}$ com uma precisão maior, através da técnica de múltiplos traçadores, do que aquelas obtidas com medidas da CMB.

Palavras-chave: Universo Primordial, Estrutura em Larga Escala, Inflação, Teoria de Perturbações Cosmológica, Espectro de Potências, Bispectro, Não-Gaussianidades Primordiais, Levantamentos de Galáxias, Técnica de Múltiplos Traçadores.

Abstract

Early Universe physics leaves distinct imprints on the Cosmic Microwave Background (CMB) and Large-Scale Structure (LSS). The current cosmological paradigm to explain the origin of the structures we see in the Universe today (CMB and LSS), named Inflation, says that the Universe went through a period of accelerated expansion. Density fluctuations that eventually have grown into the temperature fluctuations of the CMB and the galaxies and other structures we see in the LSS come from the quantization of the scalar field (inflaton) which provokes the accelerated expansion. The most simple inflationary model, which contains only one slowly-rolling scalar field with canonical kinetic term in the action, produces a power-spectrum (Fourier transform of the two-point correlation function) approximately scale invariant and an almost null bispectrum (Fourier transform of the three-point correlation function). This characteristic is called Gaussianity, once random fields that follow a normal distribution have all the odd moments null. Yet, more complex inflationary models (with more scalar fields and/or non-trivial kinetic terms in the action, etc) and possible alternatives to inflation have a non-vanishing bispectrum which can be parametrized by a non-linearity parameter $f_{\rm NL}$, whose value differs from model to model. In this work we studied the basic ingredients to understand such statements and focused on the observational evidences of this parameters and how the current and upcoming galaxy surveys are able to impose constraints to the value of $f_{\rm NL}$ with a better accuracy, through the multi-tracer technique, than those obtained by means of CMB measurements.

Keywords: Primordial Universe, Large-Scale Structure, Inflation, Cosmological Perturbation Theory, Power-spectrum, Bispectrum, Primordial Non-Gaussianities, Galaxy Surveys, Multi-Tracer Technique.

Contents

Chapter 1

Introduction

Despite the discovery of the cosmic microwave background (CMB), which was a breakthrough evidence for the standard Hot Big Bang model, it is clear nowadays the many problems this cosmological scenario possesses: the nearly flat geometry inferred from observations implies an early Universe with spatial curvature much closer to zero, leading to a fine-tuning of the initial conditions; the striking homogeneity of the CMB introduces a conundrum of causality, known as the horizon problem; and the suppression of hot relics, such as cosmic strings and magnetic monopoles generated in Grand Unified Theories, could not be explained in terms of this model [39, 53, 72, 73, 97].

The idea of Inflation, as we know it today[1], was proposed by Guth in 1981 [53]. It solved these issues and brought a bonus: a mechanism for generating the seeds of the large-scale structure of the Universe through the production of quantum fluctuations.

As in any scientific theory, observations constrain the form and parameters of the inflationary paradigm, with the scalar spectral index n_s, which probes departures from a scale-invariant ($n_s = 1$) primordial spectrum, being one of inflation's most important tests[2]. Another possible constraint concerns the non-Gaussianities present in the correlation functions of perturbations, which are manifested, at late times, in the large-scale structure (LSS) of the universe and, at early times, in the CMB. Promising constraints reachable today rely on observations of

[1] Previous works to [53] in the 60s and 70s, introduced precursor ideas that can be seen in the current inflationary models, such as the idea that the Universe would be a product of a quantum effect or the concept of a fluid with negative pressure [20, 52, 120].

[2] Current constraints gives $n_s = 0.968 \pm 0.006$, disfavouring a scale-invariant (Harrison-Zel'dovich) spectrum [99].

the gravitational spectrum in the CMB polarization, which can rule out Inflation itself[3].

From these two examples, it is clear that prospects in the science of primordial physics requires measurements on both CMB and LSS. However, these measurements must be sensitive enough such that we are able to obtain robust constraints on the cosmological parameters of interest. In the scope of CMB, there has been a rich history of such observational improvements: from COBE, launched in 1989, followed by the WMAP, in 2001, to the Planck satellite, in 2009. With the development of new galaxy surveys, which map the large-scale structure of the Universe, we might be able to achieve even better constraints on the early Universe physics, which may be competitive with experiments such as Planck [2, 9, 62].

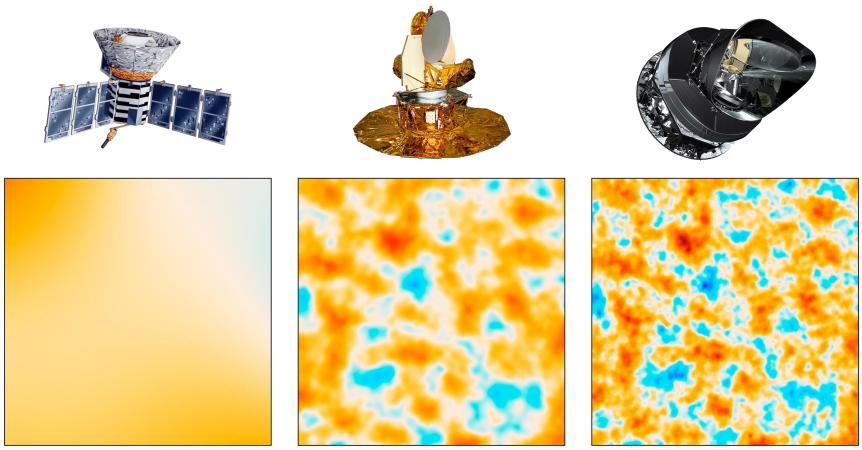

Figure 1.1: Comparison between the 10-square-degree patches of all-sky CMB maps obtained by COBE (left), WMAP (middle) and Planck (right) satellites. With the improvement of these probes, the anisotropies in the CMB became more evident and, therefore, more physical content could be extract from them. Credit: NASA/JPL-Caltech/ESA.

One of the reasons why observations of the LSS are interesting relies on the amount of information one can extract from this probe. For LSS surveys, it's reasonable to consider that the non-linear regime scales are at around $\lambda \sim 10$ Mpc [43]. Given that the volume coverage of current and upcoming surveys is in the range $V_{\rm survey} \sim 10 - 100$ Gpc^3, the amount of degrees of freedom (independent modes available) for these surveys are of the order of $10^7 - 10^8$. On the other hand, for CMB observations, scales around $\ell \sim 2200$ (observations within the angular resolution of 10 arcminutes) are the limit at which measurements are reasonably safe from secondary sources of anisotropy which supress the primordial signal we intend to measure. Given that the area mapped by these types of observations (taking the Milk Way galaxy already

[3]Ekpyrotic scenario predicts a strongly blue gravitational spectrum [65].

into account) is $\sim 2 \times 10^4$ deg^2, we have at our disposal $\sim 10^6$ degrees of freedom. Therefore, LSS measurements can bring much more information than those from CMB.

Among the parameters sensitive to primordial physics we have the scale-dependent bias [35], which is manifested in the two-point correlation function of tracers of the large-scale structure (e.g. galaxies), as well as other parameters related to non-Gaussianities. From the Quantum Field Theory approach to the inflaton, the simplest single-field slow-roll inflation, to first approximation in perturbation theory, has a harmonic oscillator spectrum (i.e. Gaussian), and the model is fully described by the two-point statistics. However, when we go from this simple scenario to the full interacting theory, the three-point correlation function (identically null for Gaussian fields) becomes non-zero, exhibiting the non-Gaussianity of the full theory. Our work focus mainly in this latter effect.

In order to take maximum advantage of what future surveys have to offer, we must completely understand how those non-Gaussian initial conditions generated by Inflation (or some other early Universe model) manifest themselves in the structures we observe today, along with possible sources of systematic errors.

One of the challenges of extracting primordial non-Gaussianities out of the LSS is due to the fact that the LSS is highly non-Gaussian owing to the non-linear evolution of matter under gravitational instability. CMB experiments are free from this issue, since physics is still very much in the linear regime at such high redshifts. Therefore, going to high redshifts in galaxy surveys will minimize such spurious contributions from the gravity sector.

There is an intrinsic limitation on cosmological observations which affects both the CMB and the LSS: it consists on the fact that we observe only one Universe, which can be thought of as one realization of an ensemble of possible Universes. It is also associated with the fact that we are only able to observe a finite patch of the Universe.

If we take many subsamples of our Universe and suppose that they fairly sample the Universe[4], these subsamples can be regarded as individual realizations of the Universe. This is known as the "ergodic hypotesis".

However, when we reach scales close to the Hubble horizon H_0^{-1} today, we no longer have subsamples of the universe which fairly represent "independent universes" and, then, it is

[4]This is directly associated with the Sampling Theorem [117], which states that a fair sample is that whose wavelength of the subsamples are much smaller than the wavelength of the whole sample. In a cosmology vocabulary, this means that the scale of the subsamples must be much smaller than the Hubble horizon today.

not possible to invoke the ergodic hypothesis to average over these subsamples anymore. This intrinsic limitation for modes close to the Hubble horizon is known as “cosmic variance”.

To partially overcome these issues, larger volumes of the Universe must be mapped in a way to increase the number of subsamples available to analysis. Just as it was seen in the CMB experiments, there is also a history of observational improvement in the mapping of the large-scale structure: until the mid-1930s, just 150000 objects had been mapped by the Harvard Observatory over 174 square degrees of the sky [112] (see Figure 1.2).

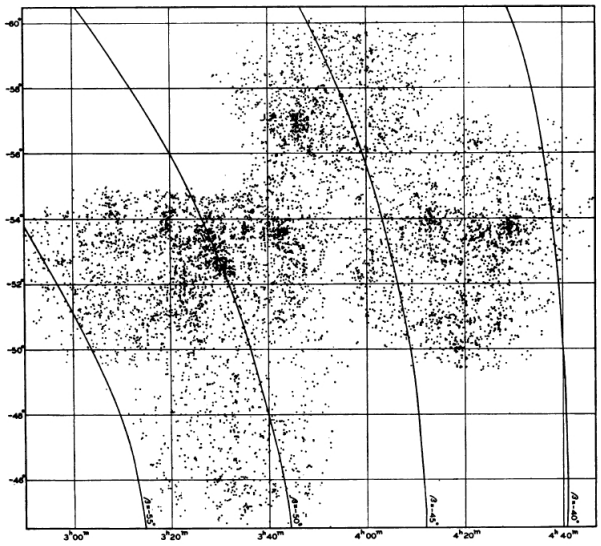

Figure 1.2: The distribution of 7900 galaxies of which only 134 were previously known, from the Harvard plates. Extracted from [112].

Later, with technological advances and better telescopes, around 1 million galaxies were surveyed by the Lick catalog, in 1967, followed by the Zwicky catalog, in 1968, which mapped another $\sim$30000 galaxies. In order to shorten the list, we can cite the Center for Astrophysics (CfA2) redshift survey, in the 1980s, covering a solid angle of 1.7 sr and ranging up to $z = 0.04$; the Las Campanas redshift survey (LCRS), in the 1990s, covering up to $z = 0.1$ [81]; and the Sloan Digital Sky Survey (SDSS), operating since 2000, that has mapped, in the first five years of operation, 8000 square degrees and measured the spectra of more than 700000 objects. The following SDSS survey, BOSS, mapped $\sim 10^4$ square degrees of the sky, measuring the redshifts of around 1.5 million luminous galaxies up to $z \approx 0.7$, as well as the Lyman-α forest absorption spectra of $\sim 1.6 \times 10^5$ quasars at redshifts in the range of $2.2 \lesssim z \lesssim 3$. Finally, eBOSS is now devoted to observing galaxies and quasars at higher redshifts, mapping in great precision the three-dimensional large-scale structure of the Universe [114].

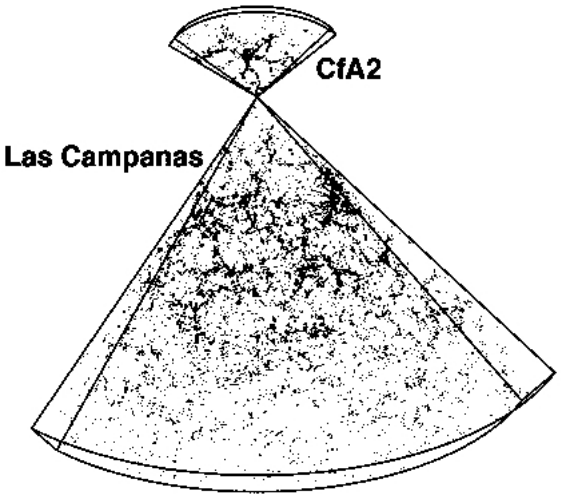

Figure 1.3: Galaxy distribution for the southern slices of the LCRS and the first slice of the CfA2 catalog at the Northern Hemisphere. Extracted from [80].

Future planned surveys will map even better the Universe. Among them we can cite (1) Euclid, which will map $\sim 1.5 \times 10^4$ square degrees of the sky and will detect, approximately, 10^{10} objects [45]; (2) Large Synoptic Survey Telescope (LSST), whose prediction is of around 37 billion stars and galaxies mapped through 3×10^4 square degrees of the sky [70, 58] and (3) Square Kilometre Array (SKA) which will map the Universe within the continuous frequency coverage from 50 MHz (6 m wavelength) to 20 GHz (1.5 cm wavelength) [118, 37].

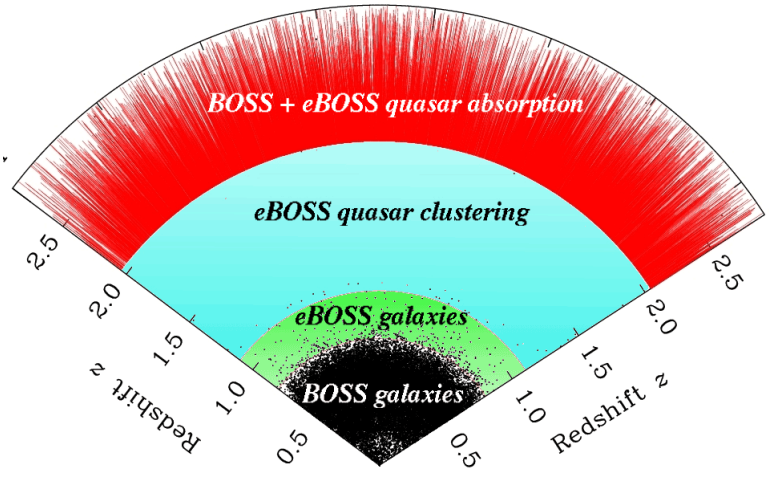

Figure 1.4: Comparison among the planned eBOSS coverage of the Universe with its previous survey BOSS. Extracted from http://www.sdss.org/surveys/eboss/ at June, 2018.

But even though mapping larger volumes increases the accuracy of long-wavelength modes, closer to the Hubble horizon, cosmic variance will always be a source of uncertainty since we have at our disposal only one Universe to observe. There is, nonetheless, a method

that allows us to mitigate cosmic variance of our samples, which consists of doing a multi-tracer analysis.

It was first shown in [110] that it is possible to eliminate the statistical fluctuations due to cosmic variance by correlating a highly biased tracer of the LSS with an unbiased one. The LSS is interesting as a venue to test these ideas because we can take advantage of this technique to improve the cosmological constraints related to bias, the growth of structures and other aspects of structure formation. Our work aims at understanding the use of the LSS to extract information about the early Universe.

We organize this dissertation as follows: in Chapter 2 we study the linear theory of cosmological perturbations from the classical and relativistic point of view, in order to extract the essential features of this theory and how the perturbations are propagated, in its simplest form, throughout the Universe. After examining perturbation theory, in Chapter 3 we apply this framework to Inflation itself and quantize the perturbations, leading to a natural explanation for the origin of the seeds of the large-scale structure we see in the Universe. This is of crucial importance to understand the link between the physics of the early Universe and the current distribution of matter we observe in LSS surveys. In Chapter 4 we look at the production of non-Gaussian features due to different models of Inflation and their imprint on the three-point function, which will eventually manifest itself in the distribution of galaxies at the late Universe. It is important to emphasize here that, although we are working specifically with Inflation, constraints on non-Gaussian parameters is of general interest and serves the purpose of discriminating among Inflation and other early Universe scenarios such as ekpyrosis. In Chapter 5 we present the log-normal prescription to generate galaxy maps and the results obtained with a numerical estimation of the bispectrum of mock galaxy catalogs generated by a code that is capable of making a multi-tracer analysis. Chapter 6 is dedicated to the present the results obtained and, finally, in Chapter 7 we conclude and give our prospects for future work.

This dissertation has two goals: the first and more objective one is to present the results obtained over these two years of a master's degree developed at USP's Institute of Physics. The second one, perhaps a bit more subjective, is to serve as a guide for new students who wish to venture into this incredible field that is cosmology, clarifying some more obscure steps which are seldom presented clearly in textbooks and reviews.

Chapter 2

Linear Theory of Cosmological Perturbations

The Cosmic Microwave Background (CMB) tells us that the universe is extremely homogeneous at very early times. However, today we observe galaxies, clusters and superclusters of galaxies, structures that were formed due to the attractive nature of gravity and that point to the non-homogeneity of the Universe at recent times. However, if we take into account very large patches of the sky, we see that, averaged over scales of more than ~ 200 Mpc, the inhomogeneities are very small. Thus, we may still study tiny perturbations on a homogeneous background, in order to explain many of the currently observed structures. This is done with the help of Linear Perturbation Theory (henceforth PT). We begin our study with cosmological perturbation theory by means of the Newtonian framework, due to its intuitive and pedagogical development. Then, once we have dealt with the Newtonian Perturbation Theory in detail, we proceed to a relativistic approach of perturbations due to the intrinsic limitations of the classical treatment.

2.1 Classical approach

2.1.1 Eulerian and Lagrangian descriptions of a fluid flow

When seen from large scales, the matter distribution is described by a continuous medium, which means we can approximate that matter content by a fluid.

There are two main treatments we can adopt in order to describe our fluid: the first is due

to Euler and the second to Lagrange. We call them, henceforth, the Eulerian and Lagrangian descriptions [19, 26, 68, 90].

The Lagrangian description of the fluid flow consists in taking the trajectories of each particle, on small enough volumes, of the fluid and describing how their properties (pressure, positions, velocity, etc.) vary along the trajectory [26]. Since the fluid elements may have their shapes altered during the motion, we need to choose an element such that its dimensions are not involved in order to circumvent this difficulty. A possible way to accomplish this is by specifying the element through its center of mass $\mathbf{q}$ at some initial time t_0. To make things clearer, we call the Lagrangian coordinate $\mathbf{q} \equiv \mathbf{q}_0$, which labels the material particle at the time at which the it started to be followed. This can be thought of as the "particle's reference frame". Hence, in order to describe the velocity of the fluid as a whole, the velocity, $\mathbf{v}(q, t)$, and initial positions of all particles are required.

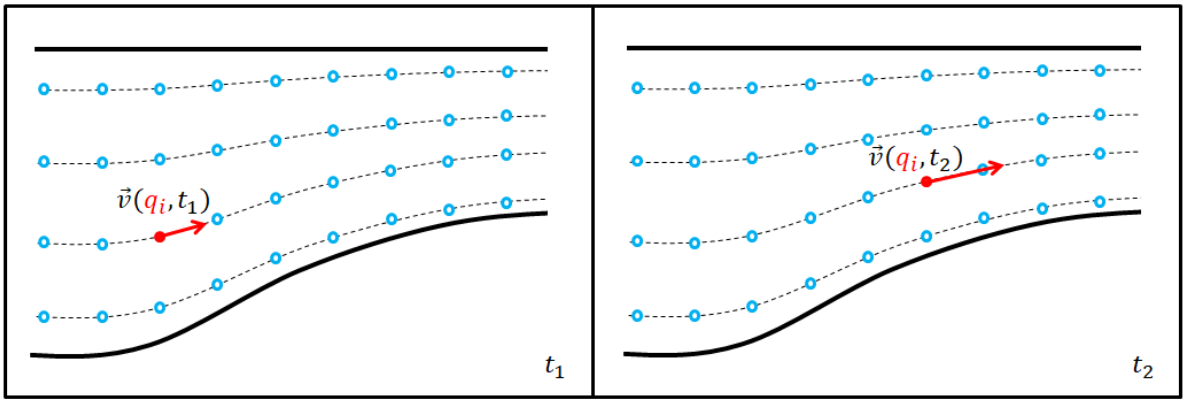

Figure 2.1: Illustration of a fluid flow described by the Lagrangian approach, where the blue circles are particles (or very small elements) of the fluid and the dashed lines represents the particles' trajectories. (*Left*) "Snapshot" of the fluid flow at some initial instant of time t_1. In this picture we follow the i-th particle marked in red, whose initial position and velocity are, respectively, $\mathbf{q_i}$ and $\mathbf{v}(\mathbf{x}_i, t_1)$. (*Right*) "Snapshot" of the fluid flow, following the same particle shown in the left panel, at some posterior time $t_2 > t_1$. We still refer to the initial position of the particle, but now the velocity is $\mathbf{v}(\mathbf{x}_i, t_2)$. Therefore, to have the whole description of the fluid represented in this figure we would need to give, for each particle in the fluid, its velocity as a function of time and initial position. Based on the figures of [77].

On the other hand, the Eulerian approach can be thought of as the description given by an observer in the "laboratory frame". That is, the spatial velocity distribution is given as a function of time. Hence, for some $\mathbf{x} = (x, y, z)$, which we will call the Eulerian position, the velocity is given at all times t: $\mathbf{u} = \mathbf{u}(\mathbf{x}, t)$.

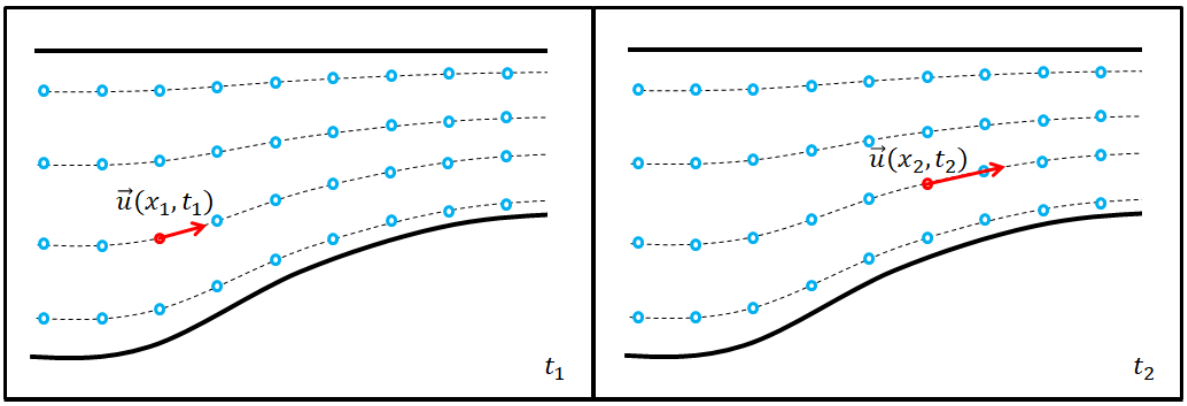

Figure 2.2: Illustration of a fluid flow described by the Eulerian approach, where the blue circles are particles (or very small elements) of the fluid and the dashed lines represents the particles' trajectories. (*Left*) "Snapshot" of the fluid flow at some initial instant of time t_1. In this picture we follow the i-th particle marked in red, whose initial position and velocity at time at time t_1 are, respectively, $\mathbf{x_1}$ and $\mathbf{u}(\mathbf{x}_1, t_1)$. (*Right*) "Snapshot" of the fluid flow, following the same particle shown in the left panel, at some posterior time $t_2 > t_1$. The velocity is $\mathbf{u}(\mathbf{x}_2, t_2)$. Therefore, to have the whole description of the fluid represented in this figure we only need the velocity field $\mathbf{u}$ as a function of $\mathbf{x}$ and t. Based on the figures of [77].

2.1.2 Fluid equations

To describe how the matter in the Universe evolves, assuming our hypothesis that it can be described as a perfect fluid, one must take into account the three main fluid equations: the Euler equation, which gives us the equations of motion of the fluid; the continuity equation, which is nothing more than the statement that matter should be conserved; and the entropy conservation, when considering adiabatic systems [26]. For the case of an external force acting upon the fluid (e.g. gravity) we must also consider the Poisson equation, which gives us the potential field ϕ acting on some element of density ρ.

I) Continuity equation

$$\frac{\partial \rho}{\partial t} + \nabla \cdot (\rho \mathbf{v}) = 0. \tag{2.1}$$

Here, $\mathbf{v}$ is the velocity field of the fluid in the Eulerian frame, so $\mathbf{v} = \mathbf{v}(\mathbf{x}, t)$, and $\rho = \rho(\mathbf{x}, t)$ is its density.

II) Euler equation

$$\frac{\partial \mathbf{v}}{\partial t} + (\mathbf{v} \cdot \nabla)\mathbf{v} + \frac{\nabla P}{\rho} + \nabla \phi = 0. \tag{2.2}$$

Notice that we are not taking into account dissipative effects, since we are assuming perfect fluids. In the above equation, $P = P(\mathbf{x}, t)$ is the pressure.

III) Entropy conservation

$$\frac{\partial S}{\partial t} + (\mathbf{v} \cdot \nabla) S = 0. \tag{2.3}$$

We take this equation into account assuming that no volume element of the fluid can exchange heat over the movement.

IV) Poisson equation

$$\nabla^2 \phi = 4\pi G \rho. \tag{2.4}$$

Notice that, in both (2.2) and (2.3), we are using the material (or convective) derivative, which denotes the rate of change of the velocity of a given fluid particle as it moves about in space instead of the rate of change of the fluid velocity at a fixed point in space [68]. For any quantity $f(\mathbf{r}(t), t)$, where $\mathbf{r} = (r_1, r_2, r_3)$, we have that

$$df = \frac{\partial f}{\partial r_1} dr_1 + \frac{\partial f}{\partial r_2} dr_2 + \frac{\partial f}{\partial r_3} dr_3 + \frac{\partial f}{\partial t} dt, \tag{2.5}$$

and hence

$$\frac{df}{dt} = \frac{\partial f}{\partial r_1}\frac{dr_1}{dt} + \frac{\partial f}{\partial r_2}\frac{dr_2}{dt} + \frac{\partial f}{\partial r_3}\frac{dr_3}{dt} + \frac{\partial f}{\partial t} = \frac{\partial f}{\partial t} + \left(\frac{d\mathbf{r}}{dt} \cdot \nabla\right) f. \tag{2.6}$$

The last term in (2.6) is responsible for the non-linearity of (2.2), that is, if $\mathbf{v}_1$ and $\mathbf{v}_1$ are two possible solutions of (2.2), $a\mathbf{v}_1 + b\mathbf{v}_2$ may not be a solution.

2.1.3 Linear perturbation theory

The whole point of perturbation theory is treating in a simple but approximate way problems that are hard to solve, by adding some small perturbation to a background whose solution is known. The simpler scenario, which we will be addressing in this chapter, is that in which we consider only the linear order in these small perturbations. That is, if a is some quantity of some system, then its background value, which will be denoted with a bar ($\bar{a}$) throughout this text, is much larger than the perturbation δa.

Static Universe without gravity

The simplest case one can start investigating is that of an isolated system, i.e. with no external forces at play. The quantities we want to determine are the pressure of the fluid

$P(\mathbf{x},t) = \bar{P}(t) + \delta P(\mathbf{x},t)$, the velocity $\mathbf{v} = \bar{\mathbf{v}}(t) + \delta\mathbf{v}(\mathbf{x},t)$ and the density $\rho(\mathbf{x},t) = \bar{\rho}(t) + \delta\rho(\mathbf{x},t)$. Since the fluid flow is assumed to be homogeneous, i.e. $\bar{\mathbf{v}}(\mathbf{x},t) = \bar{\mathbf{v}}(t)$, then we can always find a reference frame such that $\bar{\mathbf{v}} = 0$ and hence $\mathbf{v}(\mathbf{x},t) = \delta\mathbf{v}(\mathbf{x},t)$.

From the continuity equation, we obtain

$$\frac{\partial}{\partial t}(\bar{\rho} + \delta\rho) + \nabla \cdot [(\bar{\rho} + \delta\rho)\delta\mathbf{v}] = 0, \tag{2.7}$$

which leads us to the equation for the background

$$\frac{\partial\bar{\rho}}{\partial t} = 0 \Rightarrow \bar{\rho} = \text{constant in time}, \tag{2.8}$$

and for the perturbations

$$\frac{\partial\delta\rho}{\partial t} + \bar{\rho}\nabla \cdot \delta\mathbf{v} = 0. \tag{2.9}$$

The Euler equation becomes

$$\frac{\partial\delta\mathbf{v}}{\partial t} + (\delta\mathbf{v} \cdot \nabla)\,\delta\mathbf{v} + \frac{1}{\bar{\rho}}\nabla(\bar{P} + \delta P) = 0. \tag{2.10}$$

The second term in the above equation can be neglected since it gives a second-order contribution, $\nabla\bar{P} = 0$ and then the equation describing the perturbations is

$$\frac{\partial\delta\mathbf{v}}{\partial t} + \frac{\nabla\delta P}{\bar{\rho}} = 0. \tag{2.11}$$

If we assume $S(\mathbf{x},t) = \bar{S} + \delta S(\mathbf{x},t)$, then for an adiabatic fluid the entropy conservation gives us $\bar{S}$ = constant and $\delta S(\mathbf{x},t) = \delta S(\mathbf{x})$. Taking the divergence of (2.11) and the time derivative of (2.9), we obtain

$$\frac{\partial^2\delta\rho}{\partial t^2} - \nabla^2\delta P = 0. \tag{2.12}$$

Equation (2.12) can be solved if we relate δP with $\delta\rho$. This can be done via the thermodynamic relation

$$P(\mathbf{x},t) = P(\rho(\mathbf{x},t), S(\mathbf{x},t)) = P(\bar{\rho} + \delta\rho, \bar{S} + \delta S), \tag{2.13}$$

which gives us

$$\delta P = \left(\frac{\partial P}{\partial\rho}\right)_S \delta\rho + \left(\frac{\partial P}{\partial S}\right)_\rho \delta S \equiv c_s^2\delta\rho + \chi_S\delta S, \tag{2.14}$$

where $c_s^2 \equiv \left(\frac{\partial P}{\partial \rho}\right)_S$ is the square of the speed of sound and $\chi_S \equiv \left(\frac{\partial P}{\partial S}\right)_\rho$ is the adiabatic compressibility coefficient. Therefore, assuming adiabatic perturbations, $\delta S = 0$, equation (2.12) becomes

$$\frac{\partial^2 \delta\rho}{\partial t^2} - c_s^2 \nabla^2 \delta\rho = 0. \tag{2.15}$$

This is a wave equation for the density perturbations, and from it we see that these perturbations propagate with velocity c_s.

We can solve equation (2.15) by taking the Fourier transform of the function $\delta\rho(\mathbf{x}, t)$. Throughout this text, we will use the convention

$$\delta\rho(\mathbf{x}, t) = \frac{1}{(2\pi)^3} \int \delta\rho(\mathbf{k}, t) e^{i\mathbf{k}\cdot\mathbf{x}} d^3k, \tag{2.16}$$

and then

$$\frac{\partial^2}{\partial t^2}\delta\rho(\mathbf{k}, t) + c_s^2 k^2 \delta\rho(\mathbf{k}, t) = 0 \tag{2.17}$$

$$\Rightarrow \delta\rho(\mathbf{k}, t) = A_\mathbf{k} e^{i\omega(k)t} + B_\mathbf{k} e^{-i\omega(k)t}, \tag{2.18}$$

where $\omega = c_s k$ and $k = |\mathbf{k}|$. Hence, in a static Universe without gravity, density perturbations propagate as waves with constant amplitude in time:

$$\delta\rho(\mathbf{x}, t) = \int \frac{d^3k}{(2\pi)^3} \left[A_\mathbf{k} e^{i(\mathbf{k}\cdot\mathbf{x}+\omega t)} + B_\mathbf{k} e^{i(\mathbf{k}\cdot\mathbf{x}-\omega t)}\right]. \tag{2.19}$$

Static Universe with gravity

In the presence of gravity, the continuity and entropy conservation equations in a static space remains the same, yielding a constant background density and entropy. Entropy perturbations are still and density perturbations evolve according to equation (2.9).

Euler's equation, however, has the contribution of the gravitational potential $\phi(\mathbf{x}, t) = \bar{\phi} + \delta\phi(\mathbf{x}, t)$:

$$\frac{\partial \delta\mathbf{v}}{\partial t} + \underbrace{(\delta\mathbf{v}\cdot\nabla)\delta\mathbf{v}}_{\mathcal{O}(\delta^2)\sim 0} + \frac{1}{\bar{\rho}}\nabla(\bar{P} + \delta P) + \nabla(\bar{\phi} + \delta\phi) = 0, \tag{2.20}$$

$$\Rightarrow \frac{\partial \delta\mathbf{v}}{\partial t} + \frac{1}{\bar{\rho}}\nabla\delta P + \nabla\delta\phi = 0. \tag{2.21}$$

Once again, taking the divergence of the above equation and considering the time derivative of

(2.9), Euler's equation becomes

$$\frac{\partial^2 \delta\rho}{\partial t^2} - \nabla^2 \delta P - \bar{\rho}\nabla^2 \delta\phi = 0. \tag{2.22}$$

Considering the Poisson equation for the perturbations

$$\nabla^2 \delta\phi = 4\pi G \delta\rho, \tag{2.23}$$

we obtain

$$\frac{\partial^2 \delta\rho}{\partial t^2} - \nabla^2 \delta P - 4\pi G\bar{\rho}\delta\rho = 0. \tag{2.24}$$

Finally, considering (2.14), we arrive at the equation for the density perturbations in a static universe with gravity:

$$\frac{\partial^2 \delta\rho}{\partial t^2} - c_s^2 \nabla^2 \delta\rho = 4\pi G\bar{\rho}\delta\rho + \chi_S \nabla^2 \delta S. \tag{2.25}$$

Notice that this is exactly the wave equation obtained in the previous analysis, except that now the perturbations in density are sourced by both the entropy perturbations and its own gravitational effect.

There are two possible cases: (1) the one with adiabatic perturbations or (2) when there are entropy perturbations.

(1) Adiabatic perturbations

Let's consider the case where the density perturbations are generated by some adiabatic process[1], i.e. one that affects the number densities of matter and radiation equally [91]. In this case, $\delta S = 0$ and equation (2.25) becomes

$$\frac{\partial^2 \delta\rho}{\partial t^2} - c_s^2 \nabla^2 \delta\rho = 4\pi G\bar{\rho}\delta\rho, \tag{2.26}$$

or, in Fourier space,

$$\frac{\partial^2 \delta\rho}{\partial t^2} + \left(c_s^2 k^2 - 4\pi G\bar{\rho}\right)\delta\rho = 0. \tag{2.27}$$

The solution is the same we found in (2.18), except that in this case the angular frequency

[1] One of the process that generates adiabatic initial fluctuations in density, named Inflation, will be discussed further.

is given by

$$\omega(k) = \sqrt{c_s^2 k^2 - 4\pi G\bar{\rho}}. \tag{2.28}$$

We can define the Jeans wave number k_J as the value for which the angular frequency vanishes:

$$k_J \equiv \frac{1}{c_s}\sqrt{4\pi G\bar{\rho}}. \tag{2.29}$$

Then, we have the so-called Jeans length:

$$\lambda_J \equiv \frac{2\pi}{k_J} = c_s\sqrt{\frac{\pi}{G\bar{\rho}}}. \tag{2.30}$$

Therefore, we can see that the behaviour of adiabatic perturbations will depend on the scale k. If we consider modes larger than the Jeans mode, i.e. $k_J < k$ and $\lambda < \lambda_J$, then $\omega(k)^2 > 0$ and the solutions for the density perturbations are sound waves, just as in (2.18):

$$\delta\rho(\mathbf{k}, t) = A_{\mathbf{k}} e^{i\omega(k)t} + B_{\mathbf{k}} e^{-i\omega(k)t}. \tag{2.31}$$

On the other hand, if the modes are smaller than the Jeans mode, $k < k_J$ and $\lambda_J < \lambda$, then $\omega(k)^2 < 0 \Rightarrow \omega(k) \to i\omega(k)$ and

$$\delta\rho(\mathbf{k}, t) = G_{\mathbf{k}} e^{\omega(k)t} + D_{\mathbf{k}} e^{-\omega(k)t} \tag{2.32}$$

that is, the growing mode of the density perturbations are exponentially increasing with time. The term with amplitude $D_{\mathbf{k}}$ is a decaying mode which becomes negligible for sufficiently large times.

We can conclude from this analysis that, for a static space with gravity, there are two limiting situations: the one in which the pressure of the "fluid" overcomes gravity, making the density perturbations to propagate as plane waves of constant amplitude in time and the other one in which gravitational instability dominates, leading to the exponential collapse of the matter content.

(2) Entropy perturbations

Consider now some process which generates perturbations only in the matter component. At very early times, when the energy content of the Universe is dominated by radiation component, the non-relativistic matter contributions to the perturbations in the

matter-radiation fluid can be neglected, having no effects on the total energy density perturbations. However, the number of photons per particle is going to be different at distinct points in pace, leading to what we call *entropy perturbations* [84, 88, 91]. In this case, $\delta S \neq 0$.

The equation for the perturbations, (2.27), in Fourier space and in the presence of entropy perturbations becomes

$$\frac{\partial^2 \delta\rho}{\partial t^2} + \left(c_s^2 k^2 - 4\pi G\bar{\rho}\right)\delta\rho = -\chi_S k^2 \delta S. \tag{2.33}$$

The solution of (2.33) is

$$\delta\rho(\mathbf{k}, t) = \delta\rho_h(\mathbf{k}, t) + \delta\rho_p(\mathbf{k}, t), \tag{2.34}$$

where $\delta\rho_h(\mathbf{k}, t)$ and $\delta\rho_p(\mathbf{k}, t)$ are, respectively, the homogeneous (when $\delta S = 0$) and particular solutions.

The homogeneous solution is the same obtained in the adiabatic case, consisting of sound waves at scales where $\lambda < \lambda_J$ and of a exponential growth at scales such that $\lambda_J < \lambda$. The particular solution when the conservation of entropy holds, implying in a time-independent perturbation $\delta S(\mathbf{k}, t) = \delta S(\mathbf{k})$, is going to be constant with time:

$$\delta\rho_p(\mathbf{k}, t) = \delta\rho_p(\mathbf{k}) = -\frac{\chi_S k^2 \delta S(\mathbf{k})}{c_s^2 k^2 - 4\pi G\bar{\rho}}. \tag{2.35}$$

When the distance scales are large, i.e. $k \to 0$ and the effect of gravity is dominant, $\delta\rho_p(\mathbf{k}) \to 0$ and the perturbations becomes adiabatic, $\delta\rho(\mathbf{k}, t) = \delta\rho_h(\mathbf{k}, t) + \delta\rho_p(\mathbf{k}, t) \to \delta\rho_h(\mathbf{k}, t)$, meaning that adiabatic and entropy perturbations at large scales are somehow indistinguishable. For small distance scales, where $k \to \infty$ and gravitational effects are negligible compared to pressure effects, the perturbations in the density due to the entropy term are

$$\delta\rho_p(\mathbf{k}, t) = -\frac{\chi_S}{c_s^2}\delta S(\mathbf{k}) \tag{2.36}$$

and hence, in this regime,

$$\delta P_p = c_s^2 \delta\rho_p + \chi_S \delta S = -c_s^2 \frac{\chi_S}{c_s^2}\delta S + \chi_S \delta S = 0, \tag{2.37}$$

that is, perturbations in the pressure coming from the entropy contributions vanish.

Interactions violating baryon number in grand unified theories (GUTs), and even in the standard model at very high energies, which lead to the baryon-antibaryon asymmetry we observe in the Universe, produce a constant entropy per baryon [91, 97]. Besides, the Hot Big Bang model supposes that the early Universe is in thermodynamical equilibrium, therefore there are no entropy perturbations. Lastly, because recent CMB measurements point to a nearly scale-invariant spectrum, models capable of producing entropy perturbations, which generates a scale-invariant spectrum only under very special circumstances [40, 91], will not be considered. Therefore, only adiabatic perturbations are going to be studied further.

Expanding Universe with gravity

After seeing how the matter content in a static Universe moves in the presence or absence of gravity, we turn to the most interesting case: that of an expanding Universe. It is worth, thus, to spend a few lines justifying the concern with this case.

In 1929, Hubble examined the relation between the radial velocity and the distance of extra-galactic nebulae. He reported that the velocity of recession of these nebulae with respect to the Earth increases proportionally to their inferred distances. This implies that the Universe is expanding in every direction as a function of time [55, 122].

The plot of the galaxies' magnitude as a function distance is now called Hubble diagram, in honour of Hubble's original work (see Figure 1 of [55]). Recently, many measurements of distant galaxies using type Ia supernovae indicate not only the current expansion of the Universe, but also the accelerated rate with which it seems to be expanding, whose cause is attributed to the so-called dark energy.

In Figure 2.3 we show the data from the Union2.1 compilation of the Supernova Cosmology Project [123], along with fits of different flat cosmological models including dark energy and dark matter components.

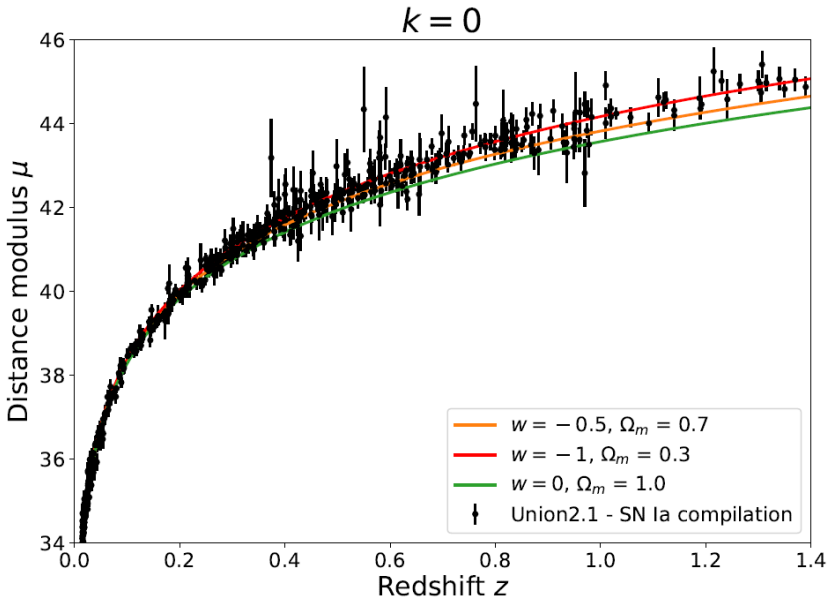

Figure 2.3: Union2.1 compilation of 557 Supernovae Ia. Solid lines represent distance modulus μ obtained in a flat Universe with varying cosmological parameters Ω_m and $\Omega_\Lambda = 1 - \Omega_m$ and dark energy equation of state w. The analysis done by Hubble, in 1929, included variable stars at maximum redshift of around $z \approx 0.0005$. Hence, due to observational limitations at that time, Hubble was only capable of analyzing what would be the equivalent of the beginning of our graph, which yields the straight line shown in [55], serving as an observational evidence for the expansion of the Universe.

When the Universe is expanding, and if we consider scales large enough so that the effects of gravity are negligible face to the cosmic expansion, all points (galaxies) in space are parting away from each other according to the law

$$\mathbf{x}(t) = a(t)\mathbf{x}(t_0), \tag{2.38}$$

where the scale factor, $a(t)$, tells us how the distances in the Universe are evolving. By examining this expression we can see that $\mathbf{x}(t)$ refers to Eulerian coordinates and $\mathbf{x}(t_0)$ are the Eulerian coordinates at some initial time t_0, i.e., $\mathbf{x}(t_0)$ are the Lagrangian coordinates, which do not evolve with time. In terms of velocity,

$$\frac{d\mathbf{x}}{dt} = \mathbf{v}(t) = \frac{da}{dt}\mathbf{x}(t_0) = \frac{\dot{a}(t)}{a(t)}\mathbf{x}(t) \equiv H(t)\mathbf{x}(t) \tag{2.39}$$

we arrive at the law observed by Hubble in 1929 [55]. In the case of an unperturbed Universe, comoving and Lagrangian coordinates coincide.

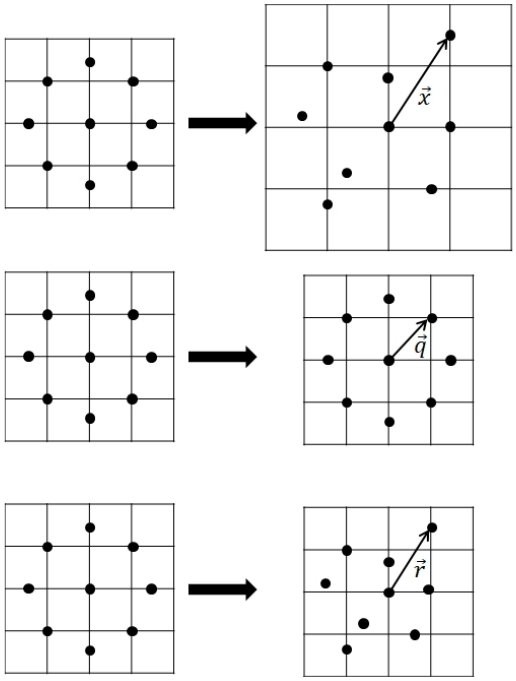

Figure 2.4: Three descriptions of fluids in Cosmology. (*Top*) Eulerian coordinates do not follow the expansion of the Universe. In this illustration, besides the Hubble flow, they are subjected to perturbations. (*Middle*) The Lagrangian coordinates are kept fixed in time. They can be thought of as comoving coordinates in the absence of perturbations, when there are no peculiar velocities induced by gravity. (*Bottom*) Comoving coordinates are the same as the Lagrangian ones, except that, in the presence of inhomogeneities, they have peculiar velocities which make displacements other than the ones due to the Hubble flow. Based on Figure 15.2 of [92].

However, when there are generate perturbations in the matter, the comoving coordinates will slightly change with time and, therefore, they will not coincide anymore with the Lagrangian coordinates (see Figure 2.4). This happens because, in addition to the Hubble flow, there is the peculiar velocity field which emerges due to the perturbations. Hence, calling $\mathbf{r}(t)$ the comoving coordinates, which are related to the proper (Eulerian) coordinates via the relation

$$\mathbf{x}(t) = a(t)\mathbf{r}(t) \tag{2.40}$$

the velocity field becomes

$$\mathbf{v}(t) = \frac{d\mathbf{x}}{dt} = H(t)\mathbf{x}(t) + a(t)\frac{d\mathbf{r}}{dt} \equiv H(t)\mathbf{x}(t) + a(t)\mathbf{u}(t) \tag{2.41}$$

The first term, $\bar{\mathbf{v}} \equiv H(t)\mathbf{x}(t)$, is the Hubble flow that describes the background over which the particles are analyzed. The second term, $\delta\mathbf{v}(t) \equiv a(t)\mathbf{u}(t)$, is the peculiar velocity field induced by the perturbations.

From (2.40) we can see that the spatial derivatives in the Eulerian coordinates can be written as

$$\nabla_{\mathbf{x}} = \frac{1}{a(t)}\nabla_{\mathbf{r}}. \tag{2.42}$$

Following (2.6), the time derivative at constant comoving coordinates is related to Eulerian coordinates through the relation

$$\frac{\partial}{\partial t}\Big|_{\mathbf{r}} = \frac{\partial}{\partial t}\Big|_{\mathbf{x}} + \frac{d\mathbf{x}}{dt}\Big|_{\mathbf{r}} \cdot \nabla_{\mathbf{x}} = \frac{\partial}{\partial t}\Big|_{\mathbf{x}} + \dot{a}\mathbf{r} \cdot \nabla_{\mathbf{x}} = \frac{\partial}{\partial t}\Big|_{\mathbf{x}} + H(t)\mathbf{r} \cdot \nabla_{\mathbf{r}}. \tag{2.43}$$

Therefore, from the Eulerian description to the comoving frame we have

$$\frac{\partial}{\partial t}\Big|_{\mathbf{x}} = \frac{\partial}{\partial t}\Big|_{\mathbf{r}} - \bar{\mathbf{v}} \cdot \nabla_{\mathbf{x}} = \frac{\partial}{\partial t}\Big|_{\mathbf{r}} - H\mathbf{r} \cdot \nabla_{\mathbf{r}}. \tag{2.44}$$

From now on we will omit the r subscript for the sake of simplicity.

Let's consider, then, the continuity equation. Now we have $\mathbf{v}(\mathbf{x}, t) = \bar{\mathbf{v}} + \delta\mathbf{v}(\mathbf{x}, t)$, where $\mathbf{x} = a(t)\mathbf{r}$ is the proper position. In these coordinates, the continuity equation becomes

$$\frac{\partial(\bar{\rho} + \delta\rho)}{\partial t}\Big|_{\mathbf{x}} + \nabla_{\mathbf{x}} \cdot [(\bar{\rho} + \delta\rho)(\bar{\mathbf{v}} + \delta\mathbf{v})] = 0, \tag{2.45}$$

leading us to the equation for the background:

$$\frac{\partial\bar{\rho}}{\partial t} + \bar{\rho}\nabla_{\mathbf{x}} \cdot \bar{\mathbf{v}} = \frac{\partial\bar{\rho}}{\partial t} + \bar{\rho}H(t)\nabla_{\mathbf{x}} \cdot \mathbf{x} = 0 \tag{2.46}$$

$$\Rightarrow \frac{\partial\bar{\rho}}{\partial t} + 3\bar{\rho}H = 0, \tag{2.47}$$

which is the conservation of mass for non-relativistic matter ($\bar{\rho} \propto a^{-3}$) and, for the perturbations,

$$\frac{\partial\delta\rho}{\partial t}\Big|_{\mathbf{x}} + \bar{\rho}\nabla_{\mathbf{x}} \cdot \delta\mathbf{v} + \bar{\mathbf{v}} \cdot \nabla_{\mathbf{x}}\delta\rho + \delta\rho\nabla_{\mathbf{x}} \cdot \bar{\mathbf{v}} = 0. \tag{2.48}$$

Equation (2.48) above is the continuity equation in the Eulerian description with proper (Euler) coordinates. We can simplify this equation by working with the comoving coordinates (2.42) and (2.44):

$$\frac{\partial\delta\rho}{\partial t} + \frac{\bar{\rho}}{a}\nabla \cdot \delta\mathbf{v} + 3H\delta\rho = 0 \tag{2.49}$$

Introducing the density contrast,

$$\delta(\mathbf{x}) \equiv \frac{\delta\rho(\mathbf{x})}{\bar{\rho}} = \frac{\rho(\mathbf{x}) - \bar{\rho}}{\bar{\rho}}, \tag{2.50}$$

equation (2.49) becomes

$$\left(\frac{\partial\bar{\rho}}{\partial t} + 3H\bar{\rho}\right)\delta + \bar{\rho}\frac{\partial\delta}{\partial t} + \frac{\bar{\rho}}{a}\nabla\cdot\delta\mathbf{v} = 0. \tag{2.51}$$

From the background equation (2.47) we see that the first term in (2.51) vanishes, resulting in

$$\frac{\partial\delta}{\partial t} + \frac{1}{a}\nabla\cdot\delta\mathbf{v} = 0. \tag{2.52}$$

The Euler equation in proper coordinates can be written as

$$\frac{\partial(\bar{\mathbf{v}} + \delta\mathbf{v})}{\partial t}\Big|_{\mathbf{x}} + \left[(\bar{\mathbf{v}} + \delta\mathbf{v})\cdot\nabla_{\mathbf{x}}\right](\bar{\mathbf{v}} + \delta\mathbf{v}) + \frac{\nabla_{\mathbf{x}}(\bar{P} + \delta P)}{\bar{\rho}} + \nabla_{\mathbf{x}}(\phi + \delta\phi) = 0, \tag{2.53}$$

which gives us the equations for the background,

$$\frac{\partial\bar{\mathbf{v}}}{\partial t}\Big|_{\mathbf{x}} + (\bar{\mathbf{v}}\cdot\nabla_{\mathbf{x}})\bar{\mathbf{v}} + \frac{\nabla_{\mathbf{x}}\bar{P}}{\bar{\rho}} + \nabla_{\mathbf{x}}\bar{\phi} = 0, \tag{2.54}$$

as well as for the perturbations at first order:

$$\frac{\partial\delta\mathbf{v}}{\partial t}\Big|_{\mathbf{x}} + (\bar{\mathbf{v}}\cdot\nabla_{\mathbf{x}})\delta\mathbf{v} + (\delta\mathbf{v}\cdot\nabla_{\mathbf{x}})\bar{\mathbf{v}} + \frac{c_s^2}{\bar{\rho}}\nabla_{\mathbf{x}}\delta\rho + \frac{\chi_S}{\bar{\rho}}\nabla_{\mathbf{x}}\delta S + \nabla_{\mathbf{x}}\delta\phi = 0. \tag{2.55}$$

Let's first consider the background. Taking the divergence of (2.54), we obtain:

$$\frac{\partial}{\partial t}\Big|_{\mathbf{x}}\nabla_{\mathbf{x}}\cdot\bar{\mathbf{v}} + \nabla_{\mathbf{x}}\cdot(\bar{\mathbf{v}}\cdot\nabla_{\mathbf{x}})\bar{\mathbf{v}} + \nabla^2_{\mathbf{x}}\phi = 0. \tag{2.56}$$

By considering the Poisson equation $\nabla^2\bar{\phi} = 4\pi G\bar{\rho}$, the Euler equation becomes

$$\frac{\partial}{\partial t}\Big|_{\mathbf{x}}\nabla_{\mathbf{x}}\cdot[H(t)\mathbf{x}] + \nabla_{\mathbf{x}}\cdot([H(t)\mathbf{x}]\cdot\nabla_{\mathbf{x}})[H(t)\mathbf{x}] = -4\pi G\bar{\rho}, \tag{2.57}$$

which is the "second" Friedmann equation:

$$\dot{H} + H^2 = -\frac{4\pi G}{3}\bar{\rho}. \tag{2.58}$$

Considering only adiabatic perturbations, the Euler equation at first order is

$$\frac{\partial \delta \mathbf{v}}{\partial t}\Big|_{\mathbf{x}} + (\bar{\mathbf{v}} \cdot \nabla_{\mathbf{x}})\delta\mathbf{v} + (\delta\mathbf{v} \cdot \nabla_{\mathbf{x}})\bar{\mathbf{v}} + \frac{c_s^2}{\bar{\rho}}\nabla_{\mathbf{x}}\delta\rho + \nabla_{\mathbf{x}}\delta\phi = 0. \tag{2.59}$$

Switching to comoving coordinates we can simplify the equation:

$$\frac{\partial \delta \mathbf{v}}{\partial t} - (\bar{\mathbf{v}} \cdot \nabla_{\mathbf{x}})\delta\mathbf{v} + (\bar{\mathbf{v}} \cdot \nabla_{\mathbf{x}})\delta\mathbf{v} + (\delta\mathbf{v} \cdot \nabla_{\mathbf{x}})H\mathbf{x} + \frac{c_s^2}{a\bar{\rho}}\nabla\delta\rho + \frac{1}{a}\nabla\delta\phi = 0 \tag{2.60}$$

$$\Rightarrow \frac{\partial \delta \mathbf{v}}{\partial t} + H\delta\mathbf{v} + \frac{c_s^2}{a\bar{\rho}}\nabla\delta\rho + \frac{1}{a}\nabla\delta\phi = 0. \tag{2.61}$$

In terms of the density contrast δ,

$$\frac{\partial \delta \mathbf{v}}{\partial t} + H\delta\mathbf{v} + \frac{c_s^2}{a}\nabla\delta + \frac{1}{a}\nabla\delta\phi = 0. \tag{2.62}$$

By substituting the Poisson equation $\nabla^2\delta\phi = 4\pi G\bar{\rho}\delta$ and the time derivative of (2.52) into the divergence of (2.62), we arrive at the equation describing how the non-relativistic matter content, when subjected to gravitational instability, evolves in an expanding Universe:

$$\boxed{\frac{\partial^2\delta}{\partial t^2} + 2H\frac{\partial\delta}{\partial t} - \frac{c_s^2}{a^2}\nabla^2\delta - 4\pi G\bar{\rho}\delta = 0}. \tag{2.63}$$

Comparing this equation with the one obtained for a static space with gravity, (2.26), we see that there is a new term, $2H\dot{\delta}$, which acts as friction. Let's now analyze how the expansion of the Universe, encoded in this new friction term, affects the matter perturbations.

General solution for adiabatic perturbations

In Fourier space (2.63) becomes

$$\frac{\partial^2\delta}{\partial t^2} + 2H\frac{\partial\delta}{\partial t} + \left(\frac{c_s^2k^2}{a^2} - 4\pi G\bar{\rho}\right)\delta = 0. \tag{2.64}$$

Unlike the Jeans length encountered in (2.30), there will be a time dependence due to the presence of $a(t)$ in the angular frequency,

$$\omega(k,t) = \sqrt{\frac{c_s^2k^2}{a^2} - 4\pi G\bar{\rho}}. \tag{2.65}$$

Therefore, the physical Jeans length, related to the comoving wavelength λ_J, is

$$\lambda_J = \frac{2\pi}{k_J} = \frac{\lambda_J^{ph}}{a(t)} = \frac{c_s}{a(t)}\sqrt{\frac{\pi}{G\bar{\rho}}}, \tag{2.66}$$

where $k_J = c_s^{-1}\sqrt{4\pi G\bar{\rho}}$ is the comoving Jeans wavenumber.

On scales much smaller than the Jeans length, $\lambda \ll \lambda_J$, $k \gg k_J$, we have

$$\frac{\partial^2\delta}{\partial t^2} + 2H\frac{\partial\delta}{\partial t} + \frac{c_s^2k^2}{a^2}\delta = 0, \tag{2.67}$$

thus it is suitable to consider the WKB method [102, 131] to solve this equation. The solutions are sound waves decaying with $\sqrt{a}$:

$$\delta(\mathbf{k}, t) \propto \frac{1}{\sqrt{c_s a}} e^{\pm i\mathbf{k}\int c_s a^{-1} dt} \tag{2.68}$$

This damping in the amplitude is expected since we are dealing with an expanding Universe. Hence, these waves are stretched with the Hubble expansion and their amplitudes decrease with time.

For large-scale perturbations gravity is dominant over pressure. In this case, we can neglect the spatial derivatives and equation (2.63) becomes

$$\frac{\partial^2\delta(\mathbf{x}, t)}{\partial t^2} + 2H\frac{\partial\delta(\mathbf{x}, t)}{\partial t} + 4\pi G\bar{\rho}(t)\delta = 0. \tag{2.69}$$

We can look for solutions of the form

$$\delta(\mathbf{x}, t) = D_+(t)\delta_g(\mathbf{x}) + D_-(t)\delta_d(\mathbf{x}), \tag{2.70}$$

where $D_+(t)$ and $D_-(t)$ are, respectively, an increasing and decreasing function of time and $\delta(x)$ is the initial density field. Plugging this into (2.69), we obtain an equation for the functions D

$$\ddot{D} + 2H(t)\dot{D} - \frac{3}{2}H^2\Omega_m(t)D = 0, \tag{2.71}$$

where we used the Friedmann equation in terms of the density parameter Ω_m to express $4\pi G\bar{\rho}_m = 3H^2\Omega_m/2$, since we are not considering spatial curvature, and we have made explicit that we are dealing with dark matter perturbations. We consider below the case of a matter dominated

Universe.

- **Matter-dominated Universe**

  Considering the case of a matter dominated Universe, $\Omega_m = 1$, the scale factor behaves as $a(t) \propto t^{2/3}$. The solutions are, thus,

$$D_+(t) \propto t^{2/3} \sim a(t) \quad \text{and} \quad D_-(t) \propto t^{-1} \sim a^{-3/2}(t) \tag{2.72}$$

  Therefore, matter perturbations in a matter dominated Universe grow with the scale factor.

2.2 Relativistic approach

The classical theory is restricted to sub-horizon scales and non-relativistic matter. The former limitation comes from the fact that, in the Newtonian framework, perturbations propagate instantaneously. The second limitation appears when one tries to treat a fluid whose constituent particles have high velocities, or when the gravitational field is strong enough to deform spacetime. At early times, when the temperature of the Universe is high enough to ionize any form of matter, the Universe is dominated by radiation. Besides, it is important to take into account perturbations whose scales exceed or are close to the Hubble radius in order to understand the formation of structures and a non-relativistic approach is wholly unsuitable in that case, owing to both the curvature of spacetime and the acausal nature of Newtonian instantaneous action at a distance. Consequently, we turn our attention to a more generalized and complete study of perturbations: the relativistic cosmological perturbation theory.

The relativistic approach leans on the theory of General Relativity. Our job, then, is to solve Einstein's equations

$$G_{\mu\nu} = R_{\mu\nu} - \frac{1}{2} R g_{\mu\nu} = 8\pi G T_{\mu\nu} \tag{2.73}$$

for small perturbations around some background solution. Above, $G_{\mu\nu}$, $R_{\mu\nu}$ and R are, respectively, the Einstein tensor, Ricci tensor and Ricci scalar. Just as was done to describe a fluid in Newtonian theory, we should to give its velocity (for the kinematic description) and thermodynamic properties. We must also solve for the metric $g_{\mu\nu} = \bar{g}_{\mu\nu} + \delta g_{\mu\nu}$, given some energy-momentum tensor $T_{\mu\nu} = \bar{T}_{\mu\nu} + \delta T_{\mu\nu}$. To make matters as clear as possible, the idea behind this treatment is that perturbations in the metric will drive to perturbations in the matter and vice-versa, since they are both coupled through Einstein's equations: $\delta g_{\mu\nu} \leftrightarrow \delta T_{\mu\nu}$.

2.2.1 Perturbing the metric

The full perturbed metric is given by

$$g_{\mu\nu} = \bar{g}_{\mu\nu} + \delta g_{\mu\nu}, \tag{2.74}$$

where $\delta g_{\mu\nu} \ll g_{\mu\nu}$ is a small deviation around a homogeneous and isotropic FLRW background metric $\bar{g}_{\mu\nu}$. This is reasonable since, on very large scales, the Universe is described to a very good approximation by the FLRW metric.

We will consider first the general form of the perturbations and then address the gauge issue emerging from this definition. Once this issue is clear, we will give a restricted form for $\delta g_{\mu\nu}$ in such a way that it is gauge independent.

The FLRW background metric is given by the line element

$$ds^2 = \bar{g}_{\mu\nu} dx^\mu dx^\nu = a^2(\tau) \left[d\tau^2 - \gamma_{ij} dx^i dx^j \right], \tag{2.75}$$

where

$$\tau \equiv \int \frac{dt}{a(t)} \tag{2.76}$$

is the conformal time, and $\gamma_{ij} = \delta_{ij} \left[1 + \frac{K}{4}(x^2 + y^2 + z^2) \right]^{-2}$ is the three-dimensional open, flat or closed metric – respectively, with $K = R^{-2}(-1, 0, 1)$, where R is the radius of curvature.

Hence, the full perturbed metric is

$$ds^2 = \bar{g}_{\mu\nu} dx^\mu dx^\nu + \delta g_{\mu\nu} dx^\mu dx^\nu. \tag{2.77}$$

2.2.2 S-V-T decomposition

Given the (3+1) symmetries of the background metric, we can split the metric perturbations into three categories of (3+1) objects: scalar, vector and tensor perturbations. An advantage of this decomposition is that, in Fourier space and at linear order in perturbations, these perturbations are completed detached from each other, i.e. they don't mix. This convenient property emerges from the helicity (or transformation properties) of the perturbations (see §2.2.2 of [39]).

Scalar perturbations

Consider the perturbed part of the metric:

$$ds^2 = \delta g_{\mu\nu} dx^\mu dx^\nu = \delta g_{00} d\tau^2 + 2\delta g_{0i} d\tau dx^i + \delta g_{ij} dx^i dx^j. \tag{2.78}$$

From the temporal part we can see that it is possible to introduce a scalar, e.g. ϕ, by considering

$$\delta g^s_{00} = 2a^2(\tau)\phi, \tag{2.79}$$

where the factor of 2 was explicitly introduced to make evident the Newtonian limit of the metric [24].

Considering the off-diagonal part, the only possible way to introduce a scalar, e.g. B, it is by taking its gradient[2] $\partial_i B$:

$$\delta g^s_{0i} = a^2(\tau)\partial_i B. \tag{2.80}$$

Finally, by considering the product of some scalar ψ with γ_{ij}, or by taking two derivatives of another scalar function, E, we can introduce scalars on the spatial part of the metric:

$$\delta g^s_{ij} = 2a^2(\tau)\psi\gamma_{ij} + 2a^2(\tau)\partial_i\partial_j E. \tag{2.81}$$

Thereby we have the scalar perturbations:

$$\delta g^s_{\mu\nu} = a^2(\tau) \begin{pmatrix} 2\phi & \partial_i B \\ \partial_i B & 2(\psi\gamma_{ij} + \partial_i\partial_j E) \end{pmatrix}, \tag{2.82}$$

or

$$ds^2 = a^2(\tau)\left[2\phi d\tau^2 + 2B_{;i} d\tau dx^i + 2(\psi\gamma_{ij} + E_{;ij}) dx^i dx^j\right]. \tag{2.83}$$

Vector perturbations

Analogously to what has been done with scalar perturbations, we can write the vector part of the perturbations $\delta g_{\mu\nu}$ using a pure 3-vector S_i, i.e. $\partial_i S_i = 0$, for the off-diagonal part,

[2]Throughout this text, ∂_i is going to denote the usual derivatives for the flat spacetime case. However, in this section it will denote the covariant derivative to save notation. Every time ∂_i appears with the γ_{ij} spatial metric component, we will be dealing with the covariant derivatives for a general curvature K.

or covariant derivatives of another pure vector F_i for the spatial part:

$$\delta g^v_{0i} = a^2(\tau) S_i \quad \text{and} \quad \delta g^v_{ij} = a^2(\tau)(\partial_i F_j + \partial_j F_i), \tag{2.84}$$

in such a way that

$$\delta g^v_{\mu\nu} = a^2(\tau) \begin{pmatrix} 0 & S_i \\ S_i & \partial_i F_j + \partial_j F_i \end{pmatrix}, \tag{2.85}$$

or

$$ds^2 = a^2(\tau) \left[2 S_i d\tau dx^i + (F_{j;i} + F_{i;j}) dx^i dx^j \right]. \tag{2.86}$$

Tensor perturbations

The only way to introduce a (3+1) tensor perturbation on the metric is by taking a symmetric, transverse and traceless 3-tensor h_{ij} satisfying $h^i_i = 0$ and $\partial_j h_{ij} = 0$. Thus,

$$\delta g^t_{\mu\nu} = a^2(\tau) \begin{pmatrix} 0 & 0 \\ 0 & h_{ij} \end{pmatrix}, \tag{2.87}$$

or simply

$$ds^2 = a^2(\tau) h_{ij} dx^i dx^j. \tag{2.88}$$

Complete form of the perturbed metric

The full perturbed metric in terms of the S-V-T decomposition is given by

$$ds^2 = a^2(\tau) \left[(1 + 2\phi) d\tau^2 + 2 B_i d\tau dx^i - (\gamma_{ij} - C_{ij}) dx^i dx^j \right], \tag{2.89}$$

where

$$B_i \equiv B_{;i} + S_i, \tag{2.90}$$

and

$$C_{ij} = 2\psi\gamma_{ij} + 2E_{;ij} + F_{j;i} + F_{i;j} + h_{ij}. \tag{2.91}$$

For a flat Universe, the full metric is simplified:

$$\boxed{ds^2 = a^2(\tau) \left[(1 + 2\phi) d\tau^2 + 2 B_i d\tau dx^i - (\delta_{ij} - E_{ij}) dx^i dx^j \right]}, \tag{2.92}$$

with $B_i = B_{,i} + S_i$ and $E_{ij} = 2\psi\delta_{ij} + 2E_{,ij} + F_{j,i} + F_{i,j} + h_{ij}$. From now on we will assume a flat Universe and ∂_i acquires back its ordinary sense of spatial derivatives.

We will see that the vector modes, associated with rotational fluid flow, will not be relevant in our study since they decay very quickly in the standard expanding Universe scenario [51, 84]. The tensor perturbations do not have non-relativistic analog and give rise to gravitational waves. Finally, scalar perturbations will be the focus of our work, since they exhibit instabilities responsible for the growth of inhomogeneities, being responsible for the structures we see today [84].

2.2.3 Gauge transformations and its consequences

As discussed in section §2.1, the perturbation theory approach relies on considering small perturbations around some background whereas the real physical quantities are obtained from the perturbed spacetime.

When we separate the full quantity into background and perturbation, we must define a correspondence – or a map Φ, in its mathematical sense – between the physical and the fictitious Universe. That is, besides the requirement that the perturbations of some physical quantity a are small[3], there is no way to determine the background $\bar{a}$ solely from the knowledge of a. Therefore, one must specify a map between the background and the physical spacetime and there is no unique way to do it [44]. There is, thus, a freedom in the choice of the mapping between universes and a change in this mapping is called a gauge transformation [14].

This gauge freedom sets up a problem in perturbation theory: it can make nonphysical perturbations appear as much as it can remove the physical ones. To illustrate this we show the argument done by Mukhanov in [84]:

> The Principle of Relativity postulates that "the laws of physics must be of such a nature that they apply to systems of reference in any kind of motion" [41]. Therefore, if we take the usual background density from the classical treatment $\bar{\rho} = \bar{\rho}(\bar{t})$, we can change to a new time coordinate t related to the former system via, e.g., $t = \bar{t} + \delta t(\bar{t}, \bar{x})$.

[3]Note that one could ask "small compared to what?". A mapping between the real perturbed spacetime and the background must be defined so that this comparison is well defined.

Then, at the new reference frame S of the time coordinates t,

$$\rho(t, \bar{x}) \equiv \bar{\rho}(\bar{t}(t, \bar{x})), \tag{2.93}$$

which leads to

$$\rho(t, \bar{x}) = \bar{\rho}(t - \delta t(\bar{t}, \bar{x})) \approx \bar{\rho}(t) - \frac{\partial \bar{\rho}}{\partial \bar{t}} \delta t \equiv \bar{\rho}(t) + \delta\rho(t, \bar{x}) \tag{2.94}$$

if we assume that $\delta t \ll \bar{t}$.

In the above equation, $\bar{\rho}(t)$ can be interpreted as the new background density in the coordinate system S whereas $\delta\rho(t, \bar{x}) = \partial_{\bar{t}}\bar{\rho}\delta t$ is a nonphysical perturbation that emerged due to this time coordinate transformation. We could also have done another transformation such that the process of eliminating a real perturbation happened instead (see Figure 2.5a).

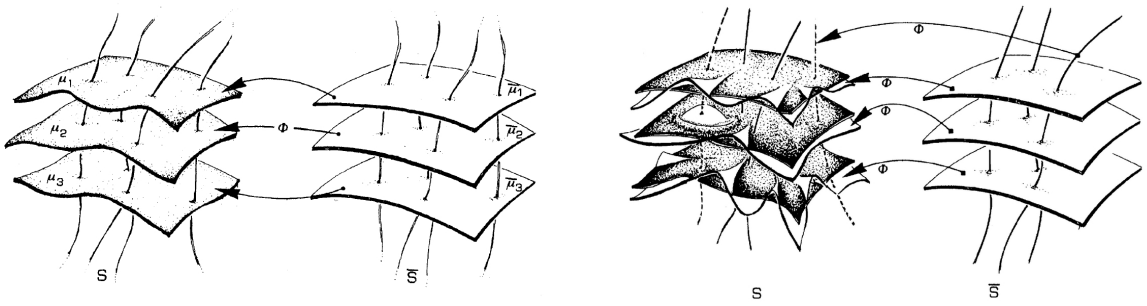

(a) Through the specific choice of Φ, it is possible to map surfaces of constant fictitious density $\bar{\rho}$ into surfaces of the real universe S with constant density ρ, that is, Φ assigns the same numerical values to $\bar{\rho}$ as ρ has on S, leading to $\delta\rho = 0$. Therefore, we can eliminate perturbations with certain choices of gauge.

(b) The mapping Φ from a fictitious universe $\bar{S}$, described by the FLRW metric, into a more accurate, real universe. With this we can define a perturbation in density $\delta\rho$, once Φ maps surfaces of constant density $\bar{\rho}$ from $\bar{S}$ into S, where they can finally be compared with the real density ρ.

Figure 2.5: Reprinted figures with permission from *Ellis, G. and Bruni, M., Covariant and gauge-invariant approach to cosmological density fluctuations, Physical Review D., v. 40, p. 1804, 1989.* Copyright (1989) by the American Physical Society.

To address this problem formally, we need to choose a system of coordinates in order to fix the background spacetime metric we are working through the manifold $\bar{S} = (\bar{x}^\mu, \bar{g}_{\mu\nu}(\bar{x}))$. We can then associate any map $\Phi : \bar{S} \to S$, at some fixed coordinate system $\bar{x}^\mu$, mapping some function $\bar{f}(\bar{x}^\mu) \in \bar{S}$ into $f(\bar{x}^\mu) \in S$. Then we can define the perturbation in this quantity through the relation

$$\delta f(p) = f(p) - \bar{f}(\Phi^{-1}(p)), \tag{2.95}$$

where $p \in S$ (see Figure 2.5b for the example of density perturbations).

However, we could choose another map, $\tilde{\Phi} : \bar{S} \to S$, which induces another set of coordinates $\tilde{x}^\mu$, such that

$$\tilde{\delta f}(p) = \tilde{f}(p) - \bar{f}(\tilde{\Phi}^{-1}(p)). \tag{2.96}$$

The change of correspondence

$$\delta f(p) \to \tilde{\delta f}(p) \tag{2.97}$$

is what we call a gauge transformation. In the context of General Relativity, it is nothing more than the coordinate transformation $x^\mu \to \tilde{x}^\mu$.

It is natural to say, then, that f is a gauge-invariant quantity if its functional dependence is the same on both coordinate systems, i.e. $f(x^\mu) = f(\tilde{x}^\mu)$. However, we cannot guarantee that $f(x^\mu) = \tilde{f}(\tilde{x}^\mu)$, meaning that δf can differ from one system to another.

Since the metric $g_{\mu\nu}(x)$ is defined on a manifold for a fixed coordinate system, we can alter the shape of the metric perturbations through a gauge transformation.

This gauge issue, and the difficulty it poses to a clear interpretation of the physical quantities in a general relativistic treatment of cosmological perturbations, has a long history. Attempts to solve this issue date back to 1960s, including one due to Hawking [54], who formulated the perturbation equations in a complete covariant form, without making any mentions to the metric tensor. However, in this work the choice of a time slicing is made to define the density perturbations, leaving the gauge matter still present, as pointed out by Bardeen [14]. Ten years later, Olson derived the equation describing the linearized perturbations of an isentropic fluid, in a flat FLRW background Universe, with gauge-independent variables [86]. Finally, four years after Olson's paper, the famous work of Bardeen [14] settled down a complete set of gauge-invariant variables that clarified the physical interpretation of the cosmological perturbations in the relativistic framework.

Gauge-invariant variables

Let's follow Bardeen's approach and consider the most general coordinate transformation

$$\tilde{x}^\mu = x^\mu + \xi^\mu, \tag{2.98}$$

where ξ^μ is an infinitesimal shift in the coordinates[4].

The simplest analysis one can perform is to check how a scalar $q(x^\mu)$, such as the density perturbations $\rho(x^\mu)$, changes under (2.98):

$$\tilde{q}(\tilde{x}^\mu) \equiv q[x^\mu(\tilde{x}^\mu)], \tag{2.99}$$

$$\bar{q}(\tilde{x}^\mu) + \tilde{\delta q} = q(\tilde{x}^\mu) - \frac{\partial q}{\partial x^\mu}\xi^\mu + \mathcal{O}(2), \tag{2.100}$$

$$= \bar{q}(\tilde{x}^\mu) + \delta q - \bar{q}_{,\mu}\xi^\mu + \mathcal{O}(2), \tag{2.101}$$

where $\mathcal{O}(2)$ represents the second and higher order terms in the perturbations δq and ξ.

Hence, at linear order a scalar transforms under (2.98) as

$$\tilde{\delta q} = \delta q - \bar{q}_{,\mu}\xi^\mu. \tag{2.102}$$

Under (2.98), the full metric $g_{\mu\nu}$ transforms as

$$\tilde{g}_{\alpha\beta}(\tilde{x}) = \frac{\partial x^\mu}{\partial \tilde{x}^\alpha}\frac{\partial x^\nu}{\partial \tilde{x}^\beta} g_{\mu\nu}(x), \tag{2.103}$$

$$\bar{g}_{\alpha\beta}(\tilde{x}) + \tilde{\delta g}_{\alpha\beta}(\tilde{x}) = \left(\delta^\mu_\alpha - \frac{\partial \xi^\mu}{\partial \tilde{x}^\alpha}\right)\left(\delta^\nu_\beta - \frac{\partial \xi^\nu}{\partial \tilde{x}^\beta}\right)(\bar{g}_{\mu\nu}(x) + \delta g_{\mu\nu}(x)), \tag{2.104}$$

$$\approx (\delta^\mu_\alpha \delta^\nu_\beta - \delta^\nu_\beta \xi^\mu_{,\alpha} - \delta^\mu_\alpha \xi^\nu_{,\beta})(\bar{g}_{\mu\nu}(x) + \delta g_{\mu\nu}(x)), \tag{2.105}$$

$$\approx \bar{g}_{\alpha\beta}(x) + \delta g_{\alpha\beta}(x) - \bar{g}_{\mu\beta}\xi^\mu_{,\alpha} - \bar{g}_{\alpha\nu}\xi^\nu_{,\beta}. \tag{2.106}$$

Since

$$\bar{g}_{\alpha\beta}(x) = \bar{g}_{\alpha\beta}(\tilde{x}) - \bar{g}_{\alpha\beta,\rho}\xi^\rho, \tag{2.107}$$

we obtain, at linear order, the following expression for the gauge transformation (2.98):

$$\tilde{\delta g}_{\alpha\beta} = \delta g_{\alpha\beta} - \bar{g}_{\alpha\beta,\rho}\xi^\rho - \bar{g}_{\mu\beta}\xi^\mu_{,\alpha} - \bar{g}_{\alpha\nu}\xi^\nu_{,\beta}. \tag{2.108}$$

By noticing that it is possible to split ξ^μ into a scalar T and a vector part, $\xi^\mu = (T, L^i)$, where $L^i = \partial^i L + \hat{L}^i$, with L a scalar and $\partial_i \hat{L}^i = 0$, and considering the case of a FLRW

[4]We could put a small factor ϵ in front of ξ to make explicit how small are these shifts from the original coordinates: $\tilde{x}^\mu = x^\mu + \varepsilon\xi^\mu$. But we will omit this factor for clarity.

background, the transformations (2.108) for the full metric lead us to

$$\tilde{\delta g}_{00} = \delta g_{00} - 2a(aT)', \tag{2.109}$$

$$\tilde{\delta g}_{0i} = \delta g_{0i} + a^2(L_i' - T_{,i}), \tag{2.110}$$

$$\tilde{\delta g}_{ij} = \delta g_{ij} + a^2(2\mathcal{H}\delta_{ij}T + L_{j,i} + L_{i,j}), \tag{2.111}$$

where $\mathcal{H} \equiv \frac{a'}{a} = aH$, and the prime corresponds to the derivative with respect to the conformal time τ, introduced in equation (2.76).

- **Gauge-invariant scalar perturbations**

  From (2.109) we have

$$a^2(1+2\tilde{\phi}) = a^2(1+2\phi) - 2a^2\mathcal{H}T - 2a^2T', \tag{2.112}$$

  which gives us

$$\tilde{\phi} = \phi - \mathcal{H}T - T'. \tag{2.113}$$

  Considering only the scalar part of L_i, (2.110) gives us

$$a^2\tilde{B}_{,i} = a^2B_{,i} + a^2(L_{,i}' - T_{,i}), \tag{2.114}$$

  and, therefore,

$$\tilde{B} = B + L' - T. \tag{2.115}$$

  Finally, (2.111) gives for the scalar contributions,

$$-a^2(1-2\tilde{\psi})\delta_{ij} + 2a^2\tilde{E}_{,ij} = -a^2(1-2\psi)\delta_{ij} + 2a^2\mathcal{H}T\delta_{ij} + a^2(2E_{,ij} + L_{,ji} + L_{,ij}), \tag{2.116}$$

  implying that

$$\tilde{\psi} = \psi + \mathcal{H}T, \tag{2.117}$$

  and

$$\tilde{E} = E + L. \tag{2.118}$$

  It was cleverly introduced by Bardeen [14] the two gauge-invariant linear combinations

of (2.113), (2.115), (2.117) and (2.118):

$$\boxed{\Phi = \phi - \frac{1}{a}\left[a(B - E')\right]'}, \tag{2.119}$$

and

$$\boxed{\Psi = \psi - \mathcal{H}(B - E')}. \tag{2.120}$$

The above equations define the two Bardeen potentials Φ and Ψ.

In the case of the a scalar quantity (2.102),

$$\tilde{\delta q} = \delta q - \bar{q}'T, \tag{2.121}$$

and the gauge invariant combination is

$$\boxed{\Delta = \delta q + \bar{q}'(B - E')}. \tag{2.122}$$

- **Gauge-invariant vector perturbations**

  Considering only the vector contributions, (2.110) gives us

$$2a^2\tilde{S}_i = 2a^2 S_i + a^2\hat{L}_i', \tag{2.123}$$

and hence

$$\tilde{S}_i = S_i + \frac{\hat{L}_i'}{2}. \tag{2.124}$$

For the spatial part of the metric, (2.111) gives for the vector contributions,

$$a^2(\tilde{F}_{i,j} + \tilde{F}_{j,i}) = a^2(F_{i,j} + F_{j,i}) + a^2(L_{i,j} + L_{j,i}), \tag{2.125}$$

implying that

$$\tilde{F}_i = F_i + \hat{L}_i. \tag{2.126}$$

These two quantities lead us to the following gauge-invariant vector variable [14]

$$\boxed{\Psi_i = S_i - F_i'}. \tag{2.127}$$

- **Gauge-invariant tensor perturbations**

  From (2.111) is immediate to see that

$$\tilde{h}_{ij} = h_{ij}, \tag{2.128}$$

  implying that the tensor perturbations are already gauge-invariant.

2.2.4 Perturbing the matter

In the previous section we consider the metric perturbations. Now we turn our attention to perturbations in the hydrodynamical matter (radiation or dark matter)[5]. Let's consider the energy-momentum tensor

$$T^{\mu}_{\ \nu} = \bar{T}^{\mu}_{\ \nu} + \delta T^{\mu}_{\ \nu}, \tag{2.129}$$

where

$$T^{\mu}_{\ \nu} = (\rho + P)u^{\mu}u_{\nu} - P\delta^{\mu}_{\ \nu}, \tag{2.130}$$

$$\bar{T}^{\mu}_{\ \nu} = (\bar{\rho} + \bar{P})\bar{u}^{\mu}\bar{u}_{\nu} - \bar{P}\delta^{\mu}_{\ \nu}, \tag{2.131}$$

and

$$\delta T^{\mu}_{\ \nu} = (\delta\rho + \delta P)\bar{u}^{\mu}\bar{u}_{\nu} + (\bar{\rho} + \bar{P})(\delta u^{\mu}\bar{u}_{\nu} + \bar{u}^{\mu}\delta u_{\nu}) - \delta P\delta^{\mu}_{\ \nu}. \tag{2.132}$$

Above we are neglecting any source of anisotropic stress Π^{i}_{j} and hence $T^{i}_{j} = 0$ for every $i \neq j$[6].

Since $g_{\mu\nu} = \bar{g}_{\mu\nu} + \delta g_{\mu\nu}$ and $u_{\mu} = \bar{u}_{\mu} + \delta u_{\mu}$, the normalization condition for the full metric and the background

$$g_{\mu\nu}u^{\mu}u^{\nu} = \bar{g}_{\mu\nu}\bar{u}^{\mu}\bar{u}^{\nu} = 1 \tag{2.133}$$

gives us, after neglecting second and higher order terms of perturbations,

$$\bar{g}_{\mu\nu}\bar{u}^{\mu}\delta u^{\nu} + \bar{g}_{\mu\nu}\delta u^{\mu}\bar{u}^{\nu} + \delta g_{\mu\nu}\bar{u}^{\mu}\bar{u}^{\nu} = 0, \tag{2.134}$$

$$\Rightarrow 2\bar{u}_{\mu}\delta u^{\mu} + \delta g_{\mu\nu}\bar{u}^{\mu}\bar{u}^{\nu} = 0. \tag{2.135}$$

From the normalization condition for the background, we see that, for a comoving observer,

[5] We could also work with different types of matter, such as scalar fields. This is going to be the case treated in the following chapter.

[6] For computations including the anisotropic stress, see chapter 2 and beyond of [39] and Appendix D of [51].

$\bar{u}^\mu = a^{-1}(\tau)\delta^\mu_0$, and using $\delta g_{00} = 2a^2(\tau)\phi$, we arrive at the conclusion that

$$\delta u^0 = -\frac{\phi}{a(\tau)}. \tag{2.136}$$

Defining $\delta u^i = v^i/a(\tau)$, we obtain

$$u^\mu = \frac{1}{a(\tau)}\left(1-\phi, v^i\right), \tag{2.137}$$

$$\text{and } u_\mu = a(\tau)\left(1+\phi, -(v_i + B_i)\right). \tag{2.138}$$

Now that we know the perturbed velocity, we can work with the energy-momentum tensor. For the background we obtain

$$\begin{aligned} \bar{T}^0_{\ 0} &= \bar{\rho}, \\ \bar{T}^i_{\ 0} &= \bar{T}^0_{\ i} = 0, \\ \bar{T}^i_{\ j} &= -\bar{P}\delta^i_{\ j}, \end{aligned} \tag{2.139}$$

and plugging in the results of velocity we found above and expanding all the terms, is straightforward to see that

$$\begin{aligned} \delta T^0_0 &= \delta\rho, \\ \delta T^i_0 &= (\bar{\rho}+\bar{P})v^i, \\ \delta T^0_j &= -(\bar{\rho}+\bar{P})(v_j + B_j), \\ \delta T^i_j &= -\delta P \delta^i_j. \end{aligned} \tag{2.140}$$

Gauge-invariant variables

The same issue we faced in the metric perturbations associated with gauge freedom appears in our current analysis. We can write gauge-invariant quantities for the perturbations of the energy-momentum tensor. It transforms as

$$\tilde{T}^\alpha_{\ \beta}(\tilde{x}) = \frac{\partial \tilde{x}^\alpha}{\partial x^\mu}\frac{\partial x^\nu}{\partial \tilde{x}^\beta}\tilde{T}^\mu_{\ \nu}(x). \tag{2.141}$$

Performing the same approximations we did for the metric,

$$\bar{T}^\alpha_{\ \beta}(\tilde{x}) + \delta\tilde{T}^\alpha_{\ \beta}(\tilde{x}) \approx \bar{T}^\alpha_{\ \beta}(x) + \delta T^\alpha_{\ \beta}(x) - \bar{T}^\alpha_{\ \nu}\xi^\nu_{,\beta} - \bar{T}^\mu_{\ \beta}\xi^\alpha_{,\mu}, \tag{2.142}$$

we obtain, at linear order, the following expression for the gauge transformation (2.98):

$$\tilde{\delta T}^{\alpha}_{\ \beta} = \delta T^{\alpha}_{\ \beta} - \bar{T}^{\alpha}_{\ \beta,\rho}\xi^{\rho} - \bar{T}^{\alpha}_{\ \nu}\xi^{\nu}_{,\beta} - \bar{T}^{\mu}_{\ \beta}\xi^{\alpha}_{,\mu}. \tag{2.143}$$

Therefore, we have that the energy-momentum tensor perturbations changes under (2.98) as

$$\tilde{\delta T}^{0}_{\ 0} = \delta T^{0}_{\ 0} - \bar{\rho}' T - 2\bar{\rho} T', \tag{2.144}$$

$$\tilde{\delta T}^{i}_{\ 0} = \delta T^{i}_{\ 0} - (\bar{\rho} - \bar{P})(\partial^{i} L + \hat{L}^{i})', \tag{2.145}$$

$$\tilde{\delta T}^{0}_{\ i} = \delta T^{0}_{\ i} - (\bar{\rho} - \bar{P}) T_{,i}, \tag{2.146}$$

$$\tilde{\delta T}^{i}_{\ j} = \delta T^{i}_{\ j} + \bar{P}' T \delta^{i}_{\ j} + 2\bar{P}(\partial^{i} L + \hat{L}^{i})_{,j}. \tag{2.147}$$

- **Gauge-invariant scalar perturbations**

  Considering only the scalar part of the energy-momentum tensor, we have that

$$\tilde{\delta\rho} = \delta\rho - \bar{\rho}' T, \tag{2.148}$$

$$\tilde{\delta P} = \delta P - \bar{P}' T, \tag{2.149}$$

$$\tilde{v} = v - L', \tag{2.150}$$

  where we wrote $v^{i} = \partial^{i} v + \hat{v}^{i}$.

  Therefore, the gauge-invariant combinations are

$$\boxed{\Delta = \delta\rho + \bar{\rho}'(B - E')} \tag{2.151}$$

  and

$$\boxed{V = v + E'}. \tag{2.152}$$

- **Gauge-invariant vector perturbations**

  For the vector part we obtain

$$\tilde{\hat{v}}^{i} = \hat{v}^{i} - \hat{L}^{i\prime}, \tag{2.153}$$

  with

$$\boxed{\hat{V}^{i} = \hat{v}^{i} + \hat{B}^{i}} \tag{2.154}$$

being a gauge-invariant quantity.

- **Gauge-invariant tensor perturbations**

  Since we are not considering anisotropic stress, there are no tensor perturbations.

In a compact way, we can write the gauge-invariant variables for the energy-momentum tensor as [83, 84]

$$\delta T^{0\,(\mathrm{gi})}_{\quad 0} = \delta T^{0}_{\quad 0} - \bar{T}^{0\,\prime}_{\quad 0}(B - E'), \tag{2.155}$$

$$\delta T^{0(\mathrm{gi})}_{\quad i} = \delta T^{0}_{\quad i} - \left(\bar{T}^{0}_{\quad 0} - \frac{\bar{T}^{i}_{\quad i}}{3}\right)(B - E')_{,i}, \tag{2.156}$$

$$\delta T^{i\,(\mathrm{gi})}_{\quad j} = \delta T^{i}_{\quad j} - \bar{T}^{i\,\prime}_{\quad j}(B - E'), \tag{2.157}$$

where $\bar{T}^{i}_{\quad i}$ is the trace of the spatial components of $\bar{T}^{\mu}_{\quad \nu}$.

2.2.5 Perturbed Einstein's equations

Let's turn to the Einstein's equations (2.73) which is written as

$$\bar{G}^{\mu}_{\quad \nu} + \delta G^{\mu}_{\quad \nu} = 8\pi G(\bar{T}^{\mu}_{\quad \nu} + \delta T^{\mu}_{\quad \nu}). \tag{2.158}$$

To derive the perturbed quantities, we need to derive the perturbed Christoffel symbols $\Gamma^{\alpha}_{\quad \beta\gamma}$, the Riemann $R^{\alpha}_{\quad \beta\mu\nu}$ and Ricci $R_{\mu\nu}$ tensor and, finally, the Ricci scalar $R = R^{\mu}_{\quad \nu}$ to write the perturbed Einstein's tensor $\delta G^{\mu}_{\quad \nu}$. These quantities can be found in [51], [83] and [97], with the note that in the latter reference the metric signature is different from ours. For a more general treatment, [5] and [15] compute up to second order all of these quantities.

- **Scalar equations in the Newtonian gauge**

  The Einstein's equations in the conformal Newtonian gauge (i.e. $E = B = 0$) gives us

$$4\pi G a^2 \delta T^{0}_{\quad 0} = \nabla^2\Psi - 3\mathcal{H}(\Psi' + \mathcal{H}\Phi), \tag{2.159}$$

$$4\pi G a^2 \delta T^{0}_{\quad i} = (\Psi' + \mathcal{H}\Phi)_{,i}, \tag{2.160}$$

$$-4\pi G a^2 \delta T^{i}_{\quad j} = \left[\Psi'' + \mathcal{H}(2\Psi + \Phi)' + (2\mathcal{H}' + \mathcal{H}^2)\Phi + \frac{1}{2}\nabla^2(\Phi - \Psi)\right]\delta^{i}_{\quad j} + \\ - \frac{1}{2}\partial^i\partial_j(\Phi - \Psi), \tag{2.161}$$

where the perturbations of the energy momentum tensor are already the gauge-invariant quantities (2.155), (2.156) and (2.157).

- **Vector equations in the Newtonian gauge**

  For the vector contributions, we have

$$16\pi G a^2 \delta T^0_{\ i(V)} = \nabla^2 \hat{V}_i, \tag{2.162}$$

$$-16\pi G a^2 \delta T^i_{\ j(V)} = (\hat{V}_{i,j} + \hat{V}_{j,i})' + 2\mathcal{H}(\hat{V}_{i,j} + \hat{V}_{j,i}), \tag{2.163}$$

  where the subscript (V) refers to the vector part of the gauge-invariant energy-momentum tensor.

- **Tensor equations in the Newtonian gauge**

  The tensor equation, describing the gravitational waves, is

$$16\pi G a^2 \delta T^i_{\ j(T)} = h^{i\,\prime\prime}_{\ j} + 2\mathcal{H} h^{i\,\prime}_{\ j} - \nabla^2 h^i_{\ j}. \tag{2.164}$$

  Notice that the left-hand side of the above equation is non-zero in case where there is anisotropic stress.

2.2.6 Hydrodynamical perturbations

Here we will see how the scalar part of the hydrodynamical perturbations evolves in a matter and radiation dominated Universe in the context of general relativity. We stress the fact that we will not solve these perturbations for a multi-component (baryons and radiation) fluid, which gives us the description of the anisotropies observed in the CMB, since this is beyond the scope of this work. However, we address the interested reader to the books by Durrer [39], Giovannini [51] and Mukhanov [84], the three solving these equations in a very complete way.

Let's consider first equation (2.161). Since $\delta T^i_{\ j} = 0$ whenever $i \neq j$, we have that $\Phi = \Psi$. Therefore, Einstein's equations (2.159) and (2.161) become

$$4\pi G a^2 \delta\rho = \nabla^2\Phi - 3\mathcal{H}(\Phi' + \mathcal{H}\Phi), \tag{2.165}$$

$$\text{and } -4\pi G a^2 \delta P = \Phi'' + 3\mathcal{H}\Phi' + (2\mathcal{H}' + \mathcal{H}^2)\Phi. \tag{2.166}$$

Notice that equation (2.165) is the Poisson equation for the case of a static universe $(\mathcal{H} = 0)$.

This is why Φ (or Ψ, in the Newtonian gauge) is called the gravitational potential.

A conserved quantity

Equation (2.166) has a first integral, which leads us to defined the curvature perturbation

$$\zeta = \Phi + \frac{2}{3}\left[\frac{\Phi' + \mathcal{H}\Phi}{\mathcal{H}(1+w)}\right], \tag{2.167}$$

which is a gauge-invariant quantity possessing the property of being conserved, i.e. $\dot{\zeta} = 0$, for adiabatic perturbations at scales larger than the Hubble radius. This conservation law is equivalent to equation (2.166) under these two conditions.

Non-relativistic matter

For the case of an universe filled with non-relativistic matter ($\delta P = 0$), perturbations will obey

$$\Phi'' + 3\mathcal{H}\Phi' + (2\mathcal{H}' + \mathcal{H}^2)\Phi = 0 \tag{2.168}$$

and $a(\tau) \propto \tau^2 \Rightarrow \mathcal{H} = 2\tau^{-1}$, leading to

$$\Phi'' + \frac{6}{\tau}\Phi' = 0, \tag{2.169}$$

whose solution is

$$\Phi_{(\mathrm{MD})}(\mathbf{x}, \tau) = C_1(\mathbf{x}) + C_2(\mathbf{x})\tau^{-5}, \tag{2.170}$$

where (MD) stands for matter-dominated. From (2.165) and recalling that $4\pi G a^2 = 3\mathcal{H}^2/(2\bar{\rho})$, we arrive at an expression for the matter perturbations

$$\frac{\delta\rho}{\bar{\rho}} = \frac{1}{6}\left[(\nabla^2 C_1 \tau^2 - 12C_1) + \tau^{-5}(\nabla^2 C_2 \tau^2) + 18C_2\right], \tag{2.171}$$

or, in terms of the density contrast in Fourier space,

$$\delta_{k(\mathrm{MD})}(\tau) = -2C_1(\mathbf{k})\left[1 + \frac{(k\tau)^2}{12}\right] + \frac{3C_2(\mathbf{k})}{\tau^5}\left[1 - \frac{(k\tau)^2}{18}\right]. \tag{2.172}$$

Neglecting the decaying mode, we can see that during the matter-dominated era, the

gravitational potential is constant,

$$\Phi(\mathbf{x},\tau)=\Phi(\mathbf{x})=C_1(\mathbf{x})\rightarrow\Phi_k^0, \tag{2.173}$$

whereas the density contrast depends on the scales in a non-trivial way

$$\delta_{k(\mathrm{MD})}(\tau)=-2C_1(\mathbf{k})\left(1+\frac{k^2\tau^2}{12}\right). \tag{2.174}$$

Hence, for long-wavelength perturbations, i.e. $k\tau\ll 1\Rightarrow k\ll\mathcal{H}\Rightarrow\gg\mathcal{H}$, called super-horizon scales (sp),

$$\delta_{k(\mathrm{MD})}^{\mathrm{sp}}\approx-2\Phi_k(\tau_i) \tag{2.175}$$

whereas for short-wavelength perturbations, $k\tau\gg 1$, hence sub-horizon scales (sb) we recover the Newtonian result,

$$\delta_{k(\mathrm{MD})}^{\mathrm{sb}}(\tau)\approx-\Phi_k(\tau_i)\frac{k^2\tau^2}{6}\propto a(\tau). \tag{2.176}$$

In the above equations, $\Phi_k(\tau_i)$ is the initial gravitational potential at the instant when the Universe begins to be dominated by matter. To bring the reader close to the standard cosmology jargon, we say that perturbations which remain constant are "frozen", thus not evolving with time.

Relativistic matter

Considering adiabatic perturbations, (2.166) becomes

$$\Phi''+3(1+c_s^2)\mathcal{H}\Phi'-c_s^2\nabla^2\Phi+[2\mathcal{H}'+(1+3c_s^2)\mathcal{H}^2]\Phi=0. \tag{2.177}$$

In the radiation era, $p=\rho/3$, $c_s^2=1/3$, $a\propto\tau\Rightarrow\mathcal{H}\tau^{-1}$ and, thus,

$$\Phi''+\frac{4}{\tau}\Phi'+\frac{k^2}{3}\Phi=0. \tag{2.178}$$

Performing the change of variables $y=k\tau/\sqrt{3}$, which implies that

$$\frac{d\Phi}{d\tau}=\frac{k}{\sqrt{3}}\frac{d\Phi}{dy}, \tag{2.179}$$

we obtain

$$\frac{d^2\Phi}{dy^2} + \frac{4}{y}\frac{d\Phi}{dy} + \Phi = 0. \tag{2.180}$$

Once again, by changing to the variable $f = y^{3/2}\Phi$, after a few simplifications we arrive at the so familiar Bessel equation [87]

$$\frac{d^2 f}{dy^2} + \frac{1}{y}\frac{df}{dx} + \left[1 - \frac{(3/2)^2}{x^2}\right] f = 0, \tag{2.181}$$

whose solutions are

$$f(y) = C_1 J_{3/2}(y) + C_2 Y_{3/2}(y), \tag{2.182}$$

where, expanding over $y \ll 1$ leads to:

$$J_{3/2}(y) = \sqrt{\frac{2}{\pi y}}\left(\frac{\sin y}{y} - \cos y\right) \approx \frac{1}{3}\sqrt{\frac{2}{\pi}} y^{3/2} + \mathcal{O}\left(y^{5/2}\right) \tag{2.183}$$

$$\text{and } Y_{3/2}(y) = \sqrt{\frac{2}{\pi y}}\left(-\sin y - \frac{\cos y}{y}\right) \approx -\frac{\sqrt{\frac{2}{\pi}}}{y^{3/2}} - \frac{\sqrt{y}}{\sqrt{2\pi}} + \mathcal{O}\left(y^{5/2}\right). \tag{2.184}$$

Since $Y_{3/2}(y)$ diverges at the origin ($\tau \to 0$), we set $C_2 = 0$ and then, switching back to the gravitational potential Φ,

$$\Phi_k(\tau) = \frac{C_1}{y^2}\left(\frac{\sin y}{y} - \cos y\right), \tag{2.185}$$

and the density contrast is

$$\delta_k(\tau) = 2C_1\left[\left(\frac{2-y^2}{y^2}\right)\left(\frac{\sin y}{y} - \cos y\right) - \frac{\sin y}{y}\right]. \tag{2.186}$$

For long-wavelength perturbations ($y \ll 1$),

$$\Phi_k(y \ll 1) \to \Phi_k^0 = \frac{1}{3}C_1 \tag{2.187}$$

and

$$\delta_k(y \ll 1) \to -2C_1 = -6\Phi_k^0, \tag{2.188}$$

where we called $\Phi_k(y \ll 1) = \Phi_k^0$ to relate to the initial gravitational potential during inflation, determined in the next chapter.

For short-wavelength perturbations ($y \gg 1$),

$$\Phi_k(y \gg 1) \to -3\Phi_k^0 \frac{\cos y}{y^2} = -\frac{9\Phi_k^0}{(k\tau)^2} \cos\left(\frac{k\tau}{\sqrt{3}}\right) \tag{2.189}$$

and

$$\delta_k(y \gg 1) \to -6\Phi_k^0 \cos y. \tag{2.190}$$

In short, during the radiation dominated era the gravitational potential has the amplitude preserved for modes with long-wavelengths, for which $y \ll 1$, whereas for $y \gg 1$ they decay.

Radiation-matter transition

Recall the definition of the curvature perturbation (2.167). Assuming that the equation of sate $w_i = P_i/\rho_i$ is a constant at some initial (radiation) era and $w_f = P_f/\rho_f$ is another constant at some final time (matter era), we can write

$$\Phi_f = \left(\frac{1+w_f}{1+w_i}\right)\left(\frac{5+3w_i}{5+3w_f}\right)\Phi_i. \tag{2.191}$$

For $w_i = 1/3$ at the radiation dominated era and $w_f = 0$ for the matter dominated case, we arrive at

$$\Phi_{(\mathrm{MD})} = \frac{9}{10}\Phi_{(\mathrm{RD})}. \tag{2.192}$$

for super-horizon scales which enter the Hubble horizon after the matter-radiation equality.

The matter power-spectrum

One of the main observables in cosmology is the power-spectrum, the Fourier transform of the two-point correlation (see Appendix A). In the case of the cosmic microwave background, it measures the correlation of the temperature anisotropies. In the case of the matter field (which can be associated with galaxies), it measures the correlation of the density contrast or the gravitational potential:

$$P_\delta(k) = \frac{2\pi^2}{k^3}|\delta|^2. \tag{2.193}$$

We saw that it is easy to analyze the behaviour of perturbations when we consider the cases $k\tau > 1$ and $k\tau < 1$, and that during the radiation era matter perturbations behave differently compared with the matter era.

As we will see in the following chapter, the theory of inflation makes the comoving Hubble radius decrease with time, that is, $d(aH)^{-1}/dt < 0$. Consider now all modes that were inside the horizon when inflation begins: with the decrease of the Hubble radius, modes of a certain wavenumber k begin to cross the horizon and, by the end of inflation, they are super-Hubble modes (i.e. are outside the horizon); however, with the cease of inflation, the Hubble radius starts growing again and these modes start to cross the horizon for the second time, so that today some modes are sub-Hubble (i.e. are inside the horizon).

Thus, we can consider the modes which entered the horizon long after matter-radiation equality, $k\tau_{eq} \ll 1$, whose evolution is obtained during the matter era, and those modes which entered well before equality, $k\tau_{eq} \gg 1$, described in a radiation-dominated Universe.

As it was previously derived, the perturbations which entered the horizon well before equality were in a radiation dominated universe and hence the density perturbations are constant. Therefore, $P(k) \propto k^{-3}$ for scales which were small enough to become sub-Hubble at the time of matter-radiation equality, that is, with modes $k \gg k_{eq}$.

On the other hand, perturbations which entered the horizon for $\tau > \tau_{\rm eq}$ were in a matter-dominated Universe, and thus the perturbations have grown with k^2 (2.176). Hence, at this regime, $P(k) \propto k$ for scales with modes $k \ll k_{eq}$.

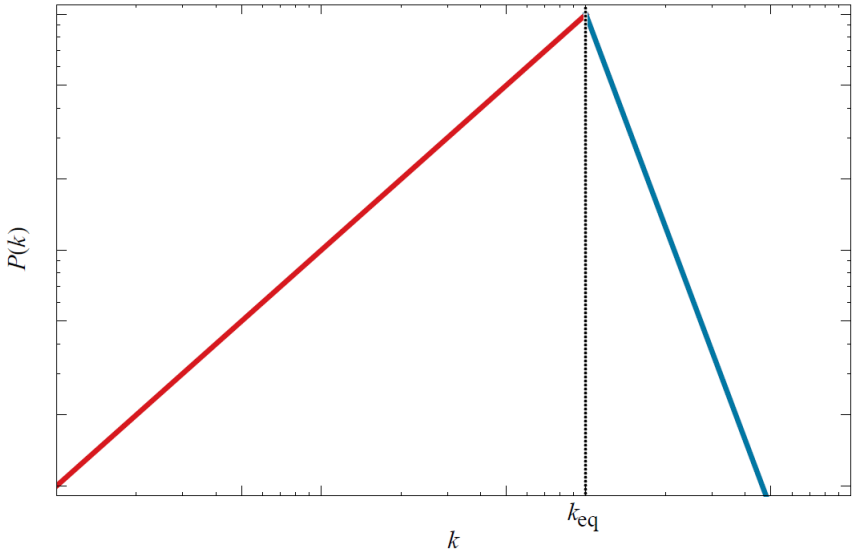

Figure 2.6: Schematic plot showing the estimated behaviour of the matter power-spectrum. In Figure A.2 we show the full power-spectrum, including all constants and features our calculations have not taken into account, and data from different types of cosmological probes.

Chapter 3

Inflationary Perturbations: an Origin for Structure

The standard theory of the Big Bang, which says that the Universe was in a very hot and dense state in the far past, leads to predictions that, nowadays, have been tested by means of different types of probes. One of these predictions, later observed by Penzias and Wilson [95], in 1964, was the Cosmic Microwave Background (CMB). Another one is the remarkable prediction of the primordial abundances of the light elements, also called primordial nucleosynthesis [8]. On very large-scales, such as those encompassed by the CMB, the Big Bang model describes the Universe very well. However, taking a closer look to this theory one is confronted by many issues. In this chapter we present inflation through its historical development up to its current status, following mainly the approach of [16, 83, 84].

3.1 Overview on inflation

One of the fundamental cornerstones of modern Cosmology is the inflationary paradigm, which provides a simple and attractive solution for some naturalness problems that emerge in the standard Hot Big Bang scenario, which is a phase of exponential expansion that generates a spatially flat and homogeneous observable Universe [39, 72, 73, 84, 97, 121]. However, the most striking feature of inflation is its capability of providing a natural explanation for the seeds

that eventually gave rise to the structures[1] we observe today.

3.1.1 Why the Universe needs to inflate?

In the standard Hot Big Bang (HBB) model[2], the initial universe is taken to be homogeneous and isotropic. These two hypothesis, known as the Cosmological Principle, lead to the Friedmann equations

$$H^2 = \frac{8\pi G}{3}\rho - \frac{K}{a^2} + \frac{\Lambda}{3}, \tag{3.1}$$

already encountered in the previous chapter, which in terms of the conformal time τ is

$$\mathcal{H}^2 = \frac{8\pi G}{3}\rho a^2 - K + \frac{\Lambda}{3}a^2, \tag{3.2}$$

where we are including the cosmological constant for completeness. Defining the density parameter $\Omega = \rho/\rho_c$, where $\rho_c = 3H^2/8\pi G$ is the critical density for which the Universe is spatially flat, we can write

$$\frac{|K|}{a^2H^2} = |\Omega_{\rm tot} - 1|, \tag{3.3}$$

where $\Omega_{\rm tot} \equiv \Omega + \Omega_\Lambda = \Omega + \Lambda/3H^2$ [72, 73, 97].

If the Universe is flat, $K = 0$, then $\Omega(t) = 1$ for all time. However, if there is some curvature in the Universe, then for the common cases of an universe dominated by matter or radiation, the density parameter increasingly deviates from one as time goes by (see Figure 3.1). Since current data strongly suggests a nearly flat Universe [99], we reach the conclusion that in the far past the spatial curvature would need to be even more irrelevant than it is today. This poses an issue if we want to avoid fine-tuning of the initial conditions of the Universe.

The second difficulty one has to face when accepting the standard HBB model concerns the CMB, the first glimpse of the Universe we can observe once the photons decouple from the matter around 380000 years after the Big Bang.

[1] The cosmic microwave background and the large-scale structure of the Universe are a manifestation of primordial inhomogeneities that evolved into temperature and density perturbations.

[2] The standard HBB model states that, at very early times, the Universe is filled with a gas of massless particles in thermal equilibrium. In addition, there is an initial singularity for $t \to 0$ which leads to an infinite temperature.

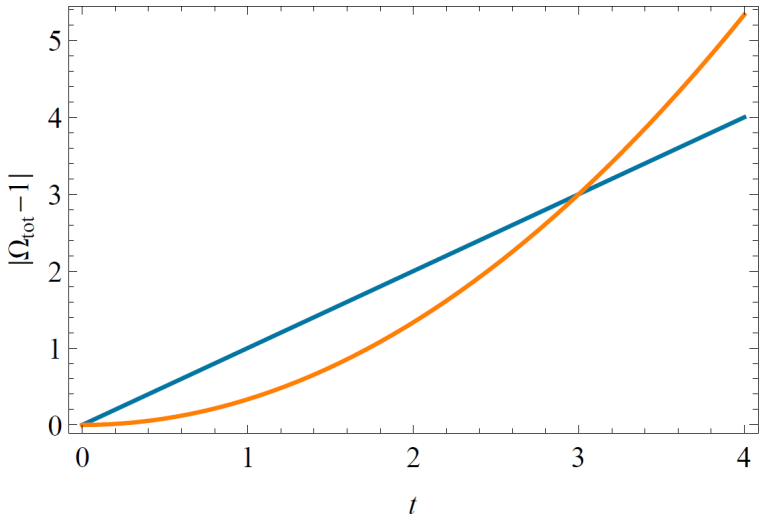

Figure 3.1: Departures from $|\Omega_{\rm tot}| = 1$ in the case of a radiation dominated universe (blue) and of a matter dominated (orange). From this figure we see that for these two cases, deviations from the critical value always increase with time. Therefore, we are led to the conclusion that if the current data supports $k \approx 0$, within the errors, then the Universe had to be much more flat in the past. We do not account for the case of a Λ dominated universe since it recently started to dominate the energy density, thus its effect does not account for the current observational constraint on the curvature of the Universe.

Since light propagates along null geodesics, for a flat homogeneous and isotropic Universe this property leads to

$$dx = \pm\frac{1}{a(t)}dt \Rightarrow \Delta x = \pm\int_{t_i}^{t_f}\frac{dt}{a(t)}. \tag{3.4}$$

We can use the relation

$$dt = \left(\frac{da}{dt}\right)^{-1}da = \frac{a}{\dot{a}}\frac{da}{a^2} = \frac{1}{aH}\frac{da}{a} = \frac{d\ln a}{aH} \tag{3.5}$$

to write (3.4) as

$$\Delta x = \pm\int_{a_i}^{a_f}\left(\frac{da}{dt}\right)^{-1}\frac{da}{a(t)} = \pm\int_{a_i}^{a_f}\frac{1}{aH}\frac{da}{a}. \tag{3.6}$$

In the case of a single-component Universe dominated by some fluid with equation of state $w = P/\rho$, we have that $1/aH = a^{(1+3w)/2}/H_0$ and, since all ordinary types of matter satisfy $w > -1/3$, the comoving particle horizon becomes

$$\Delta x = \frac{2H_0^{-1}}{1+3w}\left(a_f^{(1+3w)/2} - a_i^{(1+3w)/2}\right). \tag{3.7}$$

Assuming the HBB model, i.e. initial singularity at $t_i = 0 \Rightarrow a_i = 0$ and a radiation

dominated early Universe, $w = 1/3$, we get

$$\Delta x = \pm(aH)^{-1}, \tag{3.8}$$

that is, photons propagate a finite distance Δx, called particle horizon, between the Big Bang and some time t. This means that the light cone is limited as we look to the past, as shown in Figure 3.2.

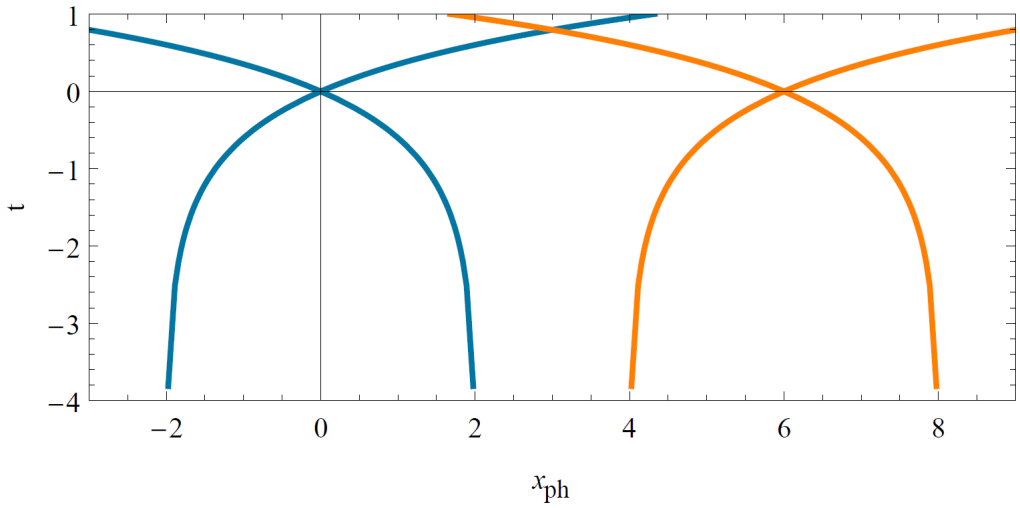

Figure 3.2: Particle horizon for a radiation dominated Universe with arbitrary unities. Clearly, for events with the origin apart on more than a certain distance, causal contact in the past was never possible. This distance is known as the particle horizon. In standard cosmology, $a(t) \propto t^p$ with $p < 1$ ($p = 1/2$ for relativistic species and $p = 2/3$ for non-relativistic matter) and then the particle horizon has a finite size.

The core of the problem relies in the fact that the CMB radiation is, to a very good approximation, isotropic, with differences between the "cold" and "hot" spots of order 10^{-5}. Since the past light cone is limited, it seems very odd that distant patches of the sky, emitting causally disconnected CMB photons, would have approximately the same temperature. Unless we are satisfied with such "cosmic coincidence", or ready to relinquish causality at the early Universe, something must address and solve this second issue.

Besides these two main problems, the suppression of relics such as monopoles, topological defects and the gravitino are also problematic to standard cosmologies. These subjects are deeply studied in [51], [75], [97] and references therein.

3.1.2 The standard solution

As a way to solve these issues Guth proposed a phase of accelerated expansion for the primordial Universe [53]. In terms of the horizon problem, we can see that a period of accelerated expansion, $\ddot{a} > 0$, implies in a shrinking particle horizon:

$$\frac{d}{dt}(aH)^{-1} = -\frac{\ddot{a}}{\dot{a}^2} \tag{3.9}$$

Moreover, looking at equation (3.3), we can see that condition (3.9) makes the difference $|\Omega_{\rm tot} - 1|$ smaller with time. Hence, this period of inflation drags $\Omega_{\rm tot}$ towards one. Besides, since the comoving Hubble radius is getting smaller, everything is well inside the particle horizon at very early times, as shown in Figure 3.3.

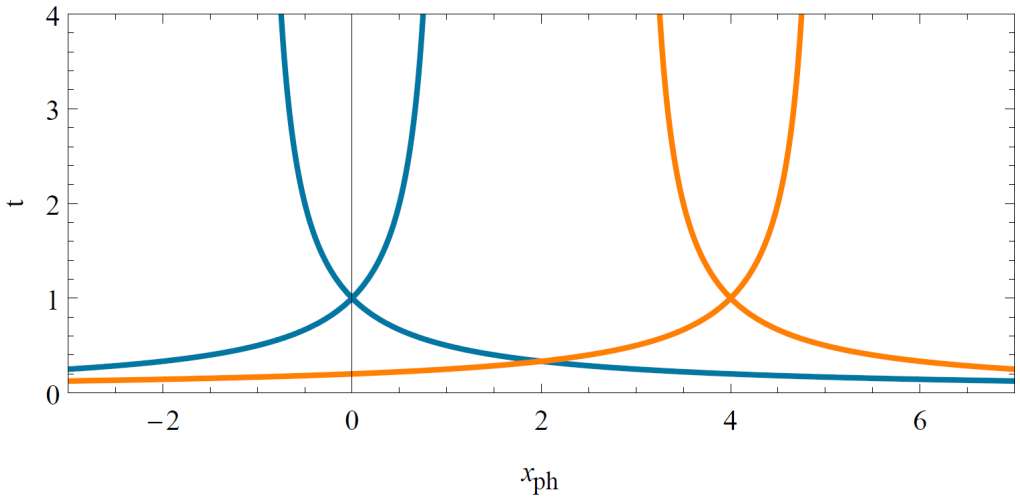

Figure 3.3: Particle horizon for an Universe with scale factor $a(t) \propto t^2$ in arbitrary unities. Clearly, a shrinking Hubble horizon puts every region in the Universe into causal contact in the very far past, thus solving the issue encountered in Figure 3.2.

Now one might ask: how to attain this accelerated expansion? If we take a look at the acceleration equation [3]

$$\frac{\ddot{a}}{a} = -\frac{8\pi G}{6}(\rho + 3P) + \frac{\Lambda}{3}, \tag{3.10}$$

is immediate that in order to get $\ddot{a} > 0$ one must have

$$\rho + 3P < 0, \tag{3.11}$$

[3] This is another Einstein equation emerging from a FLRW metric. See, for instance, [97].

or a Λ dominated universe. Assuming that the density is always positive, then during the inflationary era the Universe had to be dominated by a matter with a negative pressure equation of state (recall that for the Λ-dominated case, $P_\Lambda = -\rho_\Lambda$).

However, inflation needs to end, so it is natural to ask for how long does the inflationary era had to go on in order to solve the problems mentioned above. To quantify the duration of that phase, it is common to define the number of e-folds

$$dN = d\ln a \tag{3.12}$$

To solve the horizon problem, for example, it is reasonable to assume that the observable Universe today, given by the comoving Hubble radius $(a_0 H_0)^{-1}$ and with temperature $T_0 \approx 2.7$ K $= 10^{-4}$ eV, was smaller than the Hubble radius at the beginning of inflation $(a_i H_i)^{-1}$. Assuming that inflation ends at the Grand Unification energy scale, $T_f \sim 10^{16}$ GeV [97], and that the Universe is radiation dominated at this epoch ($\Rightarrow H \sim a^2$), then

$$\frac{(a_f H_f)^{-1}}{(a_0 H_0)^{-1}} \sim \frac{a_f}{a_0} \propto \frac{T_0}{T_f} = 10^{-29} \tag{3.13}$$

which implies that

$$(a_0 H_0)^{-1} \approx 10^{29}(a_f H_f)^{-1} < (a_i H_i)^{-1} \Rightarrow \frac{a_f}{a_i} > 10^{29} \tag{3.14}$$

and, making the assumption that $H_f \approx H_i$, which will become clear later,

$$\therefore N = \ln\left(\frac{a_f}{a_i}\right) \approx 67 \tag{3.15}$$

If the energy scale of inflation is smaller than the one assumed above, than N is smaller.

3.1.3 How to inflate the Universe

The easiest way to fill the Universe with a matter satisfying (3.11) is by considering a real scalar field[4] φ.

[4]There are inflationary models that consider complex scalar [105], vector [48, 66, 76] and tensor fields [63] as well. However, we will limit ourselves to the analysis of a real scalar field not only due to its simplicity, but because the scalar sector in particle physics is a very promising one [92].

The Lagrangian density for φ is given by

$$\mathcal{L} = \frac{1}{2} g^{\mu\nu} \partial_\mu \varphi \partial_\nu \varphi - V(\varphi), \tag{3.16}$$

and, from Noether's theorem, we derive an expression for the energy-momentum tensor

$$T^\mu_{\ \nu} = \frac{\partial \mathcal{L}}{\partial(\partial_\mu \varphi)} \partial_\nu \varphi - \delta^\mu_{\ \nu} \mathcal{L}. \tag{3.17}$$

With the metric in conformal time, we obtain

$$T^0_{\ 0} = \frac{1}{2a^2} \varphi'^2 + V(\varphi) \equiv \rho \tag{3.18}$$

and

$$T^i_{\ j} = \left[-\frac{1}{2a^2} \varphi'^2 + V(\varphi) \right] \delta^i_{\ j} \equiv -P \delta^i_{\ j}. \tag{3.19}$$

Therefore, a scalar field driven inflation is possible if $V(\varphi) > \dot{\varphi}^2$.

3.1.4 Inflationary dynamics

Now that we know why there must be a phase of inflation in the early Universe and how to achieve it, let's work on some dynamical consequences of having a FLRW universe filled with a single scalar field.

In a FLRW Universe, the Friedmann and Euler-Lagrange equations obtained from (3.16), the latter giving the equations of motion for the scalar field (also known as Klein-Gordon equation[5]) are, respectively,

Physical time

$$H^2 = \frac{8\pi G}{3} \left[\frac{1}{2} \dot{\varphi}^2 + V(\varphi) \right] - \frac{K}{a^2}; \tag{3.20}$$

$$\frac{\ddot{a}}{a} = \frac{8\pi G}{3} (V(\varphi) - \dot{\varphi}^2); \tag{3.21}$$

$$\ddot{\varphi} + 3H\dot{\varphi} + \frac{dV}{d\varphi} = 0. \tag{3.22}$$

[5]One could also obtain the Klein-Gordon equation by considering the continuity equation together with the first Friedmann equation.

Conformal time

$$\mathcal{H}^2 = \frac{8\pi G}{3}\left[\frac{1}{2}\varphi'^2 + V(\varphi)a^2\right] - K; \tag{3.23}$$

$$\mathcal{H}' = \frac{a''}{a} - \mathcal{H}^2 = -\frac{8\pi G}{3}(\varphi'^2 - V(\varphi)a^2); \tag{3.24}$$

$$\varphi'' + 2\mathcal{H}\varphi' + a^2\frac{dV}{d\varphi} = 0. \tag{3.25}$$

Taking the time derivative of the first Friedmann equation (3.20) and subtracting the product of $\dot{\varphi}$ with the Klein-Gordon equation, we get:

$$\dot{H} = -\frac{8\pi G}{2}\dot{\varphi}^2 + \frac{K}{a^3 H}. \tag{3.26}$$

From these equations we can see that it is possible to neglect the curvature, even if we are not working in a flat spacetime, since the fast growth of a during inflation makes the curvature term negligible. This is going to be the case from now on.

Slow-roll parameters

The inflationary condition (3.9) can be rewritten as

$$\frac{d}{dt}(aH)^{-1} = -\frac{\dot{a}H}{(aH)^2} - \frac{a\dot{H}}{(aH)^2} = -\frac{1}{a} + \frac{1}{a}\frac{\dot{H}}{H^2} = -\frac{1}{a}(1-\epsilon), \tag{3.27}$$

where we introduced the parameter

$$\epsilon \equiv -\frac{\dot{H}}{H^2} < 1. \tag{3.28}$$

In conformal time, it reads

$$\epsilon = 1 - \frac{\mathcal{H}'}{\mathcal{H}^2}. \tag{3.29}$$

In order to solve the problems of the standard HBB model, inflation must have happened for about 60 e-folds. Therefore, it is necessary to require that ϵ remains small for a sufficient number of e-folds. Therefore, we can introduce

$$\eta = \frac{d\ln\epsilon}{dN} = \frac{\dot{\epsilon}}{H\epsilon}, \tag{3.30}$$

which leads to the conclusion that if $|\eta| < 1$ then inflation happens for long enough so that the

issues discussed above are solved. In conformal time,

$$\eta = \frac{\epsilon'}{\mathcal{H}\epsilon}. \tag{3.31}$$

Besides, we can define the scalar field acceleration per Hubble time

$$\delta \equiv -\frac{\ddot{\varphi}}{H\dot{\varphi}}. \tag{3.32}$$

3.1.5 Slow-roll inflation

From (3.26), the condition (3.28) that must be satisfied during inflation reduces to

$$\epsilon = 8\pi G\frac{\dot{\varphi}^2}{2H^2} < 1, \tag{3.33}$$

which implies that the kinetic term $\frac{\dot{\varphi}^2}{2}$ makes a small contribution to ρ [16]. We could even extrapolate and say that $\epsilon \ll 1$. This situation is known as slow-roll inflation. The condition above also implies, for the Friedmann equation, that

$$H^2 \approx \frac{8\pi G}{3}V(\varphi) \tag{3.34}$$

and, for the Klein-Gordon equation,

$$3H\dot{\varphi} \approx -V_{,\varphi}. \tag{3.35}$$

In these approximations, we are able to rewrite ϵ as

$$\epsilon_V \equiv 4\pi G\left(\frac{V_{,\varphi}}{V}\right)^2 \ll 1 \tag{3.36}$$

and

$$|\eta_V| \equiv 8\pi G\frac{|V_{,\varphi\varphi}|}{V} \ll 1. \tag{3.37}$$

Therefore, slow-roll inflation has the property that it is completely determined by the shape of the inflaton potential.

There are two mostly common types of slow-roll inflation, namely, the large and small field inflation. They differ from each other due to the shape of the potential (Figures 3.4 and

3.5). The idea of the slow-roll inflation is that the inflaton field slowly rolls down the potential $V(\varphi)$; whence its name.

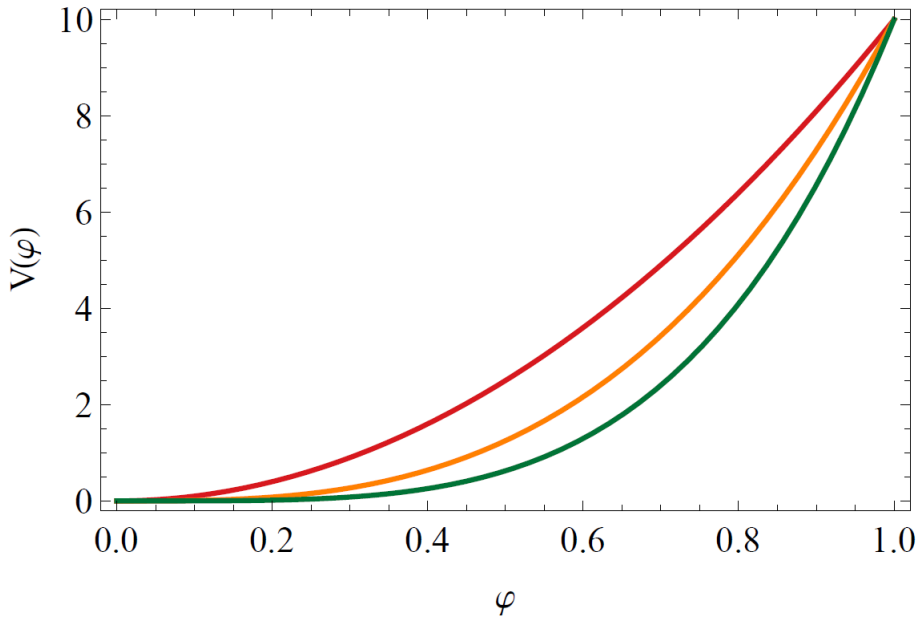

Figure 3.4: Large field inflation with potential $V(\varphi) \propto \varphi^p$. In the figure, $p = 2$ (red), $p = 3$ (orange) and $p = 4$ (green). Units are arbitrary once the image is just for illustrative purposes.

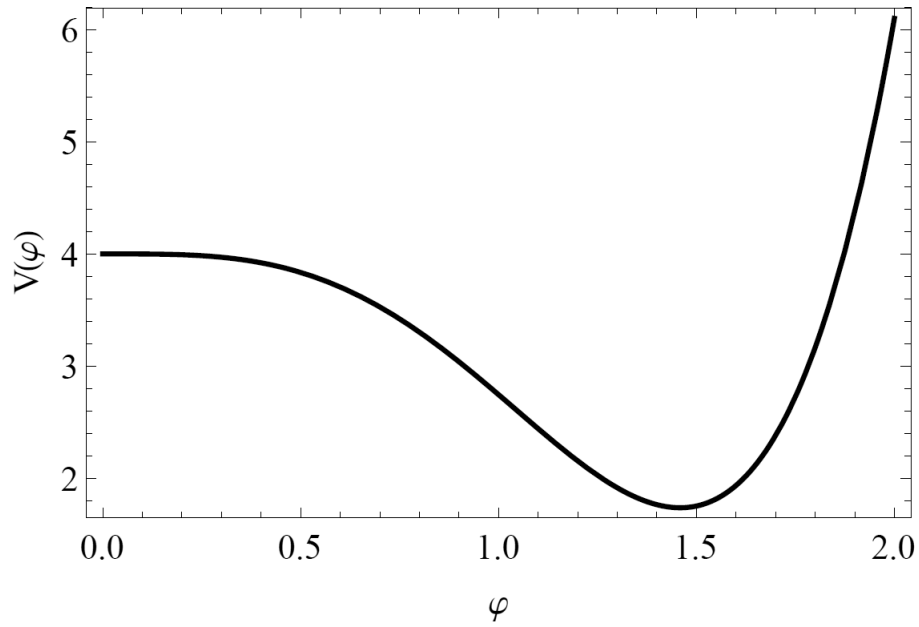

Figure 3.5: Small field inflation with a Coleman-Weinberg type of potential [39]. The units and parameters in the potential are arbitrary. The image is just for illustrative purposes.

3.1.6 Alternatives to inflation

Inflation provides a graceful solution to the problems of the standard Hot Big Bang model and current measurements of the CMB sets constraints on inflationary models. However,

many alternatives to inflation have been proposed throughout the years, although many have been discarded.

An example is the ekpyrotic/cyclic scenario, which offers an alternative to the HBB issues and accounts for the origin of the structure we see in the Universe. Until recently, it was thought that primordial gravitational waves were an exclusive feature of inflationary models, being, therefore, a smoking gun able to distinguish between inflation and cyclic Universe scenarios such as ekpyrosis. A recent work showed that it is possible to produce primordial gravitational waves, induced by magnetic fields, in an ekpyrotic universe [57]. Other ways to differentiate between these two competing models include the imprints they leave on the CMB and LSS, both in the power-spectrum and in the three-point correlation function of the perturbations. This will be discussed in the next chapter.

3.2 Perturbing the inflaton field

Besides solving the many problems of the HBB model, inflation provides a natural way to furnish the seeds for the formation of the structures we see today, through the quantum nature of the scalar field used in the model. In this section we show this accomplishment by studying how an epoch of inflation connects itself to the formation of large-scale structure in the Universe. Therefore, we turn to the study of perturbations in an universe filled with a scalar field and, in the next section, we quantize these perturbations. As we have done in the previous chapter, we will have to obtain the energy-momentum tensor and then apply it to the perturbations in a gauge-invariant treatment.

Consider the full energy-momentum tensor as

$$T^{\mu}_{\ \nu} = \bar{T}^{\mu}_{\ \nu} + \delta T^{\mu}_{\ \nu}, \tag{3.38}$$

and the inflaton field φ,

$$\varphi(\mathbf{x}, t) = \bar{\varphi}(t) + \delta\varphi(\mathbf{x}, t), \tag{3.39}$$

where $\delta\varphi(\mathbf{x}, t) \ll \bar{\varphi}(t)$.

We already derived the expressions, (2.155)-(2.157), for the gauge transformations of the energy-momentum tensor. From them we see that, choosing the Newtonian gauge ($B = E = 0$), $\delta\tilde{T}^{\mu}_{\ \nu} = \delta T^{\mu}_{\ \nu}$.

For the scalar field,

$$\delta\tilde{\varphi} = \delta\varphi - \bar{\varphi}'T, \tag{3.40}$$

Thus, there are two gauge invariant variables for the scalar field, namely

$$\delta\varphi^{(\mathrm{gi})} = \delta\varphi + \bar{\varphi}'(B - E') \tag{3.41}$$

and

$$v = a\left[\delta\varphi + \frac{\bar{\varphi}'}{\mathcal{H}}\psi\right]. \tag{3.42}$$

The latter can be related to the former through the relation

$$v = a\left[\delta\varphi^{(\mathrm{gi})} + \frac{\bar{\varphi}'}{\mathcal{H}}\Psi\right], \tag{3.43}$$

where Ψ is one of the Bardeen variables. Above, v is called the Mukhanov-Sasaki potential.

Hence, in the Newtonian gauge ($B = E = 0$), $\delta\tilde{\varphi} = \delta\varphi$ is identical to the corresponding gauge invariant quantity.

3.2.1 Scalar perturbations

Recalling the scalar part of our full perturbed metric in a flat spacetime, in the Newtonian gauge,

$$ds^2 = a^2(\tau)[(1 + 2\Phi)d\tau^2 - (1 - 2\Psi)\delta_{ij}dx^i dx^j], \tag{3.44}$$

we obtain the background energy-momentum tensor at zeroth order in the perturbations:

$$\bar{T}^0_{\ 0} = \frac{1}{2a^2}\bar{\varphi}'^2 + V(\bar{\varphi}), \tag{3.45}$$

$$\bar{T}^0_{\ i} = 0, \tag{3.46}$$

$$\bar{T}^i_{\ j} = -\left[\frac{1}{2a^2}\bar{\varphi}'^2 + V(\bar{\varphi})\right]\delta^i_{\ j}, \tag{3.47}$$

already found in section 3.1.3.

At first order in the perturbations,

$$\delta T^0_{\ 0} = \frac{1}{a^2}(-\bar{\varphi}'^2\Phi + \bar{\varphi}'\delta\varphi' + V_{,\varphi}a^2\delta\varphi), \tag{3.48}$$

$$\delta T^0_{\ i} = \frac{1}{a^2}\bar{\varphi}'\delta\varphi_{,i}, \tag{3.49}$$

$$\delta T^i_{\ j} = \frac{1}{a^2}(\bar{\varphi}'^2\Phi - \bar{\varphi}'\delta\varphi' + V_{,\varphi}a^2\delta\varphi)\delta^i_{\ j}, \tag{3.50}$$

are already gauge-invariant. Above, we used Einstein's equation (2.161), for $i \neq j$, to write $\Psi = \Phi$.

Writing (3.26) in conformal time,

$$\mathcal{H}^2 - \mathcal{H}' = \frac{8\pi G}{2}\bar{\varphi}'^2, \tag{3.51}$$

we can work out the gauge-invariant equations for the perturbations driven by a scalar field. First, the perturbed inflaton field (3.39) obeys the Klein-Gordon equation. For the background, $\bar{\varphi}$ is given by (3.25). When it comes to considering the perturbations, we can use the Klein-Gordon equation in curved spacetimes

$$\frac{1}{\sqrt{-g}}\frac{\partial}{\partial x^\alpha}\left(\sqrt{-g}g^{\alpha\beta}\frac{\partial\varphi}{\partial x^\beta}\right) + V_{,\varphi} = 0, \tag{3.52}$$

with the perturbed metric in the Newtonian gauge to get, at first order,

$$\delta\varphi'' + 2\mathcal{H}\delta\varphi' - \nabla^2\delta\varphi + V_{,\varphi\varphi}a^2\delta\varphi - 4\bar{\varphi}'\Phi' + 2V_{,\varphi}a^2\Phi = 0. \tag{3.53}$$

We derive now the three key equations for perturbations during inflation:

- Substituting (3.48) into (2.159),

$$\begin{aligned}\nabla^2\Phi - 3\mathcal{H}\Phi' - 3\mathcal{H}^2\Phi &= 4\pi G\left(-\bar{\varphi}'^2\Phi + \bar{\varphi}'\delta\varphi' + V_{,\varphi}a^2\delta\varphi\right)\\ &= -(\mathcal{H}^2 - \mathcal{H}')\Phi + 4\pi G\left(\bar{\varphi}'\delta\varphi' + V_{,\varphi}a^2\delta\varphi\right).\end{aligned}$$

Therefore, the Poisson equation becomes:

$$\nabla^2\Phi - 3\mathcal{H}\Phi' - (\mathcal{H}' + 2\mathcal{H}^2)\Phi = 4\pi G\left(\bar{\varphi}'\delta\varphi' + V_{,\varphi}a^2\delta\varphi\right). \tag{3.54}$$

- Substituting (3.49) into (2.160),

$$(\Phi' + \mathcal{H}\Phi)_{,i} = 4\pi G\bar{\varphi}'\delta_{,i}$$

and then

$$\Phi' + \mathcal{H}\Phi = 4\pi G\bar{\varphi}'\delta\varphi. \tag{3.55}$$

- Substituting (3.50) into (2.161),

$$\begin{aligned}\left[\Phi'' + 3\mathcal{H}\Phi' + (2\mathcal{H}' + \mathcal{H}^2)\Phi\right]\delta^i{}_j &= -4\pi G\left(\bar{\varphi}'^2\Phi - \bar{\varphi}'\delta\varphi' + V_{,\varphi}a^2\delta\varphi\right)\delta^i{}_j,\\ \Rightarrow \Phi'' + 3\mathcal{H}\Phi' + (2\mathcal{H}' + \mathcal{H}^2)\Phi &= -(\mathcal{H}^2 - \mathcal{H}') - 4\pi G\left(-\bar{\varphi}'\delta\varphi' + V_{,\varphi}a^2\delta\varphi\right),\end{aligned}$$

we arrive at our third equation

$$\Phi'' + 3\mathcal{H}\Phi' + (\mathcal{H}' + 2\mathcal{H}^2)\Phi = -4\pi G\left(-\bar{\varphi}'\delta\varphi' + V_{,\varphi}a^2\delta\varphi\right). \tag{3.56}$$

Let's solve the perturbation equations. By subtracting (3.54) from (3.56),

$$\Phi'' + 6\mathcal{H}\Phi' + 2(\mathcal{H} + 2\mathcal{H}^2)\Phi - \nabla^2\Phi + 8\pi G V_{,\varphi}a^2\delta\varphi = 0, \tag{3.57}$$

and writting $\delta\varphi$ in terms of Φ, from the second equation (3.55),

$$\delta\varphi = \frac{\Phi' + \mathcal{H}\Phi}{4\pi G\bar{\varphi}}, \tag{3.58}$$

we have

$$\Phi'' + 6\mathcal{H}\Phi' + 2(\mathcal{H} + 2\mathcal{H}^2)\Phi - \nabla^2\Phi + 2V_{,\varphi}a^2\frac{\Phi' + \mathcal{H}\Phi}{\bar{\varphi}} = 0. \tag{3.59}$$

Substituting the Klein-Gordon equation (3.25),

$$V_{,\varphi}a^2 = -\bar{\varphi}'' - 2\mathcal{H}\bar{\varphi}' \tag{3.60}$$

into (3.59), we arrive at the master equation for the perturbations:

$$\boxed{\Phi'' + 2\left(\mathcal{H} - \frac{\bar{\varphi}''}{\bar{\varphi}}\right)\Phi' + 2\left(\mathcal{H}' - \mathcal{H}\frac{\bar{\varphi}''}{\bar{\varphi}'}\right)\Phi - \nabla^2\Phi = 0}. \tag{3.61}$$

Note that this is an exact equation: no approximations have been done (with the exception of linearization).

In order to follow the approach of [83], we will rewrite (3.61). First,

$$\mathcal{H} - \frac{\bar{\varphi}''}{\bar{\varphi}'} = \frac{a'}{a} - \frac{\bar{\varphi}''}{\bar{\varphi}'} = \frac{\bar{\varphi}}{a}\left(\frac{a}{\bar{\varphi}'}\right)' \tag{3.62}$$

and noticing that

$$\left(\frac{\mathcal{H}}{\bar{\varphi}'}\right)' = \frac{\mathcal{H}'}{\bar{\varphi}'} - \frac{\mathcal{H}}{\bar{\varphi}'^2}\bar{\varphi}'' \to \mathcal{H}' - \mathcal{H}\frac{\bar{\varphi}''}{\bar{\varphi}'}, \tag{3.63}$$

we have

$$\boxed{\Phi'' + 2\left(\frac{a}{\bar{\varphi}'}\right)'\frac{\bar{\varphi}'}{a}\Phi' + 2\left(\frac{\mathcal{H}}{\bar{\varphi}'}\right)'\bar{\varphi}'\Phi - \nabla^2\Phi = 0}. \tag{3.64}$$

With this equation we can introduce the new variable $u = \frac{a\Phi}{\bar{\varphi}'}$ to write

$$\Phi = \left(\frac{\bar{\varphi}'}{a}\right)u, \tag{3.65}$$

$$\Phi' = \left(\frac{\bar{\varphi}'}{a}\right)'u + \left(\frac{\bar{\varphi}'}{a}\right)u', \tag{3.66}$$

$$\Phi'' = \left(\frac{\bar{\varphi}'}{a}\right)''u + 2\left(\frac{\bar{\varphi}'}{a}\right)'u' + \left(\frac{\bar{\varphi}'}{a}\right)u'', \tag{3.67}$$

and, in terms of $\theta = \frac{\mathcal{H}}{a\bar{\varphi}'}$,

$$\theta' = \frac{\mathcal{H}'}{a\bar{\varphi}'} + \mathcal{H}\left(\frac{1}{a\bar{\varphi}'}\right)', \tag{3.68}$$

$$\theta'' = \frac{\mathcal{H}''}{a\bar{\varphi}'} + 2\left(\frac{1}{a\bar{\varphi}'}\right)'\mathcal{H}' + \mathcal{H}\left(\frac{1}{a\bar{\varphi}'}\right)'', \tag{3.69}$$

we finally get, in Fourier space,

$$\boxed{u'' + \left(k^2 - \frac{\theta''}{\theta}\right)u = 0}. \tag{3.70}$$

Sub-horizon limit

Since $\theta''/\theta \sim \mathcal{H}^2$, when $\lambda_{\text{phy}} \ll H^{-1} \Rightarrow k \gg aH = \mathcal{H}$, then $k^2 \gg \theta''/\theta$ and we can neglect the last term in (3.70). Thus, in the sub-horizon limit,

$$u'' + k^2 u = 0, \tag{3.71}$$

whose solutions are

$$u(\tau) \propto e^{\pm ik\tau}. \tag{3.72}$$

Coming back to the original potential Φ, we get

$$\Phi(\tau) \sim C_1(k)\frac{\bar{\varphi}'}{a}\cos(k\tau) + C_2(k)\frac{\bar{\varphi}'}{a}\sin(k\tau), \tag{3.73}$$

or, in physical time,

$$\Phi(t) \sim C_1(k)\dot{\bar{\varphi}}\cos\left(k\int a^{-1}dt\right) + C_2(k)\dot{\bar{\varphi}}\sin\left(k\int a^{-1}dt\right). \tag{3.74}$$

From the second equation we derived, (3.55), we obtain the form of the inflaton perturbations

$$\delta\varphi_k(\tau) \sim \frac{k}{a}\frac{C_2(k)\cos(k\tau) - C_1(k)\sin(k\tau)}{4\pi G} + \frac{\bar{\varphi}''}{\bar{\varphi}'}\frac{C_1(k)\cos(k\tau) + C_2(k)\sin(k\tau)}{4\pi G a}, \tag{3.75}$$

or, in physical time,

$$\delta\varphi_k(\tau) \sim \frac{k}{4\pi G a}\left[C_2(k)\cos\left(k\int a^{-1}dt\right) - C_1(k)\sin\left(k\int a^{-1}dt\right)\right] + SR(t), \tag{3.76}$$

where we called

$$SR(t) = \left(H + \frac{\ddot{\bar{\varphi}}}{\dot{\bar{\varphi}}}\right)\frac{C_1(k)\cos\left(k\int a^{-1}dt\right) + C_2(k)\sin\left(k\int a^{-1}dt\right)}{4\pi G}. \tag{3.77}$$

which can be neglected during slow-roll inflation.

Super-horizon limit

On the other hand, when $k^2 \ll \theta''/\theta$, it is possible to neglect the spatial contributions of (3.70) to obtain

$$u'' - \frac{\theta''}{\theta}u = 0 \Rightarrow u''\theta - \theta''u = 0. \tag{3.78}$$

Writing

$$u''\theta - \theta''u + u'\theta' - u'\theta' = (\theta u' - \theta' u)' = \left[\theta^2\left(\frac{u'}{\theta} - \frac{\theta'}{\theta^2}u\right)\right]' = \left[\theta^2\left(\frac{u}{\theta}\right)'\right]' = 0, \tag{3.79}$$

we have, integrating by parts,

$$\int \frac{d}{d\tau}\theta^2 \left(\frac{u}{\theta}\right)' d\tau = \theta^2 \frac{d}{d\tau}\left(\frac{u}{\theta}\right) + \alpha = 0, \tag{3.80}$$

$$\Rightarrow \int \frac{d}{d\tau}\left(\frac{u}{\theta}\right) d\tau = C_2(k) \int \frac{d\tau}{\theta^2}, \tag{3.81}$$

$$\frac{u}{\theta} + \beta = C_2(k) \int \frac{d\tau}{\theta^2} \tag{3.82}$$

and then

$$u_k(\tau) = C_1(k)\theta(\tau) + C_2(k)\theta(\tau) \int^{\tau} \frac{d\tilde{\tau}}{\theta^2(\tilde{\tau})} = C_2\theta(\tau) \int_{\tau_0}^{\tau} \frac{d\tilde{\tau}}{\theta^2(\tilde{\tau})} \tag{3.83}$$

The decaying mode $C_1(k)\theta(\tau)$ has been absorbed into the integral by the changing the lower limit of integration. Making use of the relation (3.51) to write $\bar{\varphi}'$ in terms of $\mathcal{H}$,

$$u_k(\tau) = \frac{2C_2(k)}{8\pi G}\frac{\mathcal{H}}{a\bar{\varphi}'} \int \frac{a^2}{\mathcal{H}^2}(\mathcal{H}^2 - \mathcal{H}')d\tau, \tag{3.84}$$

$$= \frac{A(k)}{\bar{\varphi}'}\frac{\mathcal{H}}{a} \int a^2 \left[1 + \left(\frac{1}{\mathcal{H}}\right)'\right] d\tau. \tag{3.85}$$

Integrating by parts:

$$\int a^2 \left(\frac{1}{\mathcal{H}}\right)' d\tau = \frac{a^2}{\mathcal{H}} - \int \frac{2aa'}{\mathcal{H}} d\tau \tag{3.86}$$

$$= \frac{a^2}{\mathcal{H}} - 2\int a^2 d\tau. \tag{3.87}$$

Finally,

$$u_k(\tau) = \frac{A(k)}{\bar{\varphi}'}\left(a - \frac{\mathcal{H}}{a}\int a^2 d\tau\right) = \frac{A(k)}{\bar{\varphi}'}\left(\frac{1}{a}\int a^2 d\tau\right)'. \tag{3.88}$$

Coming back to Φ:

$$\Phi(\tau) = \frac{A(k)}{a}\left(\frac{1}{a}\int a^2 d\tau\right)', \tag{3.89}$$

or

$$\Phi(t) = A(k)\frac{d}{dt}\left(\frac{1}{a}\int a dt\right) = A(k)\left(1 - \frac{H}{a}\int a dt\right). \tag{3.90}$$

Writing $\delta\varphi$ from (3.55) and making use of (3.51), we obtain

$$\delta\varphi(\tau) = \frac{A(k)}{a^2}\bar{\varphi}' \int a^2 d\tau, \tag{3.91}$$

or

$$\delta\varphi(t) = \frac{A(k)}{a}\dot{\bar{\varphi}}\int a dt. \tag{3.92}$$

3.2.2 Vector perturbations

There is only one equation describing the evolution of the vector modes,

$$\Phi_i' + 2\mathcal{H}\Phi_i = 0 \tag{3.93}$$

It is straightforward to check that $\Phi_i \propto a^{-2}$ is a solution to the above equation. Hence, for any model of inflation, the vector modes decay with the square of the scale factor and then, by the end of inflation, they have been completely diluted.

3.3 Seeding the structure formation

We now turn to a key aspect of inflationary modes: the quantization of the inflaton field perturbations which will lead to the particle production responsible for the structures we see nowadays in the Universe. This quantization sets the initial conditions for the perturbation theory developed previously, thus determining the initial state of the fields[6].

3.3.1 The full action for the scalar field

Previously we found, in a gauge invariant form, how the perturbations of the scalar inflaton field are related to the metric perturbations. In this section, we shall consider the action for a scalar field about a FLRW background,

$$\begin{aligned} S &= -\frac{1}{16\pi G}\int R\sqrt{-g}\, d^4x + \int \mathcal{L}(g)\sqrt{-g}\, d^4x \\ &\equiv S_{\rm gr} + S_{\rm sf}, \end{aligned} \tag{3.94}$$

where the first term $S_{\rm gr}$ is the Einstein-Hilbert action, representing gravity, and the second term $S_{\rm sf}$ is the scalar field action [97], with $\mathcal{L}(g)$ given by (3.16).

[6]Note that the constants $C_1(k), C_2(k)$ and $A(k)$ need initial conditions to be determined.

The first order perturbation of the action gives us the background equations of motion. Hence, to study the linearized dynamics of the perturbations, we need to evaluate the action up to second order in the fluctuations, $\delta^{(2)}S$ [16]. In this case,

$$\delta^{(2)}S = \delta^{(2)}S_{\rm gr} + \delta^{(2)}S_{\rm sf} \tag{3.95}$$

and, for a flat Universe,

$$\delta^{(2)}S = \frac{1}{2}\int \left(v'^2 - \delta^{ij}v_{,i}v_{,j} + \frac{z''}{z}v^2 + \mathscr{D}\right)\, d^4x, \tag{3.96}$$

where

$$v = a\left[\delta\varphi^{(\rm gi)} + \left(\frac{\bar{\varphi}'}{\mathcal{H}}\right)\Psi\right] \equiv a\left[\delta\varphi + \left(\frac{\bar{\varphi}'}{\mathcal{H}}\right)\Phi\right] \tag{3.97}$$

is the Mukhanov-Sasaki potential already introduced in (3.43),

$$z = \frac{a\bar{\varphi}'}{\mathcal{H}}, \tag{3.98}$$

and $\mathscr{D}$ accounts for total derivatives contributions. In [83] it is shown that for the cases of hydrodynamical matter and higher derivative theories of gravity, the action reduces to this form as well, with the caveat that, for the former, c_s^2 appears multiplying the Laplacian of v.

We work, henceforth, in the Newtonian gauge ($B = E = 0 \Rightarrow \Phi = \Psi$), and the scalar-field perturbation $\delta\varphi$ appearing in (3.97) is already gauge-invariant. The complete expressions in any gauge and for any spatial curvature can be found in [83].

3.3.2 Quantizing the action

The action (3.96) describes a scalar field with time dependent mass $m^2 \equiv -z''/z$ and whose Lagrangian density is

$${}^{(2)}\mathcal{L} = \frac{1}{2}\left(v'^2 - \delta^{ij}v_{,i}v_{,j} + \frac{z''}{z}v^2\right), \tag{3.99}$$

up to total derivatives.

From the action, the Euler-Lagrange equation gives us the equation of motion

$$v'' - \nabla^2 v - \frac{z''}{z}v = 0, \tag{3.100}$$

also called Mukhanov-Sasaki equation [82, 103], which is a harmonic oscillator equation for the coupled fields $v(\tau, \mathbf{x})$ [85]. In order to decouple the oscillators, we consider the Fourier mode expansion of the field,

$$v(\tau, \mathbf{x}) = \int v_{\mathbf{k}}(\tau) e^{i\mathbf{k}\cdot\mathbf{x}} \frac{d^3k}{(2\pi)^3} \tag{3.101}$$

and then the Mukhanov-Sasaki equation becomes

$$v_{\mathbf{k}}'' + \omega_k^2(\tau) v_{\mathbf{k}} = 0, \tag{3.102}$$

where $\omega_k(\tau)^2 \equiv \left(k^2 - \frac{z''}{z}\right)$.

Here we perform the usual canonical quantization. For that, we promote v and its conjugate momentum $\pi = \partial\mathcal{L}/\partial v' = v'$ to operators $\hat{v}$ and $\hat{\pi}$ satisfying the commutation relations

$$[\hat{v}(\tau, \mathbf{x}), \hat{v}(\tau, \mathbf{x}')] = [\hat{\pi}(\tau, \mathbf{x}), \hat{\pi}(\tau, \mathbf{x}')] = 0 \quad \text{and} \quad [\hat{v}(\tau, \mathbf{x}), \hat{\pi}(\tau, \mathbf{x}')] = i\hbar\delta(\mathbf{x} - \mathbf{x}'), \tag{3.103}$$

and whose mode expansions are

$$\hat{v}(\tau, \mathbf{x}) = \int \hat{v}_{\mathbf{k}}(\tau) e^{i\mathbf{k}\cdot\mathbf{x}} \frac{d^3k}{(2\pi)^3} \quad \text{and} \quad \hat{\pi}(\tau, \mathbf{y}) = \int \hat{\pi}_{\mathbf{k}'}(\tau) e^{i\mathbf{k}'\cdot\mathbf{y}} \frac{d^3k'}{(2\pi)^3}. \tag{3.104}$$

In terms of the operators, the Mukhanov-Sasaki equation becomes

$$\hat{v}_{\mathbf{k}}'' + \omega_k^2(\tau) \hat{v}_{\mathbf{k}} = 0. \tag{3.105}$$

It is straightforward to see that, in Fourier space,

$$[\hat{v}_{\mathbf{k}}(\tau), \hat{\pi}_{\mathbf{k}'}(\tau)] = i\hbar\delta(\mathbf{k} + \mathbf{k}') \tag{3.106}$$

and, by noticing that we are working with the Heisenberg picture, that is, the operators depend on time whereas the eigenstates will remain constant, it is possible to write the mode expansion

$$\hat{v}_{\mathbf{k}}(\tau) = \frac{1}{\sqrt{2}} \left[v_k(\tau) a_{\mathbf{k}} + v_k^*(\tau) a_{-\mathbf{k}}^\dagger \right], \tag{3.107}$$

where we assume that $a_{\mathbf{k}}^\dagger$, the Hermitian conjugate of the time-independent operator $a_{\mathbf{k}}$, satisfy

the commutation relations

$$[a_{\mathbf{k}}, a_{\mathbf{k}'}] = [a^{\dagger}_{\mathbf{k}}, a^{\dagger}_{\mathbf{k}'}] = 0 \quad \text{and} \quad [a_{\mathbf{k}}, a^{\dagger}_{\mathbf{k}'}] = i\hbar\delta(\mathbf{k} - \mathbf{k}'), \tag{3.108}$$

and the mode functions $v^{*}_{\mathbf{k}}(\tau) = v_{-\mathbf{k}}(\tau)$, since the field is real, are solutions to (3.102).

The condition (3.106) implies that

$$\frac{1}{2}\left(v_{\mathbf{k}} v^{*\prime}_{\mathbf{k}'} - v^{*}_{\mathbf{k}} v'_{\mathbf{k}'}\right)[a_{\mathbf{k}}, a^{\dagger}_{\mathbf{k}'}] = i\hbar\delta(\mathbf{k} + \mathbf{k}'), \tag{3.109}$$

which leads to the normalization condition

$$v_{\mathbf{k}} v^{*\prime}_{\mathbf{k}} - v^{*}_{\mathbf{k}} v'_{\mathbf{k}} = 2i\hbar, \tag{3.110}$$

implying that $v_{\mathbf{k}}$ and $v^{*}_{\mathbf{k}}$ are linearly independent solutions of the Mukhanov-Sasaki equation. With the expansion (3.107), we have

$$\hat{v}(\tau, \mathbf{x}) = \frac{1}{\sqrt{2}} \int \left[v_k(\tau) a_{\mathbf{k}} e^{i\mathbf{k}\cdot\mathbf{x}} + v^{*}_{k}(\tau) a^{\dagger}_{\mathbf{k}} e^{-i\mathbf{k}\cdot\mathbf{x}} \right] \frac{d^3k}{(2\pi)^3}, \tag{3.111}$$

where in the second term we switched from $\mathbf{k}$ to $-\mathbf{k}$

Ambiguity of the vacuum state

The operators $a_{\mathbf{k}}$ and $a^{\dagger}_{\mathbf{k}'}$, satisfying (3.108), have the physical interpretation of creating and annihilating particles, respectively. In a mathematical sense, they construct the Fock space representation of quantum Hilbert states from the vacuum state $|0\rangle^{(a)}$. We could have defined, however, another mode function

$$u_{\mathbf{k}}(\tau) = \alpha_{\mathbf{k}} v_{\mathbf{k}}(\tau) + \beta_{\mathbf{k}} v^{*}_{\mathbf{k}}(\tau) \tag{3.112}$$

that satisfies (3.110) for $|\alpha_{\mathbf{k}}|^2 - |\beta_{\mathbf{k}}|^2 = 1$, such that

$$\hat{u}(\tau, \mathbf{x}) = \frac{1}{\sqrt{2}} \int \left[u_k(\tau) b_{\mathbf{k}} e^{i\mathbf{k}\cdot\mathbf{x}} + u^{*}_{k}(\tau) b^{\dagger}_{\mathbf{k}} e^{-i\mathbf{k}\cdot\mathbf{x}} \right] \frac{d^3k}{(2\pi)^3}. \tag{3.113}$$

With this new set of operators, $b_{\mathbf{k}}$ and $b^{\dagger}_{\mathbf{k}}$, we can built new quantum states from a new vacuum $|0\rangle^{(b)}$ as well. It is clear, then, that the particle interpretation of the theory is blurred by

this freedom in the choice of the mode functions.

Another tricky subtlety relies on the fact that usually one defines the vacuum of a theory in the case when the Hamiltonian does not depend on time. In our case, the time dependence of $\omega_k(\tau)$ leads to a time-dependent Hamiltonian. Thus, it is possible to define the vacuum, but we must allude to the instant of time τ_0 at which the vacuum is being defined. Our task is, then, to find the set of mode functions which uniquely determines the vacuum $|0\rangle^{(\tau_0)}$, that is, the instantaneous lowest-energy state of the Hamiltonian

$$H(\tau, \mathbf{x}) = \frac{1}{2}\int \left[\hat{\pi}^2 + \nabla^2\hat{v} - \frac{z''}{z}\hat{v}^2\right] d^4x \tag{3.114}$$

determined with some arbitrary mode function.

Noticing that the mode functions obey the Mukhanov-Sasaki equation (3.102), which is a harmonic oscillator with energy

$$E_k = \frac{1}{2}\left(|v_k'|^2 + \omega_k(\tau)^2|v_k|^2\right) \tag{3.115}$$

subjected to the normalization condition (3.110), we find that, by plugging in the ansatz

$$v_k = r_k e^{i\alpha_k} \tag{3.116}$$

into the normalization condition, one gets, assuming r_k and α_k real functions of the conformal time,

$$r_k^2\alpha_k' = \hbar \tag{3.117}$$

and then the energy becomes

$$E_k = \frac{1}{2}\left(r_k' + \frac{\hbar^2}{r_k^2} + \omega_k^2(\tau)r_k^2\right), \tag{3.118}$$

which is minimized if $r_k'(\tau_0) = 0$ and $r_k(\tau_0) = \omega_k^{-1/2}$, resulting in

$$v_k(\tau_0) = \frac{1}{\sqrt{\omega_k}}e^{i\alpha_k(\tau_0)} \quad \text{and} \quad v_k'(\tau_0) = i\sqrt{\omega_k}e^{i\alpha_k(\tau_0)}, \tag{3.119}$$

where we can set the phase $\alpha_k(\tau_0) = 0$ with no further problems.

3.3.3 Inflationary spectrum of scalar density perturbations

Let's go back to the Mukhanov-Sasaki equation

$$v_k'' + \left(k^2 - \frac{z''}{z}\right) v_k = 0. \tag{3.120}$$

Since

$$\frac{z''}{z} = \frac{a''}{a} + 2 - 2\frac{\mathcal{H}'}{\mathcal{H}} + \frac{\bar{\varphi}''}{\bar{\varphi}'} - 2\frac{\bar{\varphi}''}{\bar{\varphi}'}\frac{\mathcal{H}'}{\mathcal{H}} + \frac{\mathcal{H}''}{\mathcal{H}} + 2\frac{\mathcal{H}'^2}{\mathcal{H}^2}, \tag{3.121}$$

we can write, in terms of the slow-roll parameters ϵ and δ,

$$\frac{z''}{z} = (aH)^2(2 + 2\epsilon - 3\delta + \epsilon\delta + \delta^2). \tag{3.122}$$

Besides, by writing

$$\tau = -\frac{1}{aH} + \epsilon \int \frac{dt}{a} \Rightarrow aH = -\frac{1}{\tau(1-\epsilon)}, \tag{3.123}$$

we finally obtain

$$v_k'' + \left(k^2 - \frac{\nu^2 - \frac{1}{4}}{\tau^2}\right) v_k = 0, \tag{3.124}$$

where

$$\nu^2 - \frac{1}{4} = \frac{2 + 2\epsilon - 3\delta + \epsilon\delta + \delta^2}{(1-\epsilon)^2}. \tag{3.125}$$

Performing the change of variables

$$v_k(\tau) = \sqrt{-\tau} f_k(\tau), \tag{3.126}$$

equation (3.124) takes the form of a Bessel equation [87]

$$\tau^2 f_k'' + \tau f' + (\tau^2 k^2 - \nu^2) f = 0, \tag{3.127}$$

which gives us the solutions for v_k:

$$v_k(\tau) = \alpha_k \sqrt{-\tau} H_\nu^{(1)}(-k\tau) + \beta_k \sqrt{-\tau} H_\nu^{(2)}(-k\tau), \tag{3.128}$$

where $H_\nu^{(1)}$ and $H_\nu^{(2)}$ are, respectively, the Hankel functions of the first and second kind [11].

Taking the limit $\tau \to -\infty$, (3.124) becomes

$$v_k'' + k^2 v_k = 0, \tag{3.129}$$

whose solutions are, already taking into account (3.119),

$$v_k(\tau_i) = \frac{e^{-ik\tau_i}}{\sqrt{2k}}. \tag{3.130}$$

Considering the asymptotic behaviour of the Hankel functions [97],

$$\lim_{x\to\infty} H_\nu^{(1)}(x) = \sqrt{\frac{2}{\pi x}} e^{i\left(x - \frac{\pi\nu}{2} - \frac{\pi}{4}\right)} \tag{3.131}$$

$$\text{and } \lim_{x\to\infty} H_\nu^{(2)}(x) = \sqrt{\frac{2}{\pi x}} e^{-i\left(x - \frac{\pi\nu}{2} - \frac{\pi}{4}\right)}, \tag{3.132}$$

we see that, in order to get (3.130),

$$v_k(\tau) = \sqrt{\frac{\pi}{2}} \frac{1}{\sqrt{k}} \sqrt{-k\tau} H_\nu^{(1)}(-k\tau). \tag{3.133}$$

Vacuum fluctuations and the primordial power-spectrum

Once we have the mode functions, we can write

$$\hat{v}(\tau, \mathbf{x}) = \frac{1}{\sqrt{2}} \int \left[v_k(\tau) a_k e^{i\mathbf{k}\cdot\mathbf{x}} + v_k^*(\tau) a_k^\dagger e^{-i\mathbf{k}\cdot\mathbf{x}} \right] \frac{d^3k}{(2\pi)^3} \tag{3.134}$$

in terms of (3.133) and compute the vacuum expectation value $\langle \hat{v} \rangle = 0$ and the variance, calling $\mathbf{r} = \mathbf{x} - \mathbf{x}'$,

$$\langle 0|\hat{v}^\dagger(\mathbf{x}, \tau)\hat{v}(\mathbf{x}', \tau)|0\rangle = \int \frac{d^3k}{(2\pi)^3} |v_k|^2 e^{i\mathbf{k}\cdot\mathbf{r}} = \int \frac{dk}{k} \frac{k^3}{2\pi^2} |v_c|^2 \frac{\sin kr}{kr}. \tag{3.135}$$

Comparing with the definition of correlation function and power spectrum (A.13), we have

$$P_v(k) = |v_k|^2, \tag{3.136}$$

or, defining the dimensionless power-spectrum,

$$\mathcal{P}_v(k) = \frac{k^3}{2\pi^2} |v_k|^2 \tag{3.137}$$

For super-horizon scales, that is, when $k\tau \ll 1$, we find

$$\mathcal{P}_v = 2^{2\nu-3}\left[\frac{\Gamma(\nu)}{\Gamma(3/2)}\right]^2\left(\frac{H}{2\pi}\right)^2\left(\frac{k}{aH}\right)^{3-2\nu}. \tag{3.138}$$

For the case of slow-roll inflation, when $\epsilon \approx \delta \approx 0$, $\nu = 3/2$ and we obtain a scale invariant power-spectrum:

$$\mathcal{P}(k) = \left(\frac{H}{2\pi}\right)^2 \tag{3.139}$$

A constrained observable from inflation is the spectral index, defined as

$$n_s - 1 \equiv \frac{d\ln\mathcal{P}}{d\ln k} = 3 - 2\nu = 3 - \sqrt{\frac{(3-2\delta)^2 + \epsilon^2 + (4\delta+6)\epsilon}{(\epsilon-1)^2}} \approx 2\delta - 4\epsilon. \tag{3.140}$$

From the latest Planck measurements, $n_s \approx 0.968 \pm 0.006$ [101], that is, the spectrum is almost scale-invariant. Thus, we write

$$\mathcal{P}_\Phi(k) = A_s\left(\frac{k}{k_\star}\right)^{n_s-1}, \tag{3.141}$$

where A_s is called the primordial scalar power-spectrum amplitude, whose current value is set at $A_s \approx 2.2 \times 10^{-9} \pm 10^{-10}$ [101]. Therefore, our matter power-spectrum is written in terms of this amplitude and the scalar index n_s.

Chapter 4

The Physics of Non-Gaussianities

From the inflaton field quantization we have obtained the primordial spectrum generated by Inflation. However, our study was restricted to the simplest case: one scalar field slowly, rolling down the potential, to first order in perturbation theory. Besides alternatives to inflation, there are supersymmetric theories containing many scalar fields, string theory models and other higher-dimensional theories that may lead to possible inflationary scenarios [128]. Additional inflationary fields in the theory may have a role in the dynamics of inflation, leading to distinctive predictions for the power-spectrum and higher-order correlation functions [2, 9, 17, 23, 27, 67, 72, 74, 78, 101, 128]. Hence, we shall consider how the spectrum and higher-order correlation functions, such as the bispectrum, emerge.

4.1 Generating non-Gaussianities

There are two main sources of non-Gaussianities: before the horizon exit, quantum effects can lead to a non zero three-point correlation function; after horizon re-entry, the non-linear evolution due to gravity will generate non-Gaussianities. The former are called primordial non-Gaussianities whereas, the latter are secondary non-Gaussianities [17]. The great advantage of pursuing primordial non-Gaussianities in the CMB owes to the fact that, for the CMB, secondary contributions, such as those induced by gravity, are negligible.

In the realm of large-scale structure observations, however, the non-linear effects induced by gravity are the main source of contamination of the primordial signal one wishes to measure. Many works have dealt with this subject, of which we quote [10, 18, 74, 97]. We will run briefly through this issue and then we dive into our study of the primordial contributions

that come from quantum-mechanical effects during inflation.

4.1.1 Non-Gaussian features from gravitation

Consider the fluid equations we have treated in Chapter 2:

$$\frac{\partial \delta}{\partial \tau} + \nabla \cdot (1+\delta)\delta v = 0, \tag{4.1}$$

$$\frac{\partial \delta v}{\partial \tau} + \mathcal{H}\delta v + \delta v \cdot \nabla \delta v = -\nabla \Phi, \tag{4.2}$$

and

$$\nabla^2 \Phi = \frac{3}{2}\mathcal{H}^2 \Omega_m \delta, \tag{4.3}$$

where we used the description in conformal time and the Friedmann equation to write $\Omega_m = 8\pi G\rho_m/3H^2$. To make contact with [18], we will write the divergence of the peculiar velocity field as $\theta \equiv \nabla \cdot \delta v$.

Perturbation theory allows us to write

$$\delta(\mathbf{r},\tau) = \sum_{n=1}^{\infty} \delta^{(n)}(\mathbf{r},\tau) \quad \text{and} \quad \theta(\mathbf{r},\tau) = \sum_{n=1}^{\infty} \theta^{(n)}(\mathbf{r},\tau) \tag{4.4}$$

based on the assumption that we are able to expand the density and velocity fields about the linear (known) solutions $\delta^{(1)}(\mathbf{r},\tau)$.

In the non-linear regime, we can no longer count with the decoupling of different Fourier modes. Indeed, the Fourier expansion of the continuity (4.1) and Euler (4.2) equations leads to [18]

$$\frac{\partial \delta_{\mathbf{k}}(\tau)}{\partial \tau} + \theta_{\mathbf{k}}(\tau) = -\int \delta^D(\mathbf{k}-\mathbf{k}_1-\mathbf{k}_2)\alpha_{k_1k_2}\theta(\mathbf{k}_1,\tau)\delta(\mathbf{k}_2,\tau)d^3k_1 d^3k_2 \tag{4.5}$$

and

$$\frac{\partial \theta_{\mathbf{k}}(\tau)}{\partial \tau} + \mathcal{H}\theta_{\mathbf{k}}(\tau) + \frac{3}{2}\Omega_m \mathcal{H}^2 \delta_{\mathbf{k}}(\tau) = -\int \delta^D(\mathbf{k}-\mathbf{k}_1-\mathbf{k}_2)\beta_{k_1k_2}\theta_{\mathbf{k}_1}(\tau)\delta_{\mathbf{k}_2}(\tau)d^3k_1 d^3k_2, \tag{4.6}$$

where $\delta^D(x)$ is the Dirac delta function and

$$\alpha_{k_1k_2} \equiv \frac{(\mathbf{k}_1+\mathbf{k}_2)\cdot\mathbf{k}_1}{k_1^2} \quad \text{and} \quad \beta_{k_1k_2} \equiv \frac{(\mathbf{k}_1+\mathbf{k}_2)^2(\mathbf{k}_1\cdot\mathbf{k}_2)}{2k_1^2k_2^2}. \tag{4.7}$$

For the case of a flat matter-dominated (Einstein-de Sitter [42]) Universe, where $a(\tau) \propto$

τ^2 and $\mathcal{H} = 2/\tau$, and considering only the growing mode solutions, the equations of motion (4.5) and (4.6) can be solved with the perturbative expansion

$$\delta_{\mathbf{k}}(\tau) = \sum_{n=1}^{\infty} a^n(\tau)\delta^{(n)}(\mathbf{k}) \quad \text{and} \quad \theta_{\mathbf{k}}(\tau) = -\mathcal{H}(\tau)\sum_{n=1}^{\infty} a^n(\tau)\theta^{(n)}(\mathbf{k}). \tag{4.8}$$

By direct substitution of the above expansions into the equations of motion, $\delta^{(n)}(\mathbf{k})$ and $\theta^{(n)}(\mathbf{k})$ are found to be, up to second order (i.e. $n = 2$),

$$\delta^{(2)}(\mathbf{k}) = \int \delta^D(\mathbf{k} - \mathbf{k}_1 - \mathbf{k}_2)F_2(\mathbf{k}_1, \mathbf{k}_2)\delta^{(1)}(\mathbf{k}_1)\delta^{(1)}(\mathbf{k}_2)d^3k_1 d^3k_2 \tag{4.9}$$

$$\text{and } \theta^{(2)}(\mathbf{k}) = \int \delta^D(\mathbf{k} - \mathbf{k}_1 - \mathbf{k}_2)G_2(\mathbf{k}_1, \mathbf{k}_2)\theta^{(1)}(\mathbf{k}_1)\theta^{(1)}(\mathbf{k}_2)d^3k_1 d^3k_2, \tag{4.10}$$

where $\delta^{(1)}(\mathbf{k})$ is the linear solution. The integral kernels are:

$$F_2(\mathbf{k}_1, \mathbf{k}_2) = \frac{5}{7} + \frac{1}{2}\frac{\mathbf{k}_1 \cdot \mathbf{k}_2}{k_1 k_2}\left(\frac{k_1}{k_2} + \frac{k_2}{k_1}\right) + \frac{2}{7}\frac{(\mathbf{k}_1 \cdot \mathbf{k}_2)^2}{k_1^2 k_2^2}, \tag{4.11}$$

$$\text{and } G_2(\mathbf{k}_1, \mathbf{k}_2) = \frac{3}{7} + \frac{1}{2}\frac{\mathbf{k}_1 \cdot \mathbf{k}_2}{k_1 k_2}\left(\frac{k_1}{k_2} + \frac{k_2}{k_1}\right) + \frac{4}{7}\frac{(\mathbf{k}_1 \cdot \mathbf{k}_2)^2}{k_1^2 k_2^2}. \tag{4.12}$$

General expressions for F_n and G_n can be found in [18], p. 16, and [59]. We address the reader who is interested in the details leading to the above expressions to these two references and Chapter 12 of [10].

Bispectrum induced by gravity

In analogy with the power-spectrum, we define the bispectrum as[1]

$$\langle \delta(\mathbf{k}_1)\delta(\mathbf{k}_2)\delta(\mathbf{k}_3)\rangle \equiv (2\pi)^3\delta^D(\mathbf{k}_1 + \mathbf{k}_2 + \mathbf{k}_3)B(\mathbf{k}_1, \mathbf{k}_2, \mathbf{k}_3). \tag{4.13}$$

The existence of mode coupling at second order in perturbation theory, equations (4.9) and (4.10), leads to a non-vanishing bispectrum. Plugging $\delta(\mathbf{k}, \tau) = \delta^{(1)}_{\mathbf{k}}(\tau) + \delta^{(2)}_{\mathbf{k}}(\tau) + \mathcal{O}(3)$ into the definition (4.13) and assuming that the linear order term $\delta^{(1)}_{\mathbf{k}}(\tau)$ is Gaussian, we get

$$B_{\text{grav}} = 2F_2(\mathbf{k}_1, \mathbf{k}_2)P(k_1, \tau)P(k_2, \tau) + \text{perms.}, \tag{4.14}$$

[1] For details on cosmological correlation functions see Appendix A, where we present all relevant definitions for our studies.

where perms. stands for permutations of k_i and $P(k,\tau) = D_+(\tau)P_L(k)$, with $D_+(\tau)$ the growing mode and $P_L(k)$ the linear matter power-spectrum.

If we assume that all higher-order correlations are products of the two-point statistics, such as in the Gaussian case (see Appendix A), then a useful quantity to compute is the reduced bispectrum, defined as

$$Q(\mathbf{k}_1,\mathbf{k}_2,\mathbf{k}_3) \equiv \frac{B(\mathbf{k}_1,\mathbf{k}_2,\mathbf{k}_3)}{P(k_1)P(k_2)+P(k_1)P(k_3)+P(k_2)P(k_3)}. \tag{4.15}$$

which gives the deviation we have from a perfect Gaussian field and removes the redshift and scale-dependencies induced by the tree-level contributions of gravity [18, 49, **?**] .

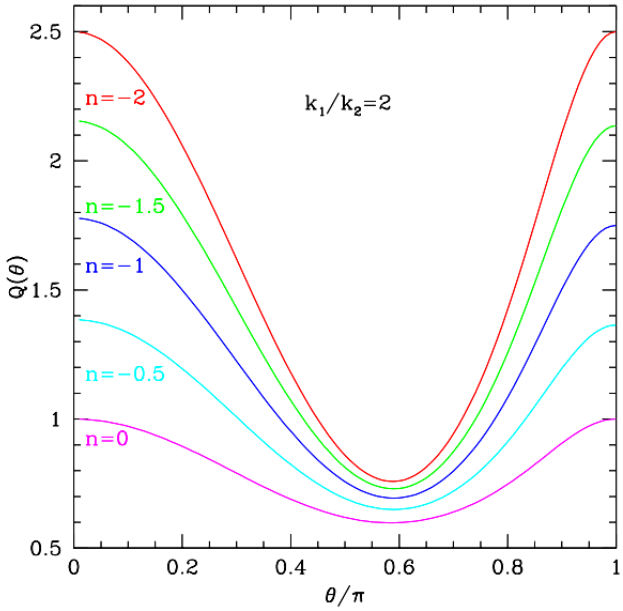

Figure 4.1: Reduced bispectrum $Q \equiv B/(P_1P_2 + P_1P_3 + P_2P_3)$ for the tree-level contribution of gravity, considering $|\mathbf{k}_1| = 2|\mathbf{k}_2|$ and $\hat{\mathbf{k}}_1 \cdot \hat{\mathbf{k}}_2 = \cos\theta$. Different curves corresponds to different spectral indices n. Extracted from [18].

4.1.2 Non-Gaussian features from inflation

So far we saw that inflation provides the initial conditions for the perturbations. According to it, the density fluctuations were created when the Universe was dominated by a slow rolling scalar field $\varphi(\mathbf{x},\tau) = \bar{\varphi}(\tau) + \delta\varphi(\mathbf{x},\tau)$. The quantization of the perturbations led us to

$$\delta\varphi = \frac{1}{\sqrt{2k}}(v_k(\tau)a_k + v_k^*(\tau)a_{-k}^\dagger), \tag{4.16}$$

where, as in the case of the harmonic oscillator, $\hat{n}_k = a_k^\dagger a_k$ is the number operator such that $\hat{n}_k|0\rangle = 0|0\rangle$, $\hat{n}_k|1_k\rangle = a_k^\dagger a_k(a_k^\dagger|0\rangle) = \delta_{kk'}|1_k\rangle = 1$, etc.

Defining the operator $\delta\varphi^\dagger\delta\varphi$, we showed that $\langle 0|\delta\varphi_k^\dagger\delta\varphi_{k'}|0\rangle = \delta_{kk'}|v_k|^2/2k$, and defined the power-spectrum. It is straightforward to see that, in this approximation,

$$\langle 0|\delta\varphi(k_1)\delta\varphi(k_2)\delta\varphi(k_3)|0\rangle = 0, \tag{4.17}$$

and that

$$\langle 0|\delta\varphi(k_1)\delta\varphi(k_2)\delta\varphi(k_3)\delta\varphi(k_4)|0\rangle \propto P(k_1)P(k_2) + \text{perms}. \tag{4.18}$$

Hence, we see that the three-point function vanishes whilst the four-point function can be written in terms of the two-point function. From a physical point of view this is obvious since the ground state of a harmonic oscillator is described by normal wave functions, whose odd moments are all null and the even ones are all functions of the second moment.

However, the simplest slow-roll single-field models of inflation have a non-vanishing three-point correlation function. In what follows we introduce two main non-Gaussian models: first we summarize the results derived by Maldacena in [78], and then we introduce one of the most studied non-Gaussian models in the literature, the local model.

Non-Gaussianities from slow-roll single-field inflation

Here we summarize the results Maldacena obtained for the three-point correlation functions of inflationary models whose action describes a minimally coupled scalar-field with potential $V(\varphi)$ and canonical kinetic term $X = -(\partial_\mu\varphi)^2/2$,

$$S = \int \left[\frac{R}{16\pi G} + X - V(\varphi)\right]\sqrt{-g}\, d^4x, \tag{4.19}$$

with the Bunch-Davies vacuum. Using the Schwinger-Keldysh formalism[2] and expanding the action up to third-order, Maldacena found [78]

[2]The Schwinger-Keldysh formalism, proposed by Schwinger [106, 107] and Keldysh [64] in the early 1960s, also known as "in-in" formalism, provides a way to calculate the expectation of some operator $Q(t)$, which is a product of perturbations – e.g. the inflaton perturbation $\delta\varphi$, or the curvature perturbation ζ, equation (2.167) – for a fixed time t: $\langle Q(t)\rangle = \langle\Omega|\delta\varphi_{k_1}\ldots\delta\varphi_{k_n}|\Omega\rangle$, where $|\Omega\rangle$ is the vacuum state of the theory. We refer the interested reader to the elucidating reviews of Baumann [17] and Chen [27], and the paper by Weinberg [130], in which the "in-in" formalism is extended to Cosmology in a pedagogical fashion.

$$\langle\zeta(\mathbf{k}_1)\zeta(\mathbf{k}_2)\zeta(\mathbf{k}_3)\rangle = (2\pi)^7\delta^D(\mathbf{k}_1+\mathbf{k}_2+\mathbf{k}_3)P_\zeta^2\frac{S^{\rm sr}}{k_1^2+k_2^2+k_3^2}, \tag{4.20}$$

where

$$S^{\rm sr} = \frac{\epsilon}{8}\left[-\left(\frac{k_1^2}{k_2k_3}+2\text{ perms.}\right)+\left(\frac{k_1}{k_2}+5\text{ perms.}\right)+\frac{8}{\sum_i k_i}\left(\frac{k_1k_2}{k_3}+2\text{ perms.}\right)\right]+ \\ +\frac{\eta}{8}\left(\frac{k_1^2}{k_2k_3}+2\text{ perms.}\right). \tag{4.21}$$

He also showed that higher-order corrections to the perturbations are suppressed by the slow-roll parameters; thus, for this reason they are negligible.

Local models

A general parametrization one can do about the gravitational potential Φ is to expand it up to second order

$$\begin{aligned}\Phi(\mathbf{x}) &= \Phi_G(\mathbf{x})+\Phi_{NG}(\mathbf{x}),\\ &= \Phi_G(\mathbf{x})+f_{NL}(\Phi_G^2(\mathbf{x})-\langle\Phi_G^2(\mathbf{x})\rangle),\end{aligned} \tag{4.22}$$

where Φ_G is the Gaussian (linear) potential and f_{NL}, called non-linearity parameter, parametrizes the deviations from the purely linear model. This type of potential gives rise to the so-called local[3] models. Another familiar expression to the local model is given in terms of the curvature perturbation $\zeta = 5\Phi/3$:

$$\zeta(\mathbf{x}) = \zeta_G(\mathbf{x})+\frac{3}{5}f_{NL}(\zeta_G^2(\mathbf{x})-\langle\zeta_G^2(\mathbf{x})\rangle). \tag{4.23}$$

In Fourier space, the quadratic term becomes a convolution

$$\Phi_{NG}(\mathbf{x}) = \frac{f_{NL}}{(2\pi)^3}\int\Phi_G(\mathbf{k}-\mathbf{k}')\Phi_G(\mathbf{k}')d^3k', \tag{4.24}$$

which leads to a non-vanishing three-point correlation function:

$$\langle\Phi(\mathbf{k}_1)\Phi(\mathbf{k}_2)\Phi(\mathbf{k}_3)\rangle = 2f_{\rm NL}(2\pi)^3\delta^D(\mathbf{k}_1+\mathbf{k}_2+\mathbf{k}_3)\left[P_\Phi(\mathbf{k}_1)P_\Phi(\mathbf{k}_2)+\right. \\ \left.+P_\Phi(\mathbf{k}_1)P_\Phi(\mathbf{k}_3)+P_\Phi(\mathbf{k}_2)P_\Phi(\mathbf{k}_3)\right]. \tag{4.25}$$

[3]Local in the sense that the potential is defined locally in real space [23].

4.2 Bispectrum

Cosmological parameters are extracted statistically from observations of the CMB or LSS. The most common tool for analyzing cosmological data is the form of the power-spectrum (or the two-point correlation function)

$$(2\pi)^3\delta^D(\mathbf{k}-\mathbf{k}')P_\Phi(k) = \langle\Phi(\mathbf{k})\Phi^*(\mathbf{k}')\rangle. \tag{4.26}$$

As shown in section §4.1.2, in the case of a Gaussian field only the even correlation functions are non-zero. But, as we saw, even the simplest model of inflation generates a non-vanishing three-point correlation function. Hence, we will consider the bispectrum (4.13) as our main statistical tool to study non-Gaussian features that emerge from primordial physics such as inflation.

The Dirac delta function appearing in the definition of the bispectrum imposes the condition that the wavevectors $\mathbf{k}$ must form a closed triangle. The three possibilities are condensed in the local (*squeezed*), equilateral and flattened configurations, as shown in Figure 4.2.

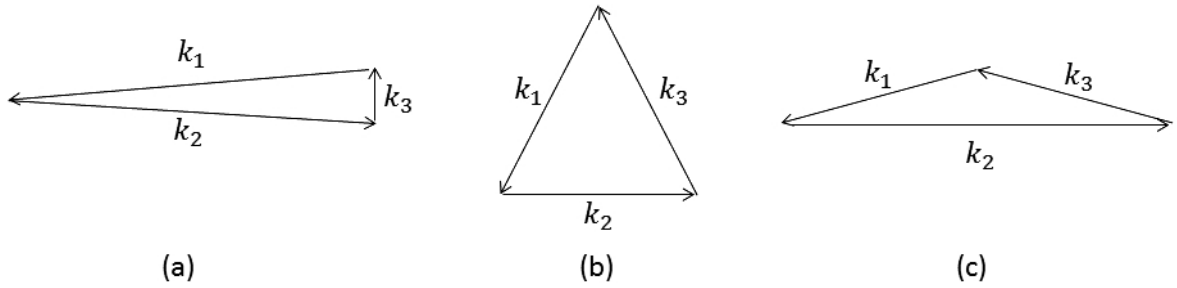

Figure 4.2: (a) Squeezed configuration ($k_3 \ll k_1, k2$); (b) Equilateral configuration ($k_1 \simeq k_2 \simeq k_3$) and (c) Flattened configuration ($k_3 \simeq k_1 + k_2$).

4.2.1 Shape of non-Gaussianities

Since the bispectrum depends on the triangular configuration determined by $\mathbf{k}_i$, we can define the bispectrum as

$$B_\Phi \equiv f_{NL}\mathcal{F}(k_1, k_2, k_3), \tag{4.27}$$

where $\mathcal{F}$ codifies the bispectrum dependence on the vector modes $\mathbf{k}_i$ and $k_3 = |k_1 - k_2|$ is needed to ensure translational invariance of the statistic.

Local Shape

Plugging the scale-invariant power-spectrum obtained from inflation, $P_\Phi(k) = \mathcal{P}_\Phi k^{-3}$, into equation (4.25) and comparing the result with the definition of the bispectrum (4.13), we can write

$$B_\Phi(k_1, k_2, k_3) \approx 2 f_{NL} \frac{\mathcal{P}_\Phi^2}{(k_1 k_2 k_3)^2} \left(\frac{k_1^2}{k_2 k_3} + \frac{k_2^2}{k_1 k_3} + \frac{k_3^2}{k_1 k_2} \right), \tag{4.28}$$

and then the shape of non-Gaussianities $S(k_1, k_2, k_3)$ can be defined as

$$S(k_1, k_2, k_3) \equiv \frac{(k_1 k_2 k_3)^2}{N} B_\Phi(k_1, k_2, k_3), \tag{4.29}$$

where N is a normalization introduced to give $S(k, k, k) = 1$ when we consider a bispectrum of the local form (4.25), i.e. $N = 6 f_{NL} \mathcal{P}_\Phi^2$.

Therefore, we define the local shape as

$$S^{\text{loc}}(k_1, k_2, k_3) = \frac{1}{3} \left(\frac{k_1^2}{k_2 k_3} + \frac{k_2^2}{k_1 k_3} + \frac{k_3^2}{k_1 k_2} \right). \tag{4.30}$$

Equilateral shape

The equilateral shape is defined, in a pure phenomenological way [74], as

$$S^{\text{eq}}(k_1, k_2, k_3) = \frac{(k_1 + k_2 - k_3)(k_2 + k_3 - k_1)(k_3 + k_1 - k_2)}{k_1 k_2 k_3}. \tag{4.31}$$

Single-field slow-roll inflation

The bispectrum derived by Maldacena can be written in terms of the local and equilateral shape:

$$S^{\text{sr}}(k_1, k_2, k_3) = (6\epsilon - 2\eta) S^{\text{loc}} + \frac{5}{3} \epsilon S^{\text{eq}}. \tag{4.32}$$

Thus, for this simple inflationary scenario we expect no significant observational signal on the non-linearity parameter, since $f_{NL} \ll 1$.

4.2.2 Correlation between different shapes

Given the huge amount of shapes that can be defined, it is natural two ask if two different shapes can be observationally distinguished. This can be done by calculating how correlated the two different shapes S and S' are. This is useful once we encounter primordial bispectra

which cannot be separated into any of the shapes we defined so far. For example, DBI inflation has a highly correlated shape to the equilateral one, although it cannot be written in terms of this shape [47].

Babich, Creminelli and Zaldarriaga [12] defined the correlation between two shapes as the integral

$$F(S,S') = \int_{V_k} S(k_1,k_2,k_3)S'(k_1,k_2,k_3)\frac{1}{k_1+k_2+k_3}dV_k, \tag{4.33}$$

where V_k is the volume enclosed by the Fourier modes k_i. Hence, $F(S,S')$ is a quantity which depends on the volume and resolution of the survey. They introduced, then, the shape correlator, defined as the cosine between the two shapes,

$$\mathcal{C}(S,S') \equiv \frac{F(S,S')}{\sqrt{F(S,S)F(S',S')}}. \tag{4.34}$$

From this definition we can say that the equilateral shape is 50% correlated to the local shape [47] and lead us to a new definition, the orthogonal shape [111], obtained from the condition that $\mathcal{C}(S^{\rm eq},S^{\rm orth}) \equiv 0$ [23]:

$$S^{\rm orth} = \frac{-3k_1^3 + 3k_1^2(k_2+k_3) + k_1\left(3k_2^2 - 8k_2k_3 + 3k_3^2\right) - 3(k_2-k_3)^2(k_2+k_3)}{k_1k_2k_3}. \tag{4.35}$$

Figures 4.3, 4.4 and 4.5 show the contributions of the primordial non-Gaussianity for different shapes on the equilateral configuration of the matter bispectrum $B(k,k,k)$, at redshift $z=1$.

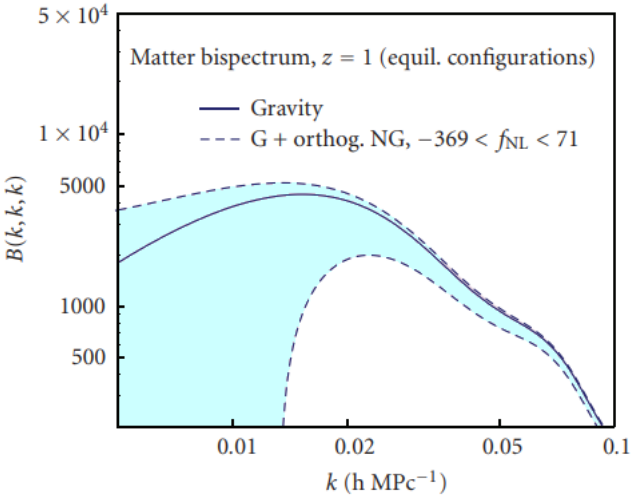

Figure 4.5: Same as Figures 4.3 and 4.5, but considering primordial non-Gaussianity of the orthogonal type varying in the range $-369 < f_{NL}^{\rm orth} < 71$ in addition to the gravity component. Extracted from [74].

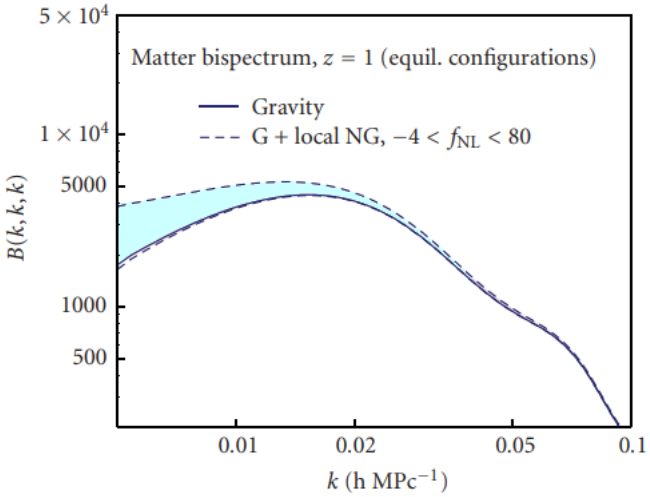

Figure 4.3: Solid line shows the gravity component of the bispectrum computed for equilateral triangles, whereas dashed lines show the contributions of primordial physics with local type of primordial non-Gaussianity varying in the range $-4 < f_{NL} < 80$ in addition to the gravity component. Extracted from [74].

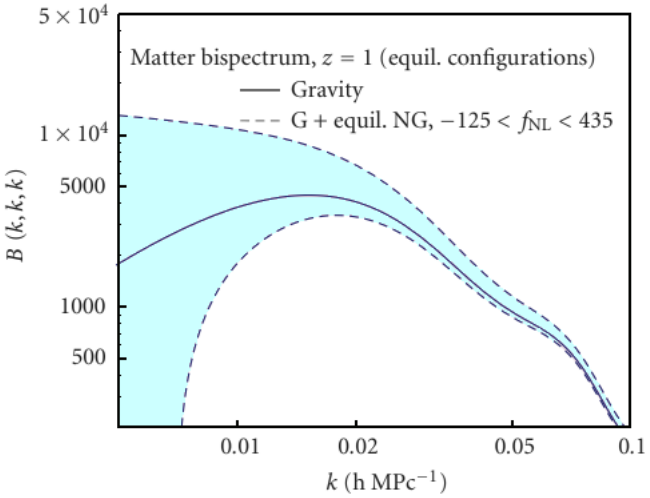

Figure 4.4: Same as Figure 4.3, but considering primordial non-Gaussianity of the equilateral type varying in the range $-125 < f_{NL}^{\rm eq} < 435$ in addition to the gravity component. Extracted from [74].

4.2.3 Contributions to the spectrum

We do not need to look for primordial signals only at the bispectrum. Another interesting probe of primordial non-Gaussianity consists on the effects it exerts on the power-spectrum.

Dalal and collaborators [35] showed that the local type of non-Gaussianity (4.22) introduces a scale dependence on the bias of dark matter halos, $b = b + \Delta b(k)$, which is manifested on the largest scales. As an extension to this work, Slosar and collaborators [116] generalized the scale-dependent bias of [35] to take into account the merging history of halos, obtaining

$$\Delta b(M,k) = 3 f_{NL}(b-p)\delta_c \frac{\Omega_m}{k^2 T(k) D(z)} \left(\frac{H_0}{c}\right)^2, \tag{4.36}$$

where $1 < p < 1.6$. For $p = 1$ we recover the expression given in [35], which only accounts for the mass of the halos. For recent mergers, $p = 1.6$ [116], and considering the merger history makes constraints more realistic when comes to tying observational bounds in f_{NL}^{loc}.

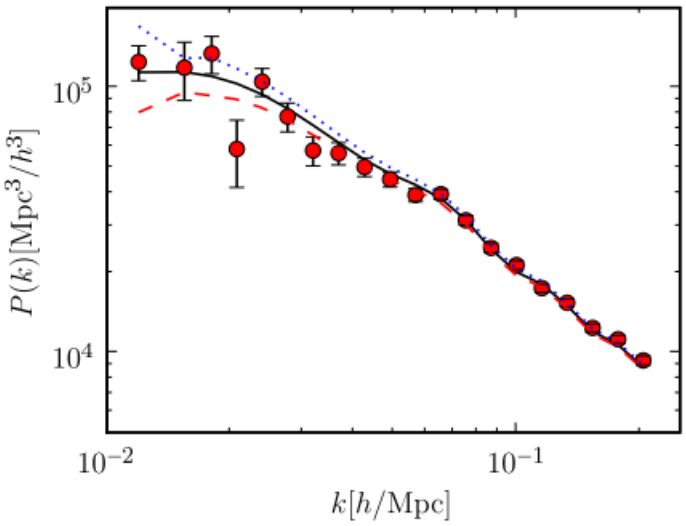

Figure 4.6: Effect of local non-Gaussianities, due to the scale-dependent bias (4.36), on the spectroscopic luminous red galaxies (red dots) power-spectrum, from Tegmark et al. [125], based on a galaxy sample that covers 4000 deg^2 of sky over the redshift range $0.16 \leq z \leq 0.47$. The black solid line shows the best fit $f_{NL}^{\text{loc}} = 0$, whereas the dashed lines show the power-spectrum for $f_{NL}^{\text{loc}} = 100$ (*blue*) and $f_{NL}^{\text{loc}} = 100$ (*red*). Slosar and collaborators [116] kept the cosmological parameters ($\omega_b = \Omega_b h^2$, $\omega_{\text{CDM}} = \Omega_{\text{CDM}} h^2$, θ (ratio of the sound horizon to the angular diameter distance at decoupling), τ (optical depth), $\log(A_s)$ and n_s) fixed during the analysis, which gave the constraint $f_{NL}^{\text{loc}} = 70^{+74}_{-83}$. Although it does not seem to have a very good constraining power, the authors combined these galaxies with other datasets and the WMAP Year 5 bispectrum data to get $f_{NL}^{\text{loc}} = 36^{+18}_{-17}$. Extracted from [116].

Chapter 5

Extracting Non-Gaussianities from Mock Galaxy Maps

In this chapter we present the basic tools used to generate and analyze mock galaxy catalogs. We begin by describing the log-normal approximation [30] used to swiftly simulate the distribution of matter, at the linear and weakly non-linear regime, and how "galaxies" can be added to the density maps previously generated via a Poisson point process. In addition to it, we go through the multi-tracer technique [3, 110] that allows one to circumvent the cosmic variance limit which appears on large-scales. Finally, we present an estimator for higher-order correlation functions [108, 60, 129] that will be used to extract statistical information out of the mocks generated by an already operating code of our group [4].

5.1 Log-normal approximation

Observations of the late Universe show how highly non-Gaussian the galaxy distribution is, i.e., by looking at real galaxy catalogs or N-body simulations one sees by eye the difference of those maps with respect to a completely Gaussian one[1]. Furthermore, approximating the density distribution $\rho(x)$ of the Universe as a Gaussian random field leads to the physical issue of having $\rho(x) < 0$.

In 1934, Hubble investigated the distribution of ~ 44000 "extra-galactic nebulae" and observed a positively skewed frequency distribution in the count N of such nebulae, which

[1] As an example, see Figure 5.1 or the distribution of galaxies shown in Figure 1 of [93]

were captured by the telescope plates during one hour exposures. Moreover, he noticed that the distribution of $\log N$ followed, approximately, a normal distribution [56]. Thus, the count of galaxies resembled a log-normal distribution[2] [13].

It was shown by Peter Coles and Bernard Jones [30] that a field whose distribution is log-normal mimics, in good approximation, the linear and weakly non-linear regime of the large-scale structure of the Universe [28], taking almost no computational cost unlike N-body simulations, even though it fails to simulate the formation of filaments observed in the matter distribution, such as those obtained through the Zel'dovich approximation [29, 133]. Besides, since the log-normal field is derived from a Gaussian random variable, one can easily extract its statistical properties.

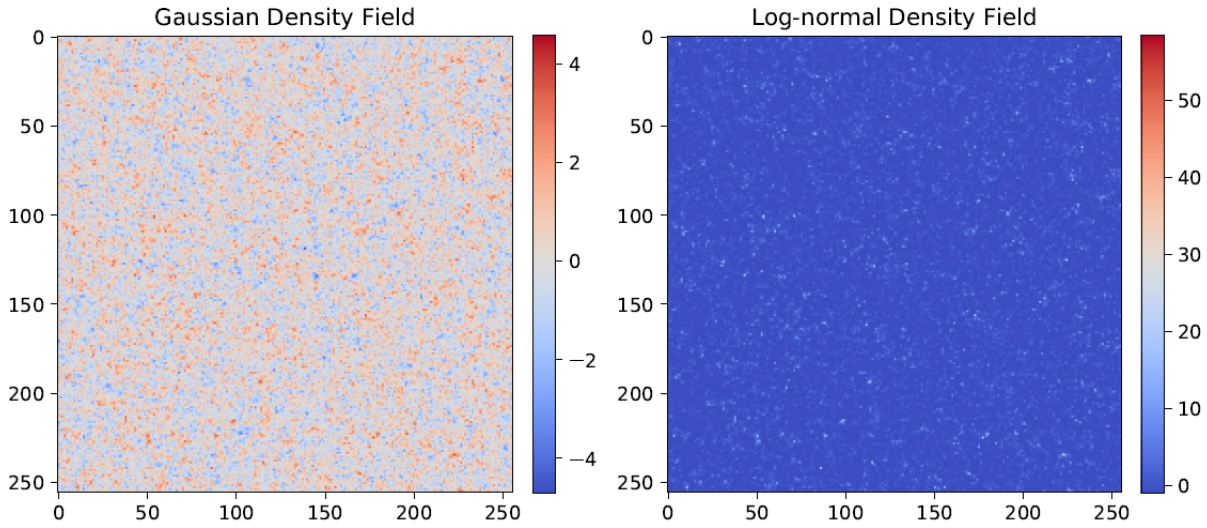

Figure 5.1: (*Left*) Gaussian density field for a box with 256^3 cells of physical size $\ell = 10$ Mpc/h. In this map we can see that the values of density represented on the box can reach any negative value within the variance of the field. (*Right*) Log-normal field generated from the left map. Notice that the smallest values of the density constrast, in this case, is $\delta = -1$, satisfying the desired condition for cosmological density fields.

5.1.1 The log-normal density field in cosmology

In the theory of LSS, one of the main quantities of interest is the density contrast

$$\delta(\mathbf{x}) \equiv \frac{\rho(\mathbf{x})}{\bar{\rho}} - 1, \tag{5.1}$$

[2] If $\log N$ has a normal distribution, then it is said that N has a log-normal distribution. This is going to be the subject of the following sections.

already introduced in (2.50).

By setting $\rho(\mathbf{x})/\bar{\rho} = e^{\delta_G(\mathbf{x})}$, where δ_G is a Gaussian random field with mean $\mu = 0$ [30], we obtain the log-normal density constrast $\delta_L(\mathbf{x})$:

$$\delta_L(\mathbf{x}) = e^{\delta_G(\mathbf{x})} - 1. \tag{5.2}$$

In what follows, the statistical properties of a random variable described by (5.2) are derived. Notice that the definition (5.2) overcomes the problem of having unphysical values of density, as shown in Figure 5.1.

5.1.2 General statistical properties of the log-normal distribution

Consider a random variable X following a normal (Gaussian) distribution with mean μ and variance σ^2, i.e. $X \sim \mathcal{N}(\mu, \sigma^2)$. The probability density function P of X is

$$P(x|\mu, \sigma) = \frac{1}{\sqrt{2\pi\sigma^2}} e^{-(x-\mu)^2/2\sigma^2}. \tag{5.3}$$

A very interesting and useful property of Gaussian distributions is that they are completely specified by their variance, statistically speaking. That is, all of its even central moments are given in terms of its variance, whereas the odd ones are null (see Appendix A):

$$\langle X^n \rangle = \begin{cases} 0 & n = 2k+1 \\ (n-1)!!\sigma^n & n = 2k \end{cases}, \tag{5.4}$$

where $k = 1, 2, 3, \ldots$[89].

A variable Y following a log-normal distribution is defined as $Y \equiv e^X$, that is, the logarithm of Y follows a Gaussian distribution. Following the notation of [7], we write for short $Y \sim \Lambda(\mu, \sigma^2)$. Since $\ln Y = X$, it is immediately seen that $Y > 0$, as this regime is sufficient to span the interval $-\infty < X < \infty$. To derive the probability density function for Y, we invoke the change of variables technique [25]: because Y is a monotonically increasing function of X, then

$$P(y|I) = P(x|I)\frac{dx}{dy}, \tag{5.5}$$

where $x = \ln y$. Accordingly, it follows that

$$P(y|\mu,\sigma) = \frac{y^{-1}}{\sqrt{2\pi\sigma^2}}\exp\left[-\frac{(\ln y - \mu)^2}{2\sigma^2}\right]. \tag{5.6}$$

It is worth stressing that μ and σ appearing in (5.6) are, respectively, the mean and standard deviation of the Gaussian variable X. The distribution function (5.6) is represented in the Figure 5.2 below.

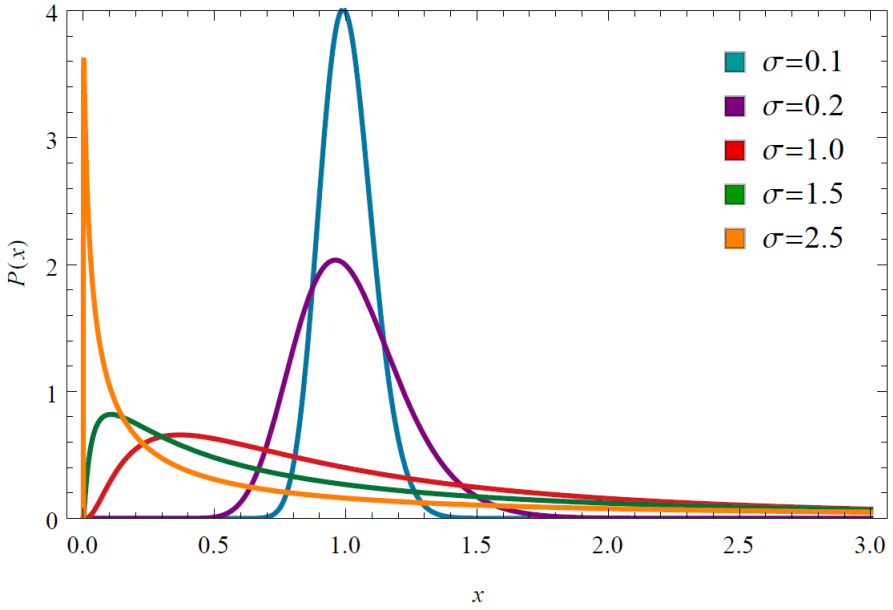

Figure 5.2: Log-normal probability density, as a function of x, with zero mean and several values for the standard deviation σ. Notice that its minimum value is zero, such as it is required for the physical density distribution $\rho(x)$.

From (5.6), the raw moments of this distribution are obtained in terms of the Gaussian parameters μ and σ:

$$\langle Y^n \rangle = e^{n\mu + n^2\sigma^2/2}. \tag{5.7}$$

5.1.3 Correlation functions of a log-normal field

In the simulations we will considered further, the matter content follows a log-normal distribution, thus its density contrast will be given by (5.2). As discussed in Appendix A, a relevant object in the quantitative analysis of cosmological density fields is the correlation function. Hence, in this section we calculate the two and three-point correlation functions for

$\delta_L(\mathbf{x})$. From the definition (2.50) of the density constrast, $\langle\delta_L(\mathbf{x})\rangle$ must be zero; therefore,

$$\delta_L(\mathbf{x}) \equiv e^{\delta_G(\mathbf{x})-\frac{\sigma_G^2}{2}} - 1. \tag{5.8}$$

Two-point correlation function

The two-point correlation function is

$$\langle\delta_L(\mathbf{x}_1)\delta_L(\mathbf{x}_2)\rangle = \left\langle \left(e^{\delta_{G_1}-\frac{\sigma_1^2}{2}} - 1\right)\left(e^{\delta_{G_2}-\frac{\sigma_2^2}{2}} - 1\right)\right\rangle \tag{5.9}$$

$$\langle\delta_L(\mathbf{x}_1)\delta_L(\mathbf{x}_2)\rangle = e^{-\frac{\sigma_1^2}{2}-\frac{\sigma_2^2}{2}}\langle e^{\delta_{G_1}+\delta_{G_2}}\rangle - e^{-\frac{\sigma_1^2}{2}}\langle e^{\delta_{G_1}}\rangle - e^{-\frac{\sigma_2^2}{2}}\langle e^{\delta_{G_2}}\rangle + 1, \tag{5.10}$$

where $\delta_G(\mathbf{x}_i) \equiv \delta_{G_i}$ for the sake of simplicity. Using the property $\delta_{G_1} + \delta_{G_2} \sim \mathcal{N}(\mu = 0, \sigma^2 = \sigma_1^2 + \sigma_2^2 + 2\xi_{12})$ [127], where ξ_{12} is the correlation between the two Gaussian variables δ_{G_1} and δ_{G_2},

$$e^{-\frac{\sigma_1^2}{2}-\frac{\sigma_2^2}{2}}\langle e^{\delta_{G_1}+\delta_{G_2}}\rangle = e^{\xi_{12}}, \tag{5.11}$$

and hence

$$\langle\delta_L(\mathbf{x}_1)\delta_L(\mathbf{x}_2)\rangle = e^{\xi_{12}} - 1. \tag{5.12}$$

Three-point correlation function

Analogously to what has been done for the two-point correlation function, we can write

$$\langle\delta_L(\mathbf{x}_1)\delta_L(\mathbf{x}_2)\delta_L(\mathbf{x}_3)\rangle = \left\langle \left(e^{\delta_{G_1}-\frac{\sigma_1^2}{2}} - 1\right)\left(e^{\delta_{G_2}-\frac{\sigma_2^2}{2}} - 1\right)\left(e^{\delta_{G_3}-\frac{\sigma_3^2}{2}} - 1\right)\right\rangle \tag{5.13}$$

$$\begin{aligned} &= e^{-\frac{1}{2}\sum_{i=1}^3\sigma_i^2}\langle e^{\delta_{G_1}+\delta_{G_2}+\delta_{G_3}}\rangle - e^{-\frac{\sigma_1^2}{2}-\frac{\sigma_2^2}{2}}\langle e^{\delta_{G_1}+\delta_{G_2}}\rangle + \\ &- e^{-\frac{\sigma_1^2}{2}-\frac{\sigma_3^2}{2}}\langle e^{\delta_{G_1}+\delta_{G_3}}\rangle - e^{-\frac{\sigma_2^2}{2}-\frac{\sigma_3^2}{2}}\langle e^{\delta_{G_2}+\delta_{G_3}}\rangle + \\ &+ e^{-\frac{\sigma_1^2}{2}}\langle e^{\delta_{G_1}}\rangle + e^{-\frac{\sigma_2^2}{2}}\langle e^{\delta_{G_2}}\rangle + e^{-\frac{\sigma_3^2}{2}}\langle e^{\delta_{G_3}}\rangle - 1. \end{aligned} \tag{5.14}$$

Once again,

$$e^{-\frac{1}{2}\sum_{i=1}^3\sigma_i^2}\langle e^{\delta_{G_1}+\delta_{G_2}+\delta_{G_3}}\rangle = e^{\xi_{12}+\xi_{13}+\xi_{23}} \tag{5.15}$$

and, finally,

$$\langle \delta_L(\mathbf{x}_1)\delta_L(\mathbf{x}_2)\delta_L(\mathbf{x}_3)\rangle = e^{\xi_{12}}e^{\xi_{13}}e^{\xi_{23}} - e^{\xi_{12}} - e^{\xi_{13}} - e^{\xi_{23}} + 2. \tag{5.16}$$

In terms of the log-normal variables δ_{L_i} and δ_{L_j} correlation, $\xi^L_{ij} \equiv \langle \delta_{L_i}\delta_{L_j}\rangle$,

$$\langle \delta_L(\mathbf{x}_1)\delta_L(\mathbf{x}_2)\delta_L(\mathbf{x}_3)\rangle = \xi^L_{12}\xi^L_{13}\xi^L_{23} + \xi^L_{12}\xi^L_{13} + \xi^L_{12}\xi^L_{23} + \xi^L_{13}\xi^L_{23}. \tag{5.17}$$

From (5.16), or (5.17), we see that the log-normal density field $\delta_L(\mathbf{x})$ has an intrinsic three-point correlation function, which was already expected since it deviates from the Gaussian distribution.

In the case of $\xi_{ij} = b^2\xi^m_{ij}$ (as it happens for galaxies which are biased tracers[3] of the matter field δ_m, i.e. $\delta_{\rm gals} = b\delta_m$.), it is worth emphasizing that the three-point correlation function of the log-normal field will scale as the fourth (b^4) or sixth power (b^6) of the bias b, depending on which term has the largest contribution to the right hand side of equation (5.17).

5.1.4 Power-spectrum and bispectrum of a log-normal field

We shall now consider the Fourier counterpart of the two and three-point correlation functions obtained in the previous section, namely, the power-spectrum and bispectrum.

Power-spectrum

The power-spectrum is defined as the Fourier transform of the correlation function $\xi(\mathbf{x})$[4]:

$$P(\mathbf{k}) = \int e^{-i\mathbf{k}\cdot\mathbf{x}}\xi(\mathbf{x})d^3x. \tag{5.18}$$

For the isotropic case,

$$P(\mathbf{k}) = P(k) = 4\pi\int \xi(|\mathbf{x}|)\frac{\sin(kx)}{kx}x^2dx. \tag{5.19}$$

Henceforward it will be assumed that the physical correlation function, $\xi_{\rm ph}(\mathbf{x})$, is described by the log-normal field: $\xi^L(\mathbf{x}) \equiv \xi_{\rm ph}(\mathbf{x})$. With this hypothesis, the log-normal corre-

[3] See section 5.2 for more details on biased tracers of the (dark) matter distribution.

[4] See Appendix A for more details on correlation functions and their use in Cosmology.

lation function can be obtained from the inverse Fourier transform of some "physical" power-spectrum, $P_{\rm ph}(\mathbf{x})$, usually taken from some Boltzmann code such as CAMB[5] or CLASS[6]:

$$\xi^L(x) = \frac{V}{2\pi^2}\int P_{\rm ph}(k)\frac{\sin(kx)}{kx}k^2 dk \tag{5.20}$$

Once ξ^L is obtained through equation (5.20), the Gaussian correlation function $\xi^G(x) = \ln(1+\xi^L(x))$ and its Fourier transform, which gives the Gaussian power-spectrum $P_G(k)$, can be obtained. The process $P_{\rm ph}(k) \rightarrow \xi^L(x) \rightarrow \xi^G(x) \rightarrow P_G(k)$ is used to perform the log-normal simulation used further. The simulation consists of generating a random Gaussian field $\delta_G(\mathbf{k})$ (the Fourier modes of the simulated box are random variables which follow a Gaussian distribution), with $P_G(k)$ as its variance, that is used to derive the log-normal ("physical") density constrast from equation (5.8).

Figure 5.3 shows the comparison between the log-normal and the Gaussian power-spectra obtained from an input ("physical") CAMB power-spectrum.

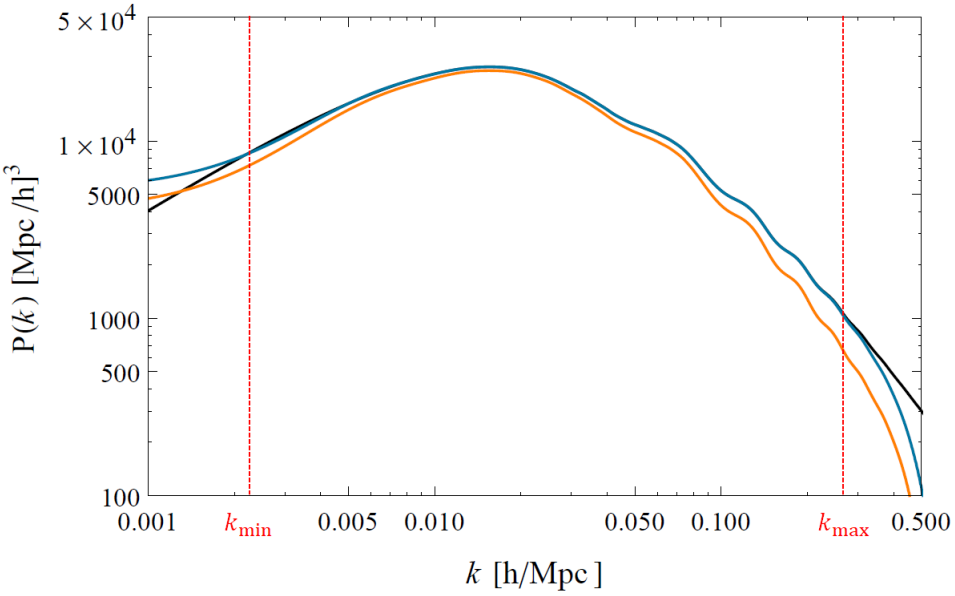

Figure 5.3: Comparison between the Gaussian (orange) power-spectrum and the input linear CAMB power-spectrum (black). From this plot it is evident the loss of power for the Gaussian spectrum, which fails to simulate the input $P_{\rm ph}$. The log-normal power-spectrum (blue) is obtained after taking the inverse Fourier transform of the log-normal correlation function ξ_{LN} in order to see the effects of the numerical integration scheme used. To overcome these numerical issues, only Fourier boxes with modes larger than $k_{\rm min}$ (left red-dashed line) and cells with modes smaller than $k_{\rm max}$ (right red-dashed line) must be considered.

[5]Code for Anisotropies in the Microwave Background - https://camb.info/
[6]Cosmic Linear Anisotropy Solving System - http://class-code.net/

Bispectrum

In analogy with the power-spectrum, the bispectrum is defined as the Fourier transform of the three-point correlation function. Here we derive an expression for the log-normal bispectrum. From scratch, in Fourier space we have:

$$\langle \delta_L(\mathbf{k}_1)\delta_L(\mathbf{k}_2)\delta_L(\mathbf{k}_3)\rangle = \left\langle \int e^{-i\mathbf{k}_1\cdot\mathbf{x}_1}\delta_L(\mathbf{x}_1)d^3x_1 \int e^{-i\mathbf{k}_2\cdot\mathbf{x}_2}\delta_L(\mathbf{x}_2)d^3x_2 \int e^{-i\mathbf{k}_3\cdot\mathbf{x}_3}\delta_L(\mathbf{x}_3)d^3x_3 \right\rangle, \tag{5.21}$$

$$= \int d^3x_1 d^3x_2 d^3x_3 e^{-i\mathbf{k}_1\cdot\mathbf{x}_1} e^{-i\mathbf{k}_2\cdot\mathbf{x}_2} e^{-i\mathbf{k}_3\cdot\mathbf{x}_3} \langle \delta_L(\mathbf{x}_1)\delta_L(\mathbf{x}_2)\delta_L(\mathbf{x}_3)\rangle, \tag{5.22}$$

$$\begin{aligned} = &\int d^3x_1 d^3x_2 d^3x_3 e^{-i\mathbf{k}_1\cdot\mathbf{x}_1} e^{-i\mathbf{k}_2\cdot\mathbf{x}_2} e^{-i\mathbf{k}_3\cdot\mathbf{x}_3} \xi^L_{12}\xi^L_{13}\xi^L_{23} + \\ &+ \int d^3x_1 d^3x_2 d^3x_3 e^{-i\mathbf{k}_1\cdot\mathbf{x}_1} e^{-i\mathbf{k}_2\cdot\mathbf{x}_2} e^{-i\mathbf{k}_3\cdot\mathbf{x}_3} \left(\xi^L_{12}\xi^L_{13} + \xi^L_{12}\xi^L_{23} + \xi^L_{13}\xi^L_{23}\right). \end{aligned} \tag{5.23}$$

We refer to the first integral of (5.23), henceforward, as the bispectrum connected piece, C_{123}, whereas the second integral will be called the disconnected piece, D_{123}. Therefore,

$$\langle \delta_L(\mathbf{k}_1)\delta_L(\mathbf{k}_2)\delta_L(\mathbf{k}_3)\rangle = C_{123} + D_{123}. \tag{5.24}$$

Considering first the connected piece,

$$C_{123} = \int \prod_{i=1}^{3} d^3x_i e^{-i\mathbf{k}_i\cdot\mathbf{x}_i} \xi^L(\mathbf{x}_1 - \mathbf{x}_2)\xi^L(\mathbf{x}_2 - \mathbf{x}_3)\xi^L(\mathbf{x}_3 - \mathbf{x}_1), \tag{5.25}$$

and rewriting the correlation function ξ in terms of the power-spectrum $P(k)$,

$$\xi_{ij} \equiv \xi(\mathbf{x}_i - \mathbf{x}_j) = \int \frac{d^3\mathbf{q}}{(2\pi)^3} e^{i\mathbf{q}\cdot(\mathbf{x}_i - \mathbf{x}_j)} P(\mathbf{q}), \tag{5.26}$$

we are led to

$$\begin{aligned} C_{123} = \int \frac{d^3q_1}{(2\pi)^3}\frac{d^3q_2}{(2\pi)^3}\frac{d^3q_3}{(2\pi)^3} P(\mathbf{q}_1)P(\mathbf{q}_2)P(\mathbf{q}_3) \int d^3x_1 e^{-i(\mathbf{k}_1 - \mathbf{q}_1 + \mathbf{q}_3)\cdot\mathbf{x}_1} \int d^3x_2 e^{-i(\mathbf{k}_2 - \mathbf{q}_2 + \mathbf{q}_1)\cdot\mathbf{x}_2} \times \\ \times \int d^3x_3 e^{-i(\mathbf{k}_3 - \mathbf{q}_3 + \mathbf{q}_2)\cdot\mathbf{x}_3} \end{aligned} \tag{5.27}$$

$$C_{123} = \int \frac{d^3q_1}{(2\pi)^3}\frac{d^3q_2}{(2\pi)^3}\frac{d^3q_3}{(2\pi)^3} P(\mathbf{q}_1)P(\mathbf{q}_2)P(\mathbf{q}_3)(2\pi)^3\delta(\mathbf{k}_1 - \mathbf{q}_1 + \mathbf{q}_3)(2\pi)^3\delta(\mathbf{k}_2 - \mathbf{q}_2 + \mathbf{q}_1)\times$$
$$\times (2\pi)^3\delta(\mathbf{k}_3 - \mathbf{q}_3 + \mathbf{q}_2) \tag{5.28}$$
$$= \int \prod_{i=1}^{3} d^3q_i P(\mathbf{q}_i)\delta(\mathbf{k}_1 - \mathbf{q}_1 + \mathbf{q}_3)\delta(\mathbf{k}_2 + \mathbf{q}_1 - \mathbf{q}_2)\delta(\mathbf{k}_3 - \mathbf{q}_3 + \mathbf{q}_2) \tag{5.29}$$
$$= \delta^D(\mathbf{k}_1 + \mathbf{k}_2 + \mathbf{k}_3)\int d^3\mathbf{q} P(|\mathbf{q} + \mathbf{k}_2|)P(|\mathbf{q} - \mathbf{k}_1|)P(|\mathbf{q}|) \tag{5.30}$$
$$= \delta^D(\mathbf{k}_1 + \mathbf{k}_2 + \mathbf{k}_3)\int d^3\mathbf{q} P(|\mathbf{q}|)P(|\mathbf{k}_1 - \mathbf{q}|)P(|\mathbf{k}_2 + \mathbf{q}|). \tag{5.31}$$

Taking into account that $\mathbf{q}\cdot\mathbf{k}_1 = qk_1\cos\theta_q$, $\mathbf{k}_1\cdot\mathbf{k}_2 = k_1k_2\cos\theta_{12}$ and $\mathbf{q}\cdot\mathbf{k}_2 = qk_2\cos\theta_{q2}$ (see Figure 5.4), equation (5.31) becomes

$$C_{123} = \delta^D(\mathbf{k}_1 + \mathbf{k}_2 + \mathbf{k}_3)\int q^2dq\sin\theta_q d\theta_q d\varphi_q P(|\mathbf{q} + \mathbf{k}_1|)P(|\mathbf{q} - \mathbf{k}_2|)P(|\mathbf{q}|), \tag{5.32}$$

where

$$|\mathbf{q} + \mathbf{k}_1| = \sqrt{q^2 + k_1^2 - 2qk_1\cos\theta_q} \tag{5.33}$$

and

$$|\mathbf{q} - \mathbf{k}_2| = \sqrt{q^2 + k_2^2 - 2qk_2\left(\cos\theta_{12}\cos\theta_q + \sin\theta_{12}\sin\theta_q\cos\varphi_q\right)}. \tag{5.34}$$

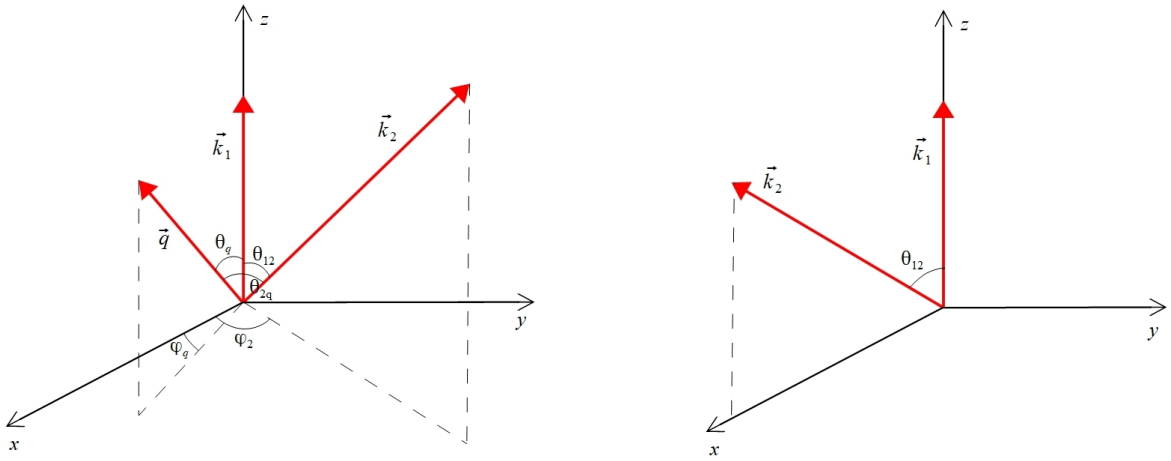

Figure 5.4: (*Left*) Schematic drawing for the vectors appearing in (5.31). In this configuration, $\mathbf{k}_1 = k_1\hat{z}$, $\mathbf{k}_2 = k_2(\cos\theta_{12}\hat{z} + \sin\theta_{12}\cos\varphi_2\hat{x} + \sin\theta_{12}\sin\varphi_2\hat{y})$ and $\mathbf{q} = q(\cos\theta_q\hat{z} + \sin\theta_q\cos\varphi_q\hat{x} + \sin\theta_q\sin\varphi_q\hat{y})$, so that $\mathbf{q}\cdot\mathbf{k}_2 = qk_2[\cos\theta_{12}\cos\theta_q + \sin\theta_{12}\sin\theta_q\cos(\varphi_q - \varphi_2)]$. (*Right*) Same scheme appearing on the left, but rotated in such a way that $\varphi_2 = 0$. Therefore, $\mathbf{q}\cdot\mathbf{k}_2 = qk_2[\cos\theta_{12}\cos\theta_q + \sin\theta_{12}\sin\theta_q\cos(\varphi_q)]$. We are omitting the $\mathbf{q}$ vector in the right drawing for clarity.

It is straightforward to see that the disconnected piece will give us the contribution

$$D_{123} = \delta^D(\mathbf{k}_1 + \mathbf{k}_2 + \mathbf{k}_3)\left[P(k_1)P(k_2) + P(k_1)P(k_3) + P(k_2)P(k_3)\right]. \tag{5.35}$$

Hence, the bispectrum is given by

$$\delta^D(\mathbf{k}_1 + \mathbf{k}_2 + \mathbf{k}_3)B(k_1, k_2, k_3) \equiv \delta^D_{123}B_{123} = \frac{C_{123} + D_{123}}{(2\pi)^3}, \tag{5.36}$$

$$\therefore B_{123} \equiv B_C + B_D \tag{5.37}$$

with

$$B_C = \frac{1}{(2\pi)^3}\int q^2 dq \sin\theta_q d\theta_q d\varphi_q P(|\mathbf{q} + \mathbf{k}_1|)P(|\mathbf{q} - \mathbf{k}_2|)P(|\mathbf{q}|) \tag{5.38}$$

and

$$B_D = \frac{1}{(2\pi)^3}\left[P(k_1)P(k_2) + P(k_1)P(k_3) + P(k_2)P(k_3)\right]. \tag{5.39}$$

In Figures 5.5 and 5.6 it is shown the separate contributions of C_{123} and D_{123}. In comparison with the disconnected piece, B_c is completely negligible.

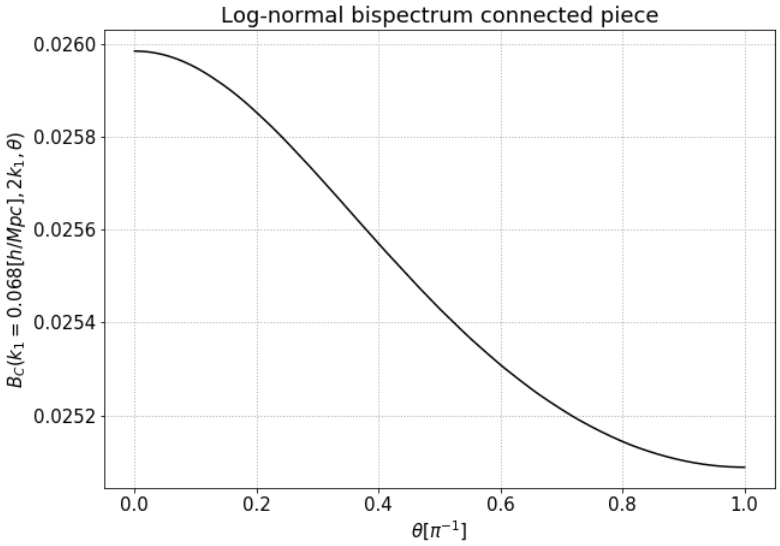

Figure 5.5: Connected part of the log-normal bispectrum (5.38) for a triangular configuration with $k_1 = 0.068[h/Mpc] = 0.5k_2$ and θ being the angle between the two vectors.

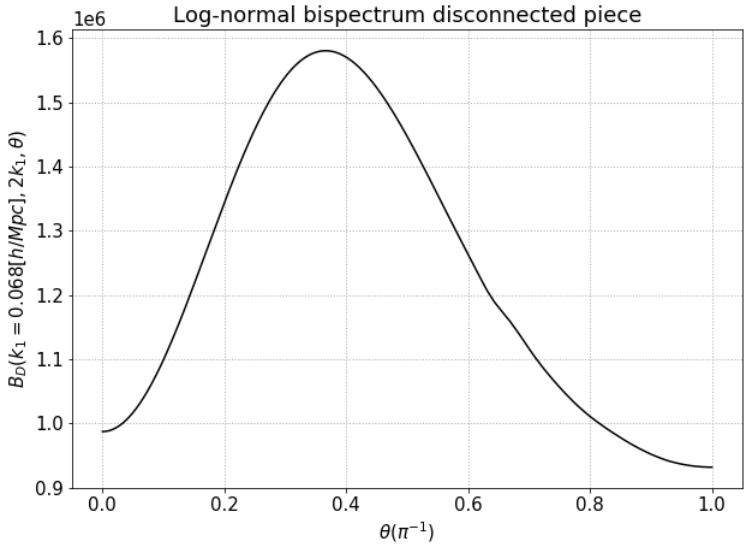

Figure 5.6: Disconnected part of the log-normal bispectrum (5.39) for the same configuration of Figure 5.5.

Figure 5.7 shows the reduced log-normal bispectrum as defined in (4.15) for the configuration $k_1 = 0.068h/Mpc, k_2 = 2k_1$. We can see that Q is a constant, $Q \approx 1$. This is what we expect from the "hierarchial form" for the three-point correlation function (or its Fourier counterpart) [30].

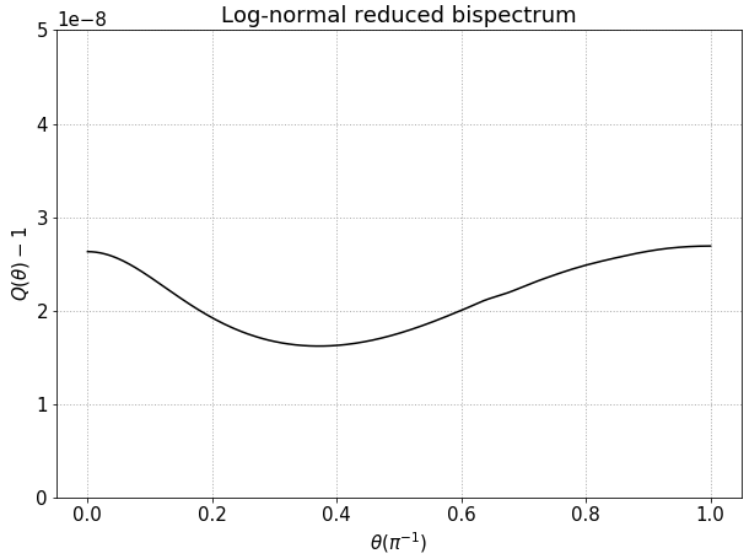

Figure 5.7: Reduced log-normal bispectrum, as defined in (4.15), for the configuration $k_1 = 0.068h/Mpc, k_2 = 2k_1$. Since the connected piece is negligible, we expect the reduced bispectrum being a constant $Q = 1$, as it is. This means that the log-normal field is completely specified by its two-point statistics.

5.2 From fields to galaxies

In the previous sections we addressed the statistics of a continuous density field, which may be thought of as the dark matter field. As studied in perturbation theory, collisionless dark matter forms structure due to gravitational instability alone.

Although it is also possible to trace the dark matter distribution by means of gravitational lensing, the most common observable in extra-galactic astronomy and cosmology is in the form of the distribution of galaxies. Besides, in this work the observational focus is on galaxy surveys. Hence, we must link the continuous statistics of the dark matter field, so far studied, to the galaxy distribution.

Firstly, unlike the simple models adopted to describe the dark matter component, galaxies are constituted by baryons, in the form of stars and hot gas, which are not only subjected to gravitational instability, but also to complex astrophysical processes which consequently changes the distribution of luminous matter in comparison to the dark matter density field. Besides, galaxies are assumed to live in dark matter halos, i.e. gravitationally bound structures containing many galaxies (e.g. groups and clusters of galaxies) [32].

Therefore, it is reasonable to assume that the galaxy density field $\delta_g(\mathbf{x})$ is a function of the dark matter field $\delta(\mathbf{x})$: $\delta_g(\mathbf{x}) = f[\delta(\mathbf{x})]$. Expanding the galaxy density contrast, we can thus define the bias parameters b_i [50],

$$\delta_g(\mathbf{x}) = b_1\delta(\mathbf{x}) + \frac{b_2}{2}\delta^2(\mathbf{x}) + \dots . \tag{5.40}$$

For simplicity, we consider throughout this work only the linear galaxy bias $b \equiv b_1$, such that $\delta_g(\mathbf{x}) = b\delta(\mathbf{x})$ [61, 113]. Therefore, it is said that galaxies trace the dark matter distribution. For this reason, two different tracers of the dark matter distribution, say α and β, will have different biases: $b_\alpha \neq b_\beta$.

We stress the fact that, by considering the Taylor expansion (5.40), the galaxy three-point correlation function depends not only on the matter three-point correlation function, but also on its four-point function statistics:

$$\langle\delta_g(\mathbf{x}_1)\delta_g(\mathbf{x}_2)\delta_g(\mathbf{x}_3)\rangle = b_1^3\langle\delta(\mathbf{x}_1)\delta(\mathbf{x}_2)\delta(\mathbf{x}_3)\rangle + b_1^2 b_2\langle\delta(\mathbf{x}_1)\delta(\mathbf{x}_2)\delta(\mathbf{x}_3)\delta(\mathbf{x}_3)\rangle + \dots . \tag{5.41}$$

Hence, considering only the linear bias leads to

$$\langle \delta_g(\mathbf{x}_1)\delta_g(\mathbf{x}_2)\delta_g(\mathbf{x}_3)\rangle \propto b_1^3\langle \delta(\mathbf{x}_1)\delta(\mathbf{x}_2)\delta(\mathbf{x}_3). \tag{5.42}$$

Secondly, in catalogs such as those obtained through redshift surveys, galaxies are treated as point-like objects distributed in the survey field and, if we ignore their individual properties, the distribution is a function solely of the positions [94]. Accordingly, there emerges the question on how the continuous matter field, as described by the log-normal distribution, for example, is related to the discrete count of galaxies in a survey.

5.2.1 Galaxy distribution as a point process

What galaxy surveys really measure are the position of individual galaxies in the sky, parametrized by the right ascension, declination and redshift. Analogously to what has been defined for the matter density contrast $\delta(\mathbf{x}) \equiv [\rho(\mathbf{x}) - \bar{\rho}]/\bar{\rho}$, we define the density contrast of galaxies as

$$\delta_g(\mathbf{x}) \equiv \frac{N(\mathbf{x}) - \bar{N}}{\bar{N}}, \tag{5.43}$$

where $N(\mathbf{x}) = n(\mathbf{x})\Delta V$ is the count of objects in a cell with volume ΔV and $n(\mathbf{x})$ is the number density of objects. The counts-in-cells can also be assigned a probability that a randomly placed cell of volume ΔV contains, on average, $N(\mathbf{x})$ objects.

Therefore, there are two processes which determine how the galaxies are going to be distributed in the sky: a continuous random process which characterizes the mass distribution $\rho(\mathbf{x})$, coming from theories such as inflation, and a point process generating a random discrete distribution over the continuous random field $\rho(\mathbf{x})$. This second process codifies the randomness of the counts of galaxies found in a survey.

The simplest distribution describing the statistics of counts of discrete objects is the Poisson distribution[7],

$$P(N|\lambda) = \frac{\bar{N}^N}{N!}e^{-\bar{N}}, \tag{5.44}$$

[7]To give a physical motivation to this distribution, here we cite the work of Saslaw and Hamilton, who showed, in 1984, that the probability of finding N galaxies in a volume V of arbitrary shape is given by $P(N|\bar{N}) = \frac{\bar{N}(1-b)}{N!}[\bar{N}(1-b)+Nb]^{N-1}e^{-\bar{N}(1-b)-Nb}$, where b encodes the ratio of the gravitational potential and kinetic energy of a system whose members interact in pairs, and $\bar{N} = \bar{n}V$ [104]. In the case of no gravitational interaction, $b = 0$, we recover the Poisson distribution (5.44) with $\lambda = \bar{N}$.

which gives the probability that a randomly placed cell i of volume V_i contains N individual objects (galaxies).

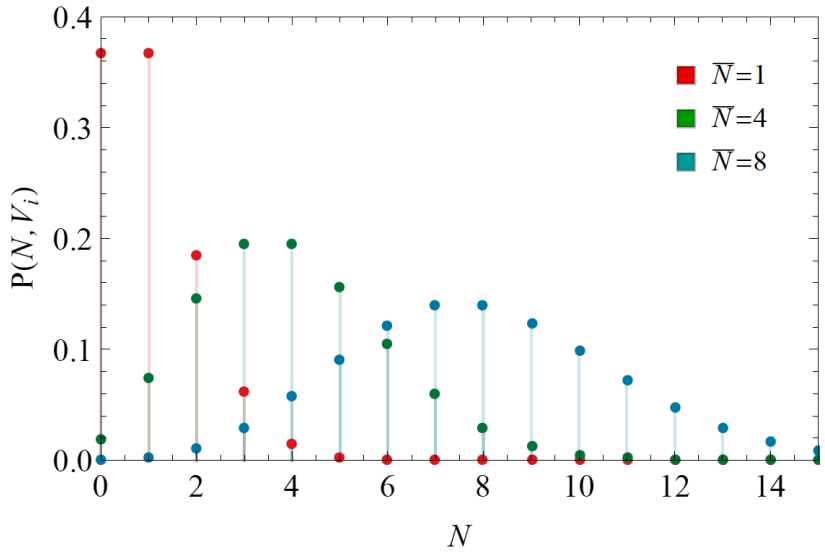

Figure 5.8: Poisson distribution (5.44) for three different values of $\bar{N}$, as a function of the number of galaxies (or occurances)

The first three moments of the Poisson distribution (5.44) are:

$$\begin{aligned} \langle N \rangle &= \bar{N}, \\ \langle N^2 \rangle &= \bar{N}(\bar{N}+1), \\ \langle N^3 \rangle &= \bar{N}(\bar{N}^2+3\bar{N}+1). \end{aligned} \tag{5.45}$$

From this we can see that $\bar{N}$ fully specifies the Poisson statistics. Also notice that for the case of small enough volumes dV_i such that the counts-in-cells is either one or zero, that is, the probability of finding more than one galaxy per cell is zero, from the moments of the Poisson distribution (5.45) we see that $\langle N^2 \rangle - \langle N \rangle^2 = \bar{N}$ and $\langle N^3 \rangle - 3\langle N \rangle \langle N^2 \rangle + 2\langle N \rangle^3 = \bar{N}$. That is, the central moments of the Poisson distribution in the case of occupation numbers either one or zero are all equal to $\bar{N}$.

Finally, the discrete galaxy distribution can related to the continuous random field $\delta_g(\mathbf{x})$ by writing (5.43) in terms of the number density of galaxies $n(\mathbf{x}) = N(\mathbf{x})/\Delta V$ as

$$n(\mathbf{x}) \equiv \bar{n}[1+\delta_g(\mathbf{x})]. \tag{5.46}$$

Two-point galaxy correlation function

In Appendix A is discussed the formal definitions of the correlation functions and spectral densities (such as the power-spectrum or bispectrum) for continuous random variables. However, galaxies are point-like objects, so let's think about discrete objects.

From (5.46), the probability of finding a galaxy in some volume element dV_i is $dP_i = n(\mathbf{x}_i)dV_i$. In the case of discrete variables, such as $n(\mathbf{x})$, we define the two-point correlation function as the excess probability of finding one galaxy a distance $\mathbf{r}_{ij} \equiv \mathbf{x}_j - \mathbf{x}_i$ apart from another galaxy or, as put by [94], as the probability of finding a pair with one galaxy in both dV_i and dV_j a distance $\mathbf{r}_{ij}$ apart from each other, that is

$$\begin{aligned} dP_{ij} &= \langle n(\mathbf{x}_i)n(\mathbf{x}_j)\rangle dV_i dV_j \\ &= \bar{n}^2(1 + \langle \delta_g(\mathbf{x}_i)\delta_g(\mathbf{x}_j)\rangle)dV_i dV_j \\ &= \bar{n}^2[1 + \xi_g(\mathbf{x}_i, \mathbf{x}_j)]dV_i dV_j. \end{aligned} \tag{5.47}$$

We emphasize that (5.47) is the discrete two-point correlation function of the random variable $n(\mathbf{x})$. Assuming the probability density function of the underlying continuous field, $\delta(\mathbf{x}_i)$ and $\delta(\mathbf{x}_j)$, to be a generic function $f(\mathbf{x}_i, \mathbf{x}_j)$, the expectation value of the number density of galaxies is related to the density field $\delta(\mathbf{x})$ as

$$\langle n(\mathbf{x}_i)n(\mathbf{x}_j)\rangle = \int f(\mathbf{x}_i, \mathbf{x}_j)\langle n(\mathbf{x}_i)n(\mathbf{x}_j)\rangle d^3x_i d^3x_j, \tag{5.48}$$

$$= \sum_{i,j} f(\mathbf{x}_i, \mathbf{x}_j)\langle n(\mathbf{x}_i)n(\mathbf{x}_j)\rangle, \tag{5.49}$$

$$= \sum_{i=j} f(\mathbf{x}_i, \mathbf{x}_j)\langle n(\mathbf{x}_i)\rangle dV_i + \sum_{i\neq j} f(\mathbf{x}_i, \mathbf{x}_j)\langle n(\mathbf{x}_i)n(\mathbf{x}_j)\rangle dV_i dV_j, \tag{5.50}$$

where to go from (5.49) to (5.50) we assumed the Poisson distribution for $n(\mathbf{x})$ in the limit of small enough cells, so that the occupation number is either one or zero, i.e. $\langle n^2\rangle = \langle n\rangle = \bar{n}$. In the continuum limit we have:

$$\langle n(\mathbf{x}_i)n(\mathbf{x}_j)\rangle = \int f(\mathbf{x}_i, \mathbf{x}_j)\bar{n}_i d^3x_i + \int f(\mathbf{x}_i, \mathbf{x}_j)\bar{n}_i\bar{n}_j\left[1 + \xi_g(\mathbf{x}_i, \mathbf{x}_j)\right] d^3x_i d^3x_j, \tag{5.51}$$

$$= \int f(\mathbf{x}_i, \mathbf{x}_j)\left(\bar{n}_i\delta^D(\mathbf{x}_i - \mathbf{x}_j) + \bar{n}_i\bar{n}_j\left[1 + \xi_g(\mathbf{x}_i, \mathbf{x}_j)\right]\right) d^3x_i d^3x_j. \tag{5.52}$$

By comparing (5.48) with (5.52), we see that the discrete two-point correlation function of

galaxies is related to the continuous distribution as

$$\langle n(\mathbf{x}_i)n(\mathbf{x}_j)\rangle = \bar{n}_i\delta^D(\mathbf{x}_i - \mathbf{x}_j) + \bar{n}_i\bar{n}_j\left[1 + \xi_g(\mathbf{x}_i, \mathbf{x}_j)\right]. \tag{5.53}$$

From (5.46), the Fourier transform of the density contrast field is

$$\delta_g(\mathbf{k}) = \frac{1}{\bar{n}}\sum_i e^{-i\mathbf{k}\cdot\mathbf{x}_i} - \delta^D(\mathbf{k}), \tag{5.54}$$

and then the two-point correlation function of the galaxies number density can be written as

$$\langle n(\mathbf{x}_1)n(\mathbf{x}_2)\rangle = \bar{n}^2[1 + \xi_g(\mathbf{r}_{12})] + \bar{n}\delta^D(\mathbf{x}_2 - \mathbf{x}_1). \tag{5.55}$$

Hence, the density correlation function is

$$\langle \delta_g(\mathbf{x}_1)\delta_g(\mathbf{x}_2)\rangle \equiv \xi_g(\mathbf{r}_{12}) = b^2\xi(\mathbf{r}_{12}) + \frac{1}{\bar{n}}\delta^D(\mathbf{x}_2 - \mathbf{x}_1). \tag{5.56}$$

where we used the fact that galaxies are a biased tracers of the matter density field, leading to $\xi_g(\mathbf{r}_{12}) = b^2\xi(\mathbf{r}_{12})$. Equation (5.56) above has a correction of $\bar{n}^{-1}$ to the continuous density field $\xi_g(\mathbf{r}_{12})$ coming from the discrete nature of the galaxies. This correction is known as Poisson shot-noise.

Galaxy power-spectrum

Taking the Fourier transform of (5.56), we obtain

$$P_g(\mathbf{k}) = b^2P(\mathbf{k}) + \frac{1}{\bar{n}}. \tag{5.57}$$

Three-point galaxy correlation function

Just as it has been done for the two-point correlation function, the three-point correlation function is written as the excess probability of finding a galaxy in each dV_1, dV_2 and dV_3 a distance $\mathbf{r}_{12}$, $\mathbf{r}_{13}$ and $\mathbf{r}_{23}$ apart from each other, that is

$$dP = \langle n(\mathbf{x}_1)n(\mathbf{x}_2)n(\mathbf{x}_3)\rangle dV_1dV_2dV_3, \tag{5.58}$$

$$dP = \bar{n}^3(1 + \langle\delta_g(\mathbf{x}_1)\delta_g(\mathbf{x}_2)\rangle + \langle\delta_g(\mathbf{x}_1)\delta_g(\mathbf{x}_3)\rangle + \langle\delta_g(\mathbf{x}_2)\delta_g(\mathbf{x}_3)\rangle + \\ + \langle\delta_g(\mathbf{x}_1)\delta_g(\mathbf{x}_2)\delta_g(\mathbf{x}_3)\rangle)dV_1dV_2dV_3, \\ = \bar{n}^3[1 + \xi_g(\mathbf{x}_1, \mathbf{x}_2) + \xi_g(\mathbf{x}_1, \mathbf{x}_3) + \xi_g(\mathbf{x}_2, \mathbf{x}_3) + \zeta_g(\mathbf{x}_1, \mathbf{x}_2, \mathbf{x}_3)dV_1dV_2dV_3. \tag{5.59}$$

Following the same steps we did for the two-point function,

$$\langle\delta_g(\mathbf{x}_1)\delta_g(\mathbf{x}_2)\delta_g(\mathbf{x}_3)\rangle \equiv \zeta_g(\mathbf{r}_{123}) = b^3\zeta(\mathbf{r}_{123}) + \frac{b^2}{\bar{n}}\left[\delta^D_{12}\xi_{12} + \delta^D_{13}\xi_{13} + \delta^D_{23}\xi_{23}\right] + \bar{n}^{-2}\delta^D_{12}\delta^D_{23}. \tag{5.60}$$

Galaxy bispectrum

Taking the Fourier transform of (5.60), we obtain

$$B_g(\mathbf{k}_1, \mathbf{k}_2, \mathbf{k}_3) = b^3B(\mathbf{k}_1, \mathbf{k}_2, \mathbf{k}_3) + \frac{b^2}{\bar{n}}\left[P(\mathbf{k}_1) + P(\mathbf{k}_2) + P(\mathbf{k}_3)\right] + \frac{1}{\bar{n}^2}. \tag{5.61}$$

5.2.2 Biased log-normal densities

In order to address the fact that galaxies are biased tracers of the matter density, we define the log-normal density field as [4]

$$\delta_L(\mathbf{x}) = e^{b\delta_G(\mathbf{x}) - b^2\frac{\sigma^2}{2}} - 1, \tag{5.62}$$

where b is the bias of the tracer we seek to simulate. Therefore, the log-normal (physical) correlation function is related to the Gaussian one through the relation

$$b^2\xi_L = \ln\left(e^{b^2\xi_G} - 1\right). \tag{5.63}$$

After these maps are generated, applying the Poisson statistics creates "galaxy" maps over the log-normal density field and each of the tracers are going to have their own mean number density $\bar{n}$ over the biased "matter" field. A code capable of generating these mock maps of large-scale structure has already been developed within our group by Raul Abramo, Lucas Secco and Arthur Loureiro (see reference [4] for more details).

5.2.3 Multi-tracer technique for galaxy surveys

The most familiar tracers of the dark matter distribution are in the form of galaxies. However, quasars, Lyman-α forest, galaxy clusters, among many other objects, can also be used to trace the large-scale distribution of matter, sharing the property of being biased tracers of the matter density contrast, i.e. $\delta_\alpha = b_\alpha \delta$, where α refers to some particular tracer.

Table 5.1 below shows the commonly used values for the biases of different tracers of LSS, at redshift $z \sim 0$.

	b	$\bar{\mathbf{n}}$ [h^3 Mpc^{-3}]
LRGs	$\sim 1.5 - 2$	$\sim 10^{-4}$
ELGs	$\sim 0.8 - 1.5$	$\sim 10^{-2} - 10^{-3}$
QSOs	~ 2	$\sim 10^{-5}$
Groups	~ 1	$\sim 10^{-2}$
Clusters	> 2	$\sim 10^{-4}$

Table 5.1: Examples of bias b and mean number density $\bar{n}$, around redshift $z = 0$, for some tracers of the large-scale structure: luminous red galaxies (LRGs), emission line galaxies (ELGs), quasars (QSOs), groups and clusters of galaxies. Values are spread throughout the literature, but can be found, e.g., in [110], [116] and [126].

The development of surveys with increasing sky coverage allows us to obtain many tracers and different ways to probe the matter distribution, therefore decreasing statistical uncertainties. However, surveys are only capable of covering a finite volume of the sky and this limits the number of modes k we can analyze. This problem is known as cosmic variance and it is the main source of limitation for large-scale measurements.

It was shown by Seljak that the limitation imposed by cosmic variance can be mitigated by correlating tracers with different biases b, improving the constraints of non-Gaussian parameters such as f_{NL}. The main idea is that, in the absence of primordial non-Gaussianities, the relative bias of two different tracers b_α/b_β does not depend on scale, being limited only by the Poisson shot noise [110]. Not restricted to primordial non-Gaussianities, the multi-tracer technique also improves the constraints on bias sensitive parameters [3].

In Figure 5.9 we present a forecast for two future surveys, Euclid and SKA, done by Yamauchi and collaborators [132], which shows the improvement on the constraints of $f_{NL}^{\rm eq}$ and $f_{NL}^{\rm orth}$ when the multi-tracer technique is applied to the bispectrum.

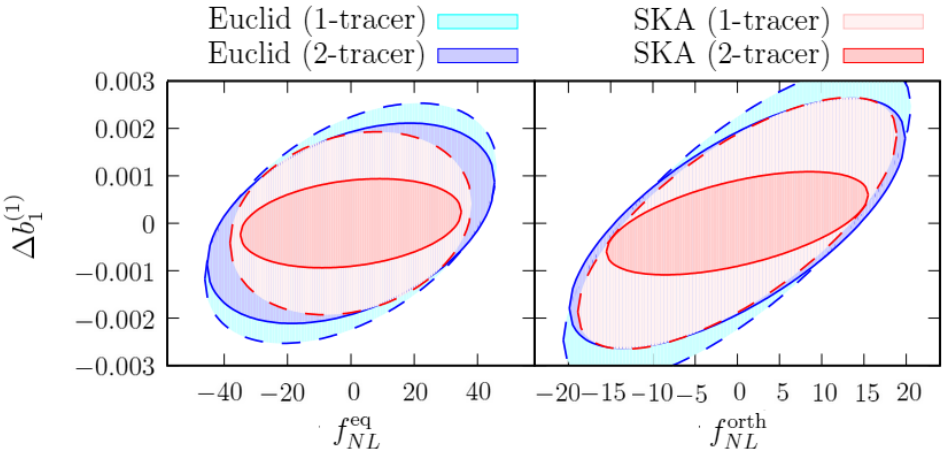

Figure 5.9: 1σ constraints on the bias parameter b_1 of one tracer and the two non-linear shapes $f_{NL}^{\rm eq}$ and $f_{NL}^{\rm orth}$. It was accounted in the analysis the cases with one and two tracers for Euclid [45], and SKA Phase-2 [22] forecasts. The forecasts done by Yamauchi and collaborators gave $\sigma(f_{NL}^{\rm eq}) = 25.1$ (1-tracer) and 23.0 (2-tracer) for the SKA phase-2, and $\sigma(f_{NL}^{\rm eq}) = 30.4$ (1-tracer) and 30.0 (2-tracer) for Euclid. For the orthogonal shape, forecasts gave $\sigma(f_{NL}^{\rm orth}) = 12.4$ (SKA 1-tracer), 13.6 (Euclid 1-tracer) and 10.2 (SKA 2-tracer), 13.1 (Euclid 2-tracer). The conclusions from [132] is that SKA is better suited to multi-tracer technique than Euclid, since the low-z source density is expected to be higher than Euclid's, and that SKA survey thus can improve the Planck constraints ($\sigma(f_{NL}^{\rm eq}) = 43$, $\sigma(f_{NL}^{\rm orth}) = 21$) [100] by a factor of ~ 2. Extracted from [132].

5.3 Extracting higher-order statistics

In this section we describe a way to obtain the bispectrum by means of the FFT bispectrum estimator, following the derivations of Donghui Jeong's PhD thesis [60], chapter 7, and of the recent paper by Catherine Watkinson and collaborators [129]. For initial (but unmentioned) use of this estimator see the work of Román Scoccimarro [108].

5.3.1 The FFT Bispectrum Estimator

Consider the discrete Fourier transform

$$\delta(\mathbf{x}) = \frac{1}{V}\sum \delta(\mathbf{k}) e^{i\mathbf{k}\cdot\mathbf{x}} \quad \text{and} \quad \delta(\mathbf{k}) = \frac{V}{N_{\rm pix}}\sum \delta(\mathbf{x}) e^{-i\mathbf{k}\cdot\mathbf{x}}, \tag{5.64}$$

where $\delta(\mathbf{x})$ is the density field one wishes to analyse, $\delta(\mathbf{k})$ is its discrete Fourier transform and $N_{\rm pix} = N^3$ is the total number of pixels (cells) within the volume V. The polyspectra $\mathscr{P}$, defined as

$$(2\pi)^3 \mathscr{P}(\mathbf{k}_1, \ldots, \mathbf{k}_p)\delta^D(\mathbf{k}_1 + \ldots + \mathbf{k}_p) = \Big\langle \delta(\mathbf{k}_1)\ldots\delta(\mathbf{k}_p)\Big\rangle, \tag{5.65}$$

must be translated to its discrete version since the grids of simulations contain pixelised data. The connection between the Dirac and Kronecker deltas, respectively denoted by δ^D and δ^K, is

$$\delta^D(\mathbf{k}) = \frac{1}{k_{\rm F}^3}\delta^K(\mathbf{m}) = \frac{V}{(2\pi)^3}\delta^K(\mathbf{m}), \tag{5.66}$$

where $\mathbf{m}$ is the dimensionless pixel coordinate (m_x, m_y, m_y), i.e. maps the grid points, such that $\mathbf{k} = \frac{2\pi}{L}\mathbf{m} \equiv k_{\rm F}\mathbf{m}$, and $\mathbf{L} = (L_x, L_y, L_z)$ is the length of the simulated box sides. For the case of an unnormalized FFT routine, the FFT of the input density constrast, $\Delta(k_{\rm F}\mathbf{m})$, is related to the Fourier density constrast as

$$\Delta(k_{\rm F}\mathbf{m}) = \frac{N_{\rm pix}}{V}\delta(\mathrm{k}) \tag{5.67}$$

where the$\Delta(k_{\rm F}\mathbf{m})$ is the Fast Fourier Transform (FFT) of the input density constrast, which can be easily obtained through numerical libraries such as the `numpy.fft`, in Python, or `FFTW`, in C. Therefore, the discrete version of (5.65) is:

$$\mathscr{P}(\mathbf{k}_1, \ldots, \mathbf{k}_p)\delta^K(\mathbf{m}_1 + \ldots + \mathbf{m}_p) \approx \frac{V^{p-1}}{N_{\rm pix}^p}\Big\langle \Delta(k_{\rm F}\mathbf{m}_1)\ldots\Delta(k_{\rm F}\mathbf{m}_p)\Big\rangle. \tag{5.68}$$

The equality of equation (5.65) becomes an approximation in (5.68) since the average is performed within a binwidth of, at least, $k_{\rm F}$ [129]. By enforcing the Kronecker delta on the right hand side of (5.68),

$$\begin{aligned}\mathscr{P}(\mathbf{k}_1, \ldots, \mathbf{k}_p) &\approx \frac{V^{p-1}}{N_{\rm pix}^p}\left\langle \prod_{i=1}^{p}\delta^K(\mathbf{m}_1 + \ldots + \mathbf{m}_p)\Delta(k_{\rm F}\mathbf{m}_i)\right\rangle; \\ &\approx \frac{V^{p-1}}{N_{\rm pix}^p}\frac{\sum_{\mathbf{m}_1\simeq\mathbf{n}_1}\cdots\sum_{\mathbf{m}_p\simeq\mathbf{n}_p}\prod_{i=1}^{p}\delta^K(\mathbf{m}_1 + \ldots + \mathbf{m}_p)\Delta(\mathbf{m}_i)}{\sum_{\mathbf{m}_1\simeq\mathbf{n}_1}\cdots\sum_{\mathbf{m}_p\simeq\mathbf{n}_p}\prod_{i=1}^{p}\delta^K(\mathbf{m}_1 + \ldots + \mathbf{m}_p)},\end{aligned} \tag{5.69}$$

where $\sum_{\mathbf{m}_i\simeq\mathbf{n}_i}$ formally means the sum over all $\mathbf{m}_i$ vectors that fall within some arbitrary bin of width $\mathbf{s}$ and $\mathbf{n} = \left(\frac{N_x x}{L_x}, \frac{N_y y}{L_y}, \frac{N_z z}{L_z}\right)$, with N_x, N_y, N_z the number of pixels on each side of the box. By noticing that

$$\delta^K(\mathbf{m}_1 + \ldots + \mathbf{m}_p) = \frac{1}{N_{\rm pix}}\sum_{n}^{N_{\rm pix}}\prod_{i=1}^{p}e^{2\pi i n\cdot m_i/N_{\rm side}}, \tag{5.70}$$

with $N_{\rm side}$ being the number of pixels on each side of the cube, the polyspectrum estimator is written as

$$\mathscr{P}(\mathbf{k}_1,\ldots,\mathbf{k}_p) \approx \frac{V^{p-1}}{N_{\rm pix}^p}\frac{\sum_{\mathbf{n}}^{N_{\rm pix}}\prod_{i=1}^{p}\delta(\mathbf{n},\mathbf{k}_i)}{\sum_{\mathbf{n}}^{N_{\rm pix}}\prod_{i=1}^{p}I(\mathbf{n},\mathbf{k}_i)}, \tag{5.71}$$

where

$$\delta(\mathbf{n},\mathbf{k}_i) = \sum_{\mathbf{m}_i\in\mathbf{k}_i\pm s/2}\Delta(\mathbf{m}_i)e^{2\pi i\mathbf{n}\cdot\mathbf{m}_i/N_{\rm side}}, \tag{5.72}$$

and

$$I(\mathbf{n},\mathbf{k}_i) = \sum_{\mathbf{m}_i\in\mathbf{k}_i\pm s/2}e^{2\pi i\mathbf{n}\cdot\mathbf{m}_i/N_{\rm side}}. \tag{5.73}$$

Notice that, for the case of $p = 3$, $I(\mathbf{n},\mathbf{k}_i)$ is the total number of independent triangles with sides (k_1, k_2, k_3) [60]. The procedure to obtain $\mathscr{P}$ is illustrated in Figure 5.10 for the case of the bispectrum, i.e. $p = 3$.

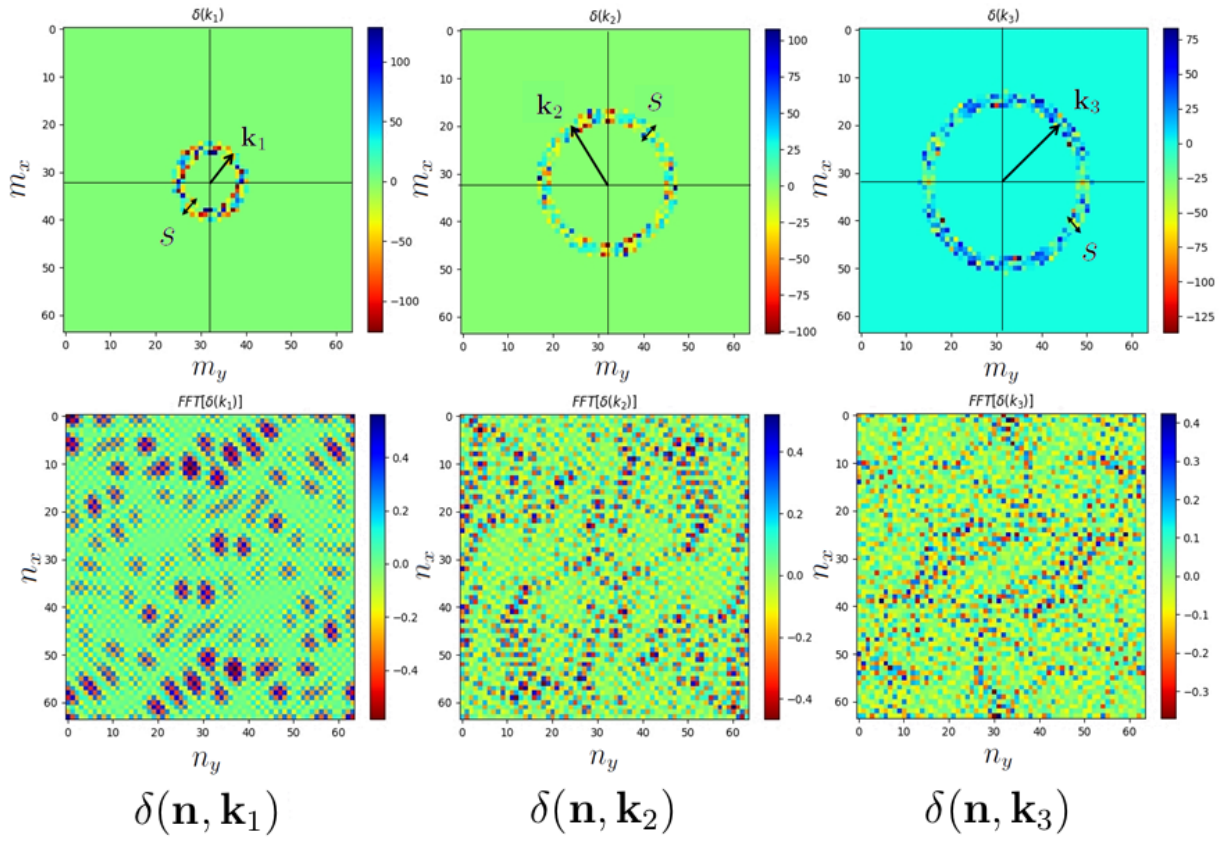

Figure 5.10: The process of obtaining $\delta(\mathbf{n},\mathbf{k}_i)$. We begin by getting the normalization factors $I(\mathbf{n},\mathbf{k}_i)$ which are one whenever a pixel matches the condition $\mathbf{m}_i \in \mathbf{k}_i \pm s/2$. Then, $\delta(\mathbf{n},k_i) = I(\mathbf{n},k_i)\delta_{\rm gal}$. (*Top*) Point selection for which the FFT of the galaxies density field $\delta_{\rm gal}$ falls into a bin of width s, separated from the origin by $|\mathbf{k}_i|$. (*Bottom*) Inverse transform of the objects shown in the top figure. This process introduces the $\mathbf{n}$ in $\delta(\mathbf{k}_i)$.

Compared to the direct sampling method (see [60], p. 268), which computes the bispectrum as

$$B(\mathbf{k}_1, \mathbf{k}_2, \mathbf{k}_3) = \frac{1}{(2\pi)^3} \frac{1}{N_{\rm tri}} \sum_{m \in {\rm Tri}_{123}} \Delta(k_{\rm F}\mathbf{m}_1)\Delta(k_{\rm F}\mathbf{m}_2)\Delta(k_{\rm F}\mathbf{m}_3), \tag{5.74}$$

where $N_{\rm tri}$ is the total number of triangles and ${\rm Tri}_{123}$ is the set of $\{\mathbf{m}_1, \mathbf{m}_2, \mathbf{m}_3\}$ which form the triangles with $\mathbf{k}_1 + \mathbf{k}_2 + \mathbf{k}_3 = 0$, the main disadvantage of the direct measurement, (5.74), one must account for all the possible triangle configurations available and this process poses a computational challenge to estimate the bispectrum, which is of order $N^3_{\rm pix}$ (all possible combinations of pixels forming the triangles of interest).

What happens in the case of the FFT-estimator is that there is no need to select the possible configurations; instead, the spherical shells containing $\delta(k_i)$ (top panels of Figure 5.10), when Fourier transformed to real space, take care of all the possible triangles defined by $\mathbf{k}_1, \mathbf{k}_2$ and $\mathbf{k}_3$; i.e., in the bottom panels showed in Figure 5.10, only the points of the density contrast field forming the triangles which satisfies $\mathbf{k}_1 + \mathbf{k}_2 + \mathbf{k}_3 = 0$ are selected. This reduces the number of operations to a fairly small amount of operations: since the grid and the thickness s of the spherical shells are finite, the number of shells is limited.

To summarize the results, we have that

$$P(\mathbf{k}_1, -\mathbf{k}_1) = P(k) \approx \frac{V}{N^2_{\rm pix}} \frac{\sum_{\mathbf{n}}^{N_{\rm pix}} \delta(\mathbf{n}, k)\delta(\mathbf{n}, k)}{\sum_{\mathbf{n}}^{N_{\rm pix}} I(\mathbf{n}, k)I(\mathbf{n}, k)} \tag{5.75}$$

and

$$B(\mathbf{k}_1, \mathbf{k}_2, \mathbf{k}_3) \approx \frac{V^2}{N^3_{\rm pix}} \frac{\sum_{\mathbf{n}}^{N_{\rm pix}} \delta(\mathbf{n}, \mathbf{k}_1)\delta(\mathbf{n}, \mathbf{k}_2)\delta(\mathbf{n}, \mathbf{k}_3)}{\sum_{\mathbf{n}}^{N_{\rm pix}} I(\mathbf{n}, \mathbf{k}_1)I(\mathbf{n}, \mathbf{k}_2)I(\mathbf{n}, \mathbf{k}_3)} \tag{5.76}$$

are, respectively, the power and bispectrum FFT-estimators.

The estimators described above have been implemented during this work and, in the next chapter, the results obtained from applying (5.75) and (5.76) to mocks of galaxy catalogs generated using the log-normal approximation and the Poisson process studied so far are presented.

Chapter 6

Results

In this chapter we present the main results obtained within this work using the code we developed to compute the bispectrum of mock catalogs of multiple tracers of large-scale structure. We compared the bispectra of different tracers and observed the improvement in the error bars of the estimates.

6.1 Simulating galaxy maps

In order to test the FFT bispectrum estimator, the log-normal approximation and the Poisson process are used to generate the mocks of galaxy catalogs in an efficient way. For that, the code developed by Raul Abramo, Lucas Secco and Arthur Loureiro [4] was used. Besides being capable of generating the maps for several tracers, the code also computes the power-spectrum and its covariance matrices using an optimal multi-tracer estimator.

In our simulation we use the fiducial ΛCDM cosmology given by the 2015 Planck measurements [99]: $\Omega_{\rm cdm} = 0.258$, $\Omega_b = 0.0484$, $\Omega_k = 0$, $H_0 = 67.8$ km s^{-1} Mpc^{-1}, $n_s = 0.9667$, $w_0 = -0.999$[1], $\ln_{10} e^{10} A_s = 3.0904$ and $z_{\rm re} = 8.8$. The physical cell size ℓ in the simulations have units of Mpc h^{-1}. Therefore, if the simulation box has n_x, n_y and n_z cells on each side, then they all have length $L_x = n_x \ell$ Mpc h^{-1} and so on.

In the following section, the essentials of the selection function used to simulate the galaxy maps are presented.

[1]The package we use to perform cosmological calculations, `NumCosmo` (https://numcosmo.github.io/), does not accept $w_0 = -1$. Therefore, we use the approximation $w_0 = -0.999$.

6.1.1 Selection function

A common strategy to build a galaxy catalog in a redshift survey is by setting a magnitude limit $m_{\rm lim}$, that is, galaxies with $m > m_{\rm lim}$ cannot be seen in the survey or are not considered [81]. Hence, in a magnitude-limited survey, the number of objects is a function of the distance from the observer. In order to perform statistical analysis of the sample, we must quantify this effect. One way to do this is by means of the selection function $\bar{n}(r)$, which gives an estimate of the probability that a galaxy brighter than a certain cutoff is detected by the survey.

In our simulations, we model the selection function $\bar{n}(r)$ as a Gaussian

$$\bar{n}(r) = n_0 \exp\left[-\frac{(r-c_1)^2}{c_2^2}\right], \tag{6.1}$$

where n_0 gives a mean number density of objects in grid units, r is the distance from Earth to the slices in depth of the sky.

Below, the effects of the selection function on simulated maps of three different tracers, i.e. with different biases, are presented. Examples of one-dimensional selection function profiles are shown in Figures 6.1, 6.4 and 6.7.

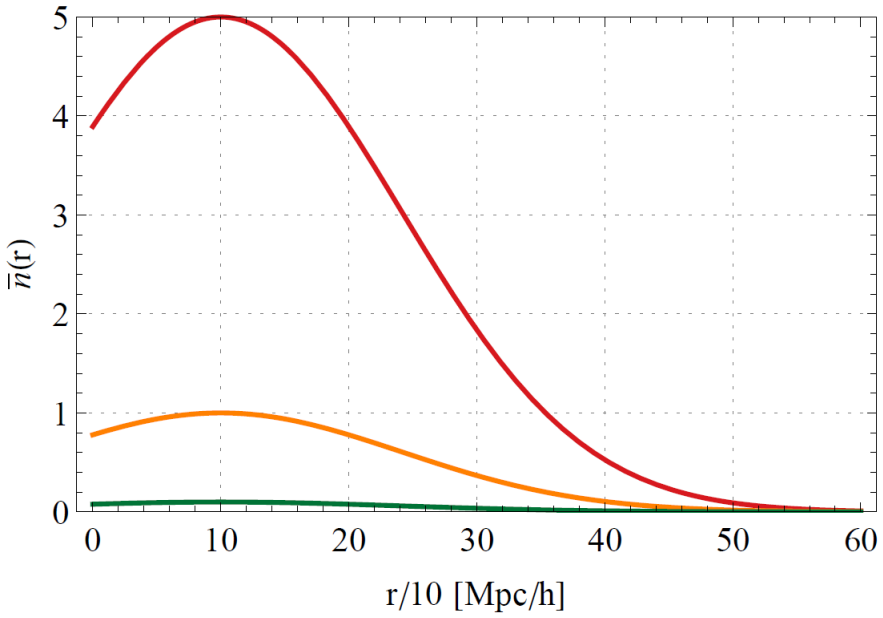

Figure 6.1: Selection function profile with constant $c_1 = 10$ Mpc h^{-1} and $c_2 = 20$ Mpc h^{-1}, but with $n_0 = 5$ h^3 Mpc^{-3} (*red*), $n_0 = 1$ h^3 Mpc^{-3} (*orange*) and $n_0 = 0.1$ h^3 Mpc^{-3} (*green*). Comparing these values of n_0 with $\bar{n}$ presented in Table 5.1 for several tracers of LSS, one can see how large the values of n_0 are. The reason why we have chosen these values is to completely neglect the Poisson shot-noise, calculated in section §5.2.1, for the power-spectrum, equation (5.57), and the bispectrum, equation (5.61).

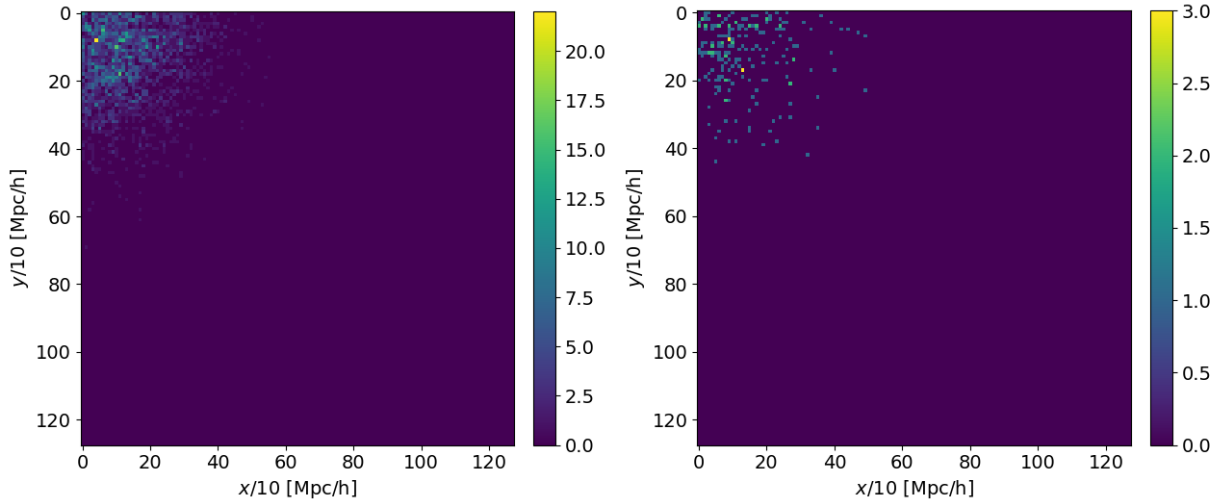

Figure 6.2: Mock galaxy map simulated with the selection function (6.1) for a tracer with bias $b = 1$, $n_0 = 5$ h^3 Mpc^{-3}, $c_1 = 10$ Mpc h^{-1} and $c_2 = 20$ Mpc h^{-1} at redshift $z = 2$. (*Left*) Slice taken at $z = 100$ Mpc h^{-1}. (*Right*) Slice taken at $z = 400$ Mpc h^{-1}.

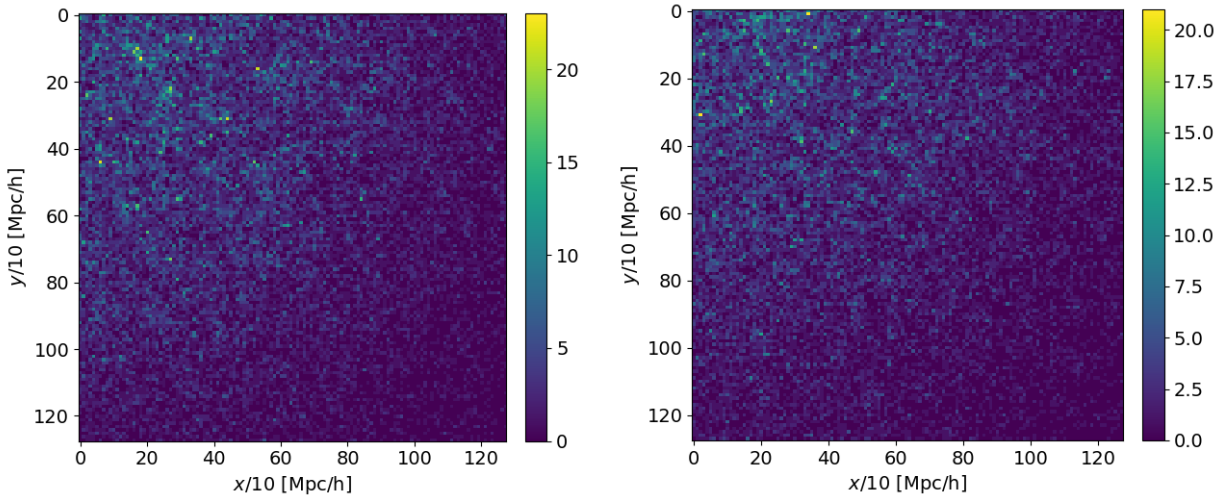

Figure 6.3: Mock galaxy map simulated with the selection function (6.1) for a tracer with bias $b = 1$, $n_0 = 5$ h^3 Mpc^{-3}, $c_1 = 1$ Mpc h^{-1} and $c_2 = 100$ Mpc h^{-1} at redshift $z = 2$. (*Left*) Slice taken at $z = 100$ Mpc h^{-1}. (*Right*) Slice taken at $z = 400$ Mpc h^{-1}.

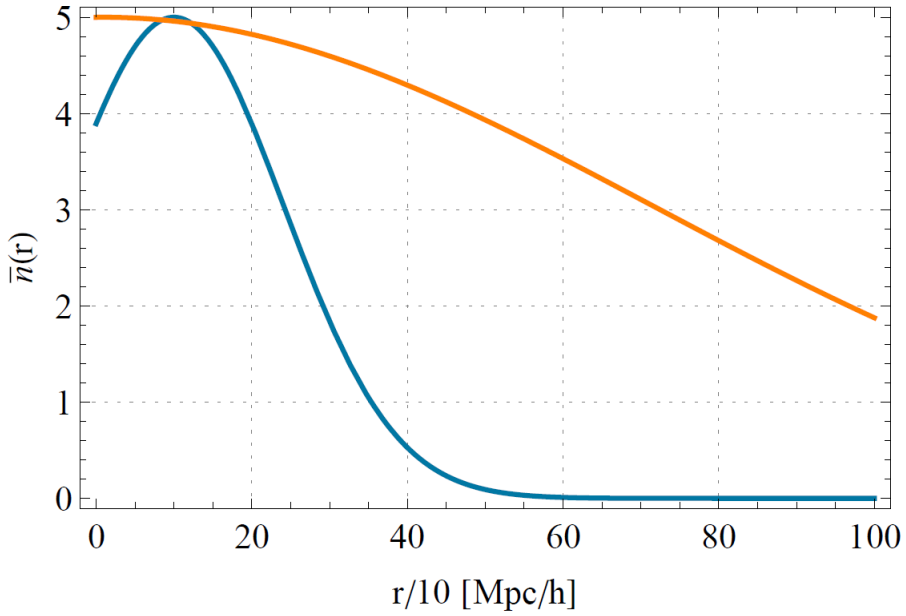

Figure 6.4: Selection function profile with constant $n_0 = 5$ h^3 Mpc^{-3}, but with $c_1 = 10$ Mpc h^{-1} and $c_2 = 20$ Mpc h^{-1} (*blue*) and $c_1 = 1$ Mpc h^{-1} and $c_2 = 100$ Mpc h^{-1} (*orange*).

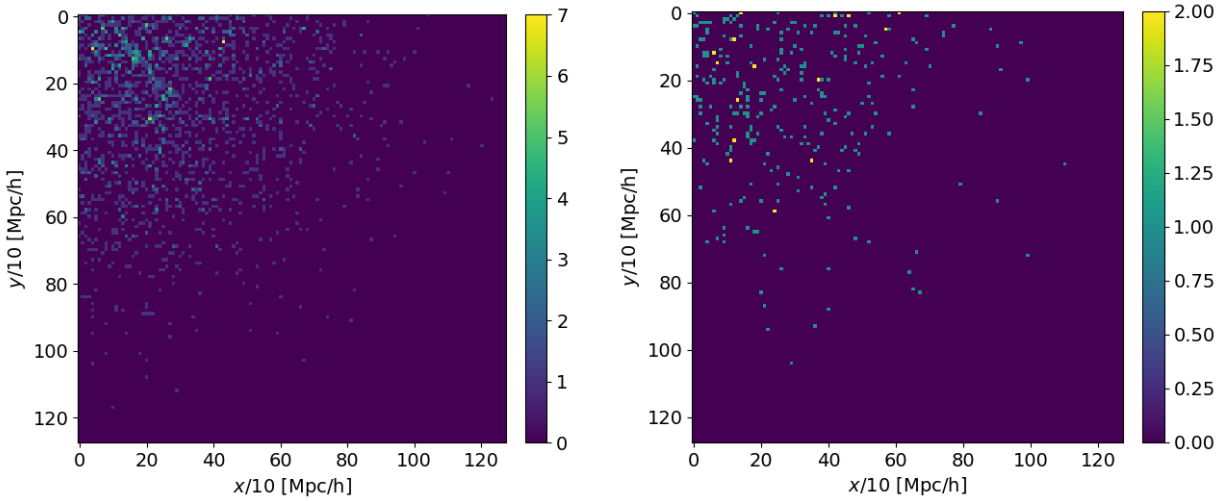

Figure 6.5: Mock galaxy map simulated with the selection function (6.1) for a tracer with bias $b = 1.3$, $n_0 = 1$ h^3 Mpc^{-3}, $c_2 = 1$ Mpc h^{-1} and $c_1 = 50$ Mpc h^{-1} at redshift $z = 2$. (*Left*) Slice taken at $z = 100$ Mpc h^{-1}. (*Right*) Slice taken at $z = 700$ Mpc h^{-1}.

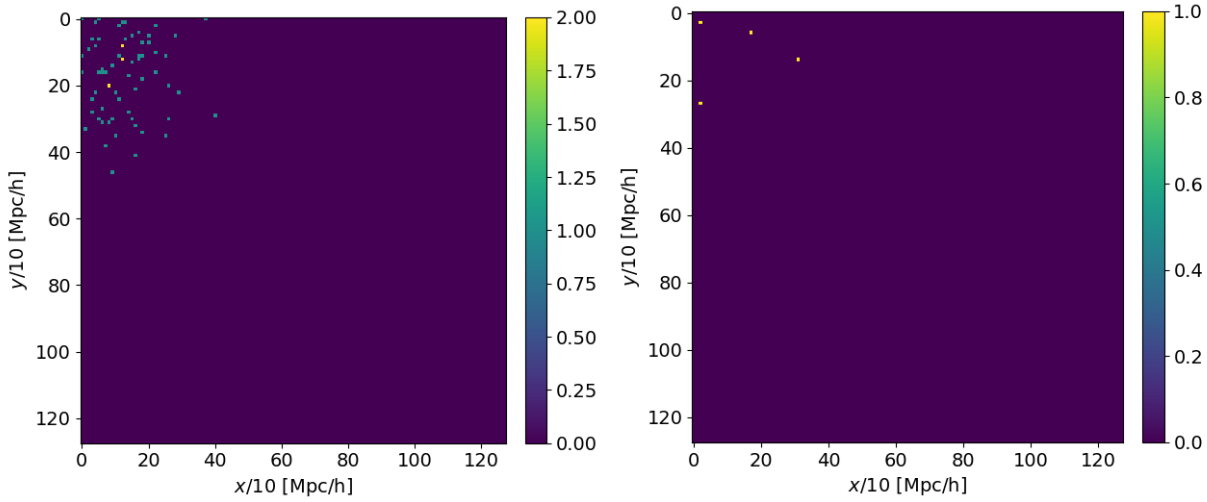

Figure 6.6: Mock galaxy map simulated with the selection function (6.1) for a tracer with bias $b = 1.6$, $n_0 = 0.1$ h^3 Mpc^{-3}, $c_2 = 10$ Mpc h^{-1} and $c_1 = 20$ Mpc h^{-1} at redshift $z = 2$. (*Left*) Slice taken at $z = 100$ Mpc h^{-1}. (*Right*) Slice taken at $z = 400$ Mpc h^{-1}.

The selection function of constant profile, showed in Figure 6.7, was used to generate the maps shown in Figure 6.8.

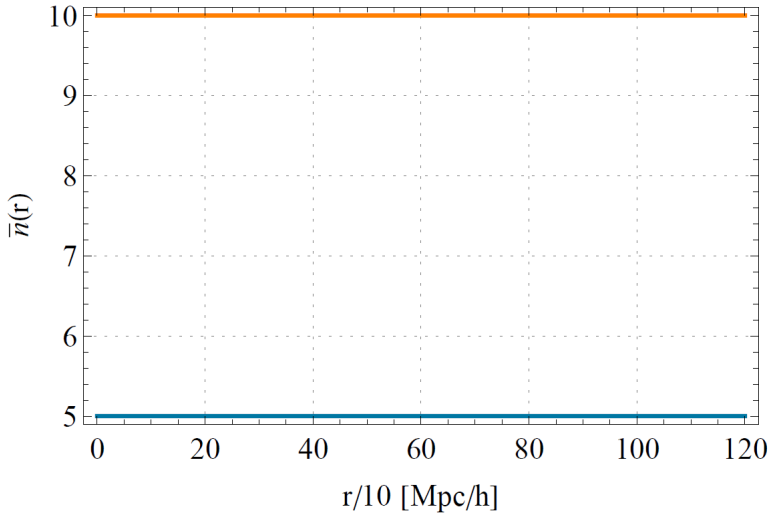

Figure 6.7: Selection function profile for constant $n_0 = 5$ h^3 Mpc^{-3} (blue) and $n_0 = 10$ h^3 Mpc^{-3} (orange) for fixed $c_1 = 10$ and $c_2 = 2 \times 10^4$. Notice that, in this case, the selection is constant throughout the grid. Therefore its effects may be neglected during the analysis. Once again, also notice how huge the value of n_0 is if compared to those values of $\bar{n}$ shown in Table 5.1.

For the purposes of our study, only these maps (with $n_0 = 10\text{h}^3\text{Mpc}^{-3}$ and constant selection function) are going to be considered, for the following reasons: there will be no shot-noise, since the number density per cell is large enough to make the Poisson noise contributions, appearing in equations (5.57) and (5.61), negligible (they are proportional to $\bar{n}^{-1}$ and $\bar{n}^{-2}$) and,

for the constant profile, there will not be any selection effects that would need to be modeled, such as those appearing in the previous cases (Figures 6.2, 6.5 and 6.6).

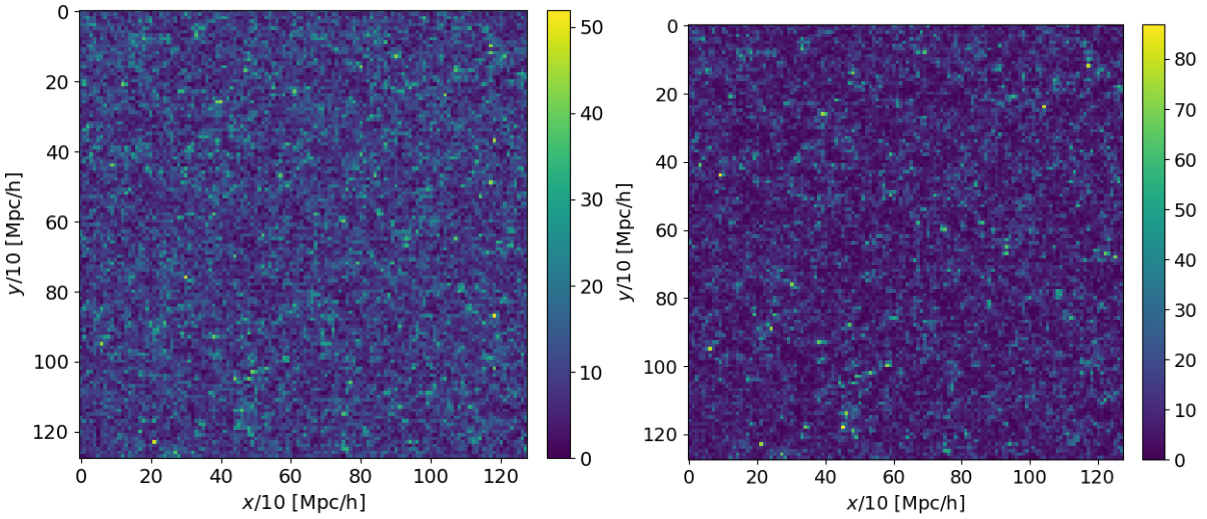

Figure 6.8: Slices of three dimensional galaxy maps simulated with selection function parameters $c_1 = 10$, $c_2 = 2 \times 10^4$ and $n_0 = 10\mathrm{h}^3\mathrm{Mpc}^{-3}$ for two tracers with bias $b = 1.0$ (*left*) and $b = 1.6$ (*right*), both at redshift $z = 2.0$.

6.2 Estimating the power-spectrum

For consistency, the power-spectrum was obtained by means of the FFT estimator (5.75), since its shape and possible sources of problems are more familiar to us.

In Figures 6.9 and 6.10, the estimated power-spectra $\hat{P}$ already normalized by the bias, i.e. $\hat{P} = P_{\mathrm{mocks}}/b^2$, for three different tracers are presented. In Figure 6.10, we see that for small scales around $k \approx 0.1$ h Mpc^{-1}, the estimator (5.75) does not recover the power-spectrum that well.

The reason why this happens concerns the way the maps were created. As pointed out in section §5.2.2, in order to make biased maps of large-scale structure the log-normal approximation needs to be modified as

$$b^2\xi_G = \ln(b^2\xi_L + 1) \tag{6.2}$$

This modification introduces spectral distortions at small scales [4]. The code accounts for these corrections in order to compute the multi-tracer power-spectrum. However, there are

many subtleties involved in the process of correcting these distortions so that there was not enough time to look at them and to see how the FFT estimator could be corrected. Thus, it must be kept in mind that, for small scales, our estimator will be limited due to the nature of our code. In Figure 6.11, the spectral distortions due to the log-normal approximation are shown.

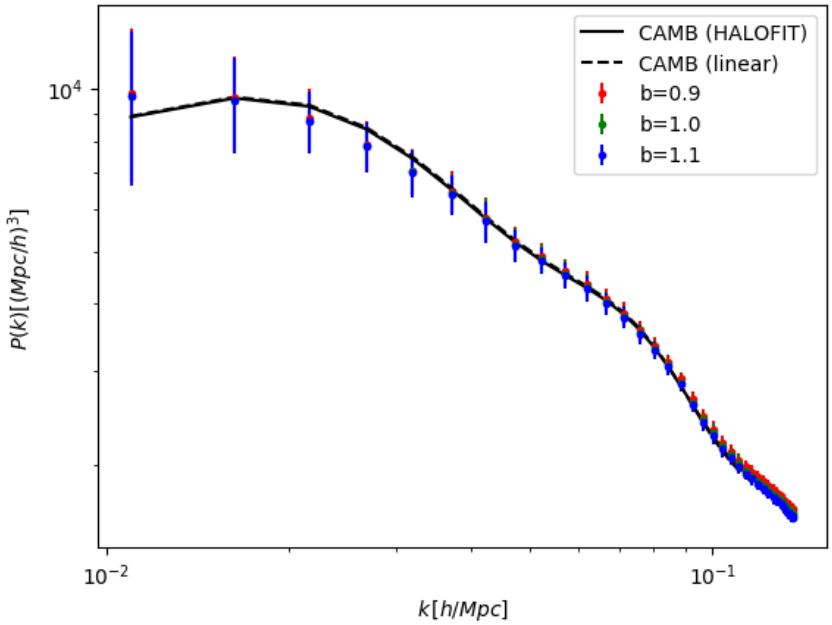

Figure 6.9: Estimated power, through (5.75), from 50 realizations done with the linear CAMB spectrum at $z = 1.0$.

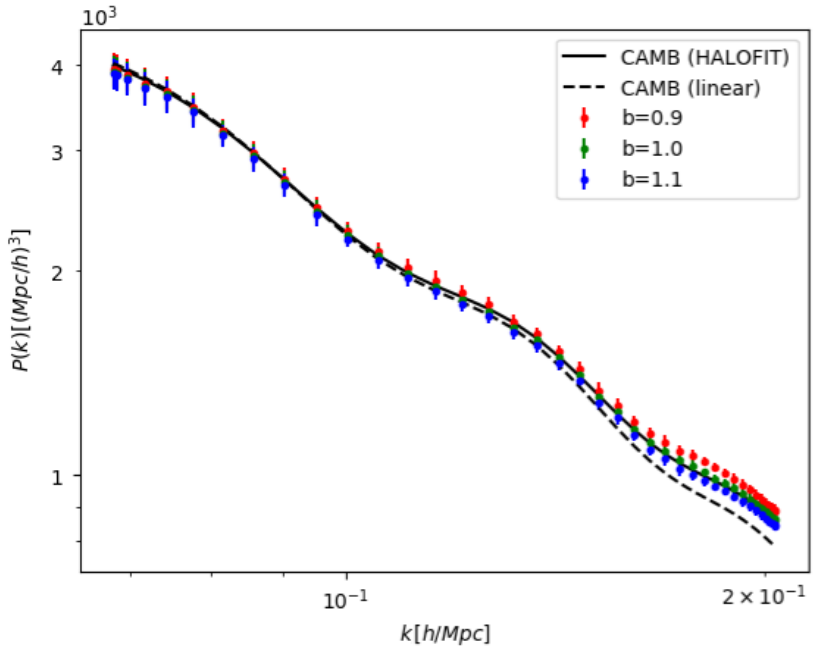

Figure 6.10: Estimated power, through (5.75), from 50 realizations done with the non-linear (HALOFIT) CAMB spectrum at $z = 1.0$. Spectral distortions introduce the scale dependence effects we observe on small scales.

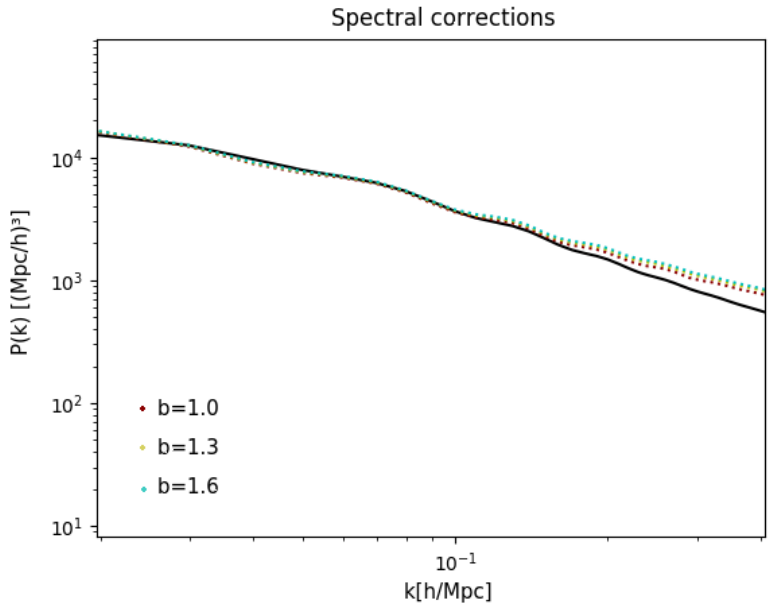

Figure 6.11: Spectral corrections obtained with the multi-tracer code for the usual power-spectrum estimation.The black curve is the non-linear CAMB spectrum.

With the exception of the spectral distortions at small scales, the FFT estimator reproduces well the power spectrum. Therefore, in the next section the bispectrum estimates of the mocks are presented.

6.3 Estimating the bispectrum

We start our analysis by computing the bispectrum for different triangular configurations. Figures 6.12 and 6.13 show the bispectrum as a function of the angle between k_1 and k_2, the two sides of some triangle. The squeezed limit corresponds to $\theta \to 0$. In these two plots, the bispectrum is already normalized by the bias, i.e. $\hat{B} = B_{\rm mocks}/b^4$. The b^4 dependence comes from the contribution of the disconnected piece of the log-normal bispectrum, which is dominant over the connected one (see discussion in §5.1.4, Figures 5.5 and 5.6). Black lines correspond to the full theoretical log-normal bispectrum (5.37) derived in the previous chapter and the error bars were computed as the standard deviation of the 50 samples of bispectrum obtained from 50 simulated maps.

Despite the feature of the error bars being large if compared to the values of the estimated bispectrum, the estimator reproduces very well the expected theoretical bispectrum shape. An extra normalization has been included to the estimator, but because the multi-tracer technique is the focus of future analysis, this normalization gets canceled when the ratio between the

bispectra is considered.

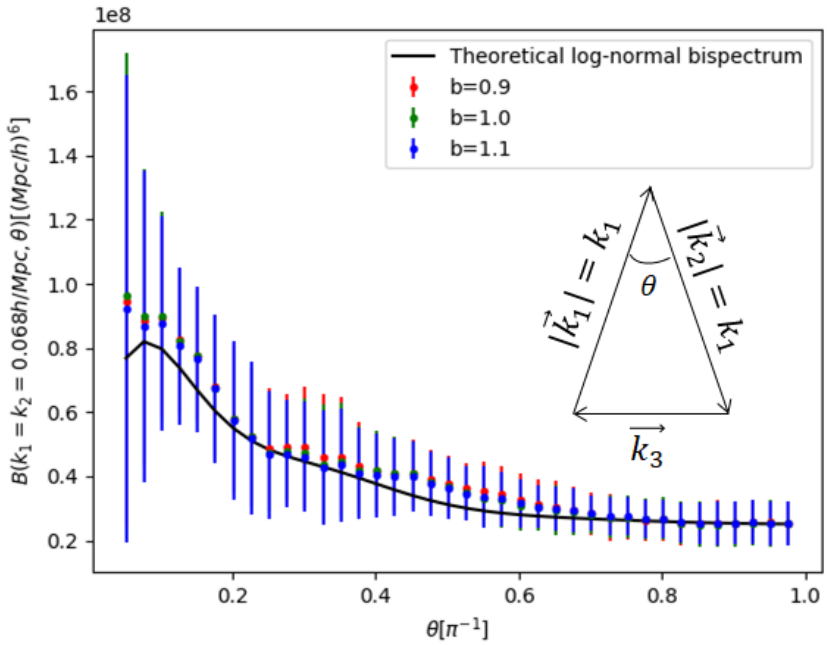

Figure 6.12: Estimated bispectrum from (5.76) for the same 50 realizations considered in Figure 6.9. The form of the triangles used to compute the bispectrum are shown in the figure.

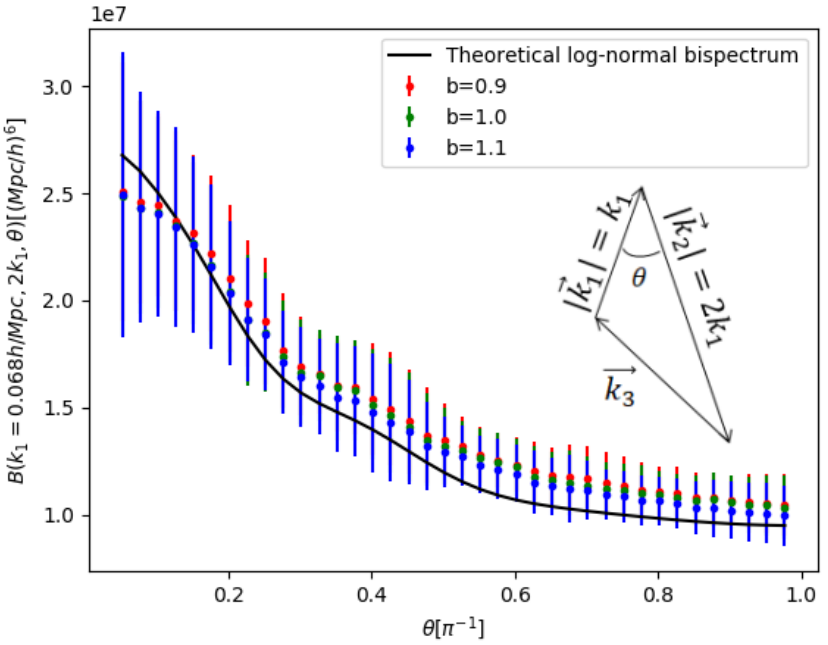

Figure 6.13: Estimated bispectrum from (5.76) for the same 50 realizations considered in Figure 6.10. The form of the triangles used to compute the bispectrum are shown in the figure.

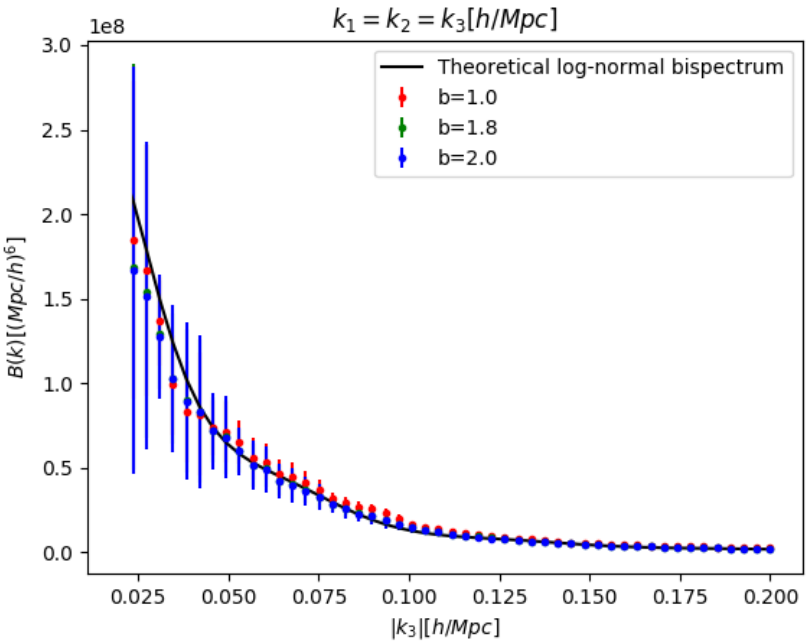

Figure 6.14: Equilateral bispectrum computed for k in the range of $k_{\min} = 0.0250$ h Mpc^{-1} and $k_{\max} = 0.2$ h Mpc^{-1} at redshift $z = 1$.

6.4 Cross-correlations

To reduce the sample variance at large scales and get rid of the possible sources of error, such as the arbitrary normalization included previously, the code which computes (5.75) and (5.76) was generalized to perform a cross-correlation of the several galaxy maps, that is, for the case of the bispectrum,

$$B_{\alpha\beta\gamma}(\mathbf{k}_1, \mathbf{k}_2, \mathbf{k}_3) \approx \frac{V^2}{N_{\text{pix}}^3} \frac{\sum_{\mathbf{n}}^{N_{\text{pix}}} \delta_\alpha(\mathbf{n}, \mathbf{k}_1)\delta_\beta(\mathbf{n}, \mathbf{k}_2)\delta_\gamma(\mathbf{n}, \mathbf{k}_3)}{\sum_{\mathbf{n}}^{N_{\text{pix}}} I_\alpha(\mathbf{n}, \mathbf{k}_1)I_\beta(\mathbf{n}, \mathbf{k}_2)I_\gamma(\mathbf{n}, \mathbf{k}_3)}, \tag{6.3}$$

where α, β and γ represents different tracers ($b_\alpha \neq b_\beta \neq b_\gamma$).

Once this was done, the ratio between the different bispectra,

$$\frac{B_{\alpha\beta\gamma}}{B_{\alpha'\beta'\gamma'}} \propto f(b_\alpha, b_\beta, b_\gamma), \tag{6.4}$$

where f is a function of the different biases, was calculated.

Figure 6.15 shows the ratio (6.4) for the bispectra $B_{\alpha\beta\gamma}$ and $B_{\alpha'\beta'\gamma'}$ resulting of a sample with 10 realizations for three tracers with biases $b_1 = 1$, $b_2 = 1.3$ and $b_3 = 1.6$ at redshift $z = 0.5$. It is possible to see that the multi-tracer approach, i.e. considering $B_{\alpha\alpha\alpha}/B_{\beta\beta\beta}$, reduces considerably the relative errors, $\Delta\sigma = \sigma(B)/B$, in comparison with the ones obtained

through the samples of only one type of tracer $B_{\alpha\alpha\alpha}$, that is,

$$\frac{\sigma(B_{\alpha\beta\gamma}/B_{\alpha'\beta'\gamma'})}{B_{\alpha\beta\gamma}/B_{\alpha'\beta'\gamma'}} \ll \frac{\sigma(B_{\alpha\beta\gamma})}{B_{\alpha\beta\gamma}}. \tag{6.5}$$

Since the multi-tracer generator code used in this work was built to reproduce the two-point statistics and not to analyze higher-order correlations, the results obtained for the bispectrum, "recovering" the bias, is surprisingly good.

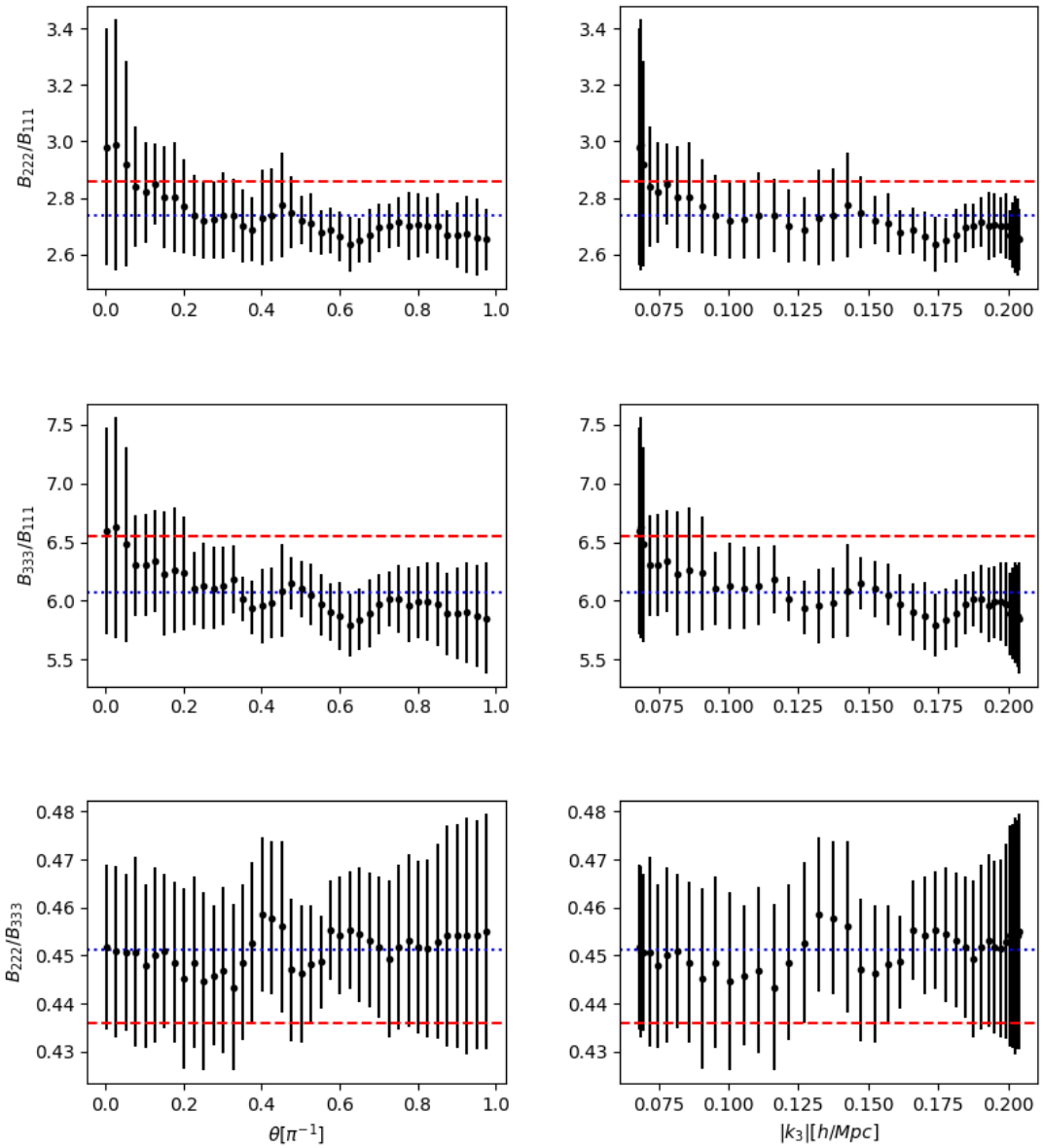

Figure 6.15: Ratio between the bispectra $B_{\alpha\alpha\alpha}/B_{\beta\beta\beta}$, at redshift $z = 0.5$, with their respective sample means (dotted blue lines) and the expected value b_α^4/b_β^4 (dashed red lines), once the connected piece C_{123} of the bispectrum may be neglected if compared to the disconnected piece $D_{123} \propto P^2$. This "expected" value is only shown for completeness. Indices 1, 2 and 3 refer two the tracers with bias $b_1 = 1$, $b_2 = 1.3$ and $b_3 = 1.6$.

Figure 6.16 shows the ratio of the cross-correlation bispectrum. The scale-dependence appearing in the estimates (more evident in the behaviour seen on the ratios B_{222}/B_{112}, B_{333}/B_{113}, B_{122}/B_{112}, B_{133}/B_{113} and $B113/B_{111}$) comes from the spectral distortions inherent to the code. This hinders the extraction of the bias parameters, although it improves a lot the errors.

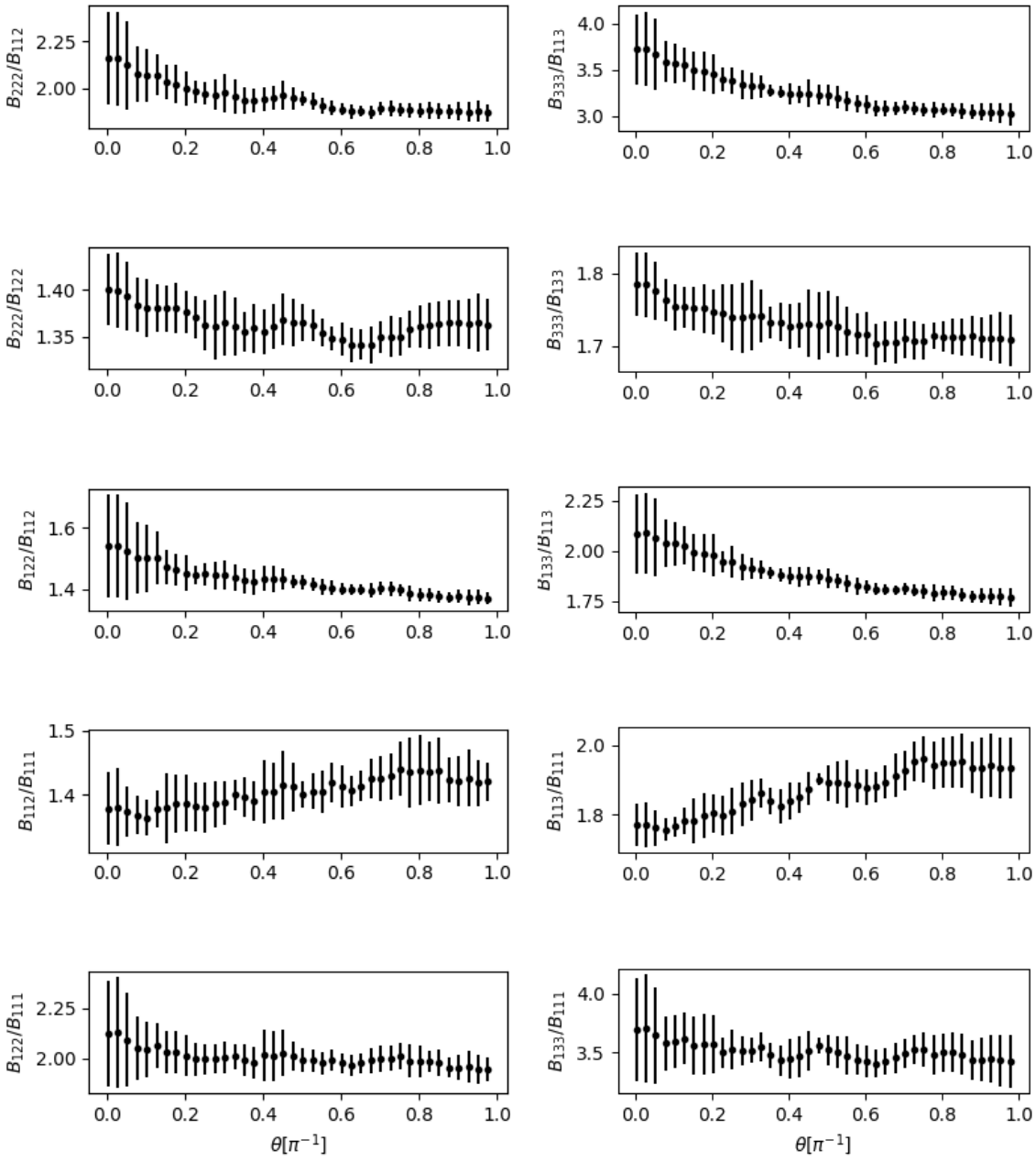

Figure 6.16: Ratio between the bispectra $B_{\alpha\beta\gamma}/B_{\alpha'\beta'\gamma'}$, at redshift $z = 0.5$, for the possible combinations among tracers with bias $b_1 = 1.0$ and $b_2 = 1.3$ (*left*) and $b_1 = 1.0$ and $b_3 = 1.6$ (*right*).

To make our point clearer about the scale-dependence being a consequence of the method used to generate the mocks, the ratio between the cross-correlations for increasing redshift

($z = 1.0$. $z = 1.5$ and $z = 2$) is presented in Figures 6.17 and 6.18. It is possible to observe in these Figures that the scale-dependence diminishes as we go to higher redshifts.

The reason behind this behaviour consists on the fact that the correlation function, and hence the power-spectrum, goes with $a^2(t)$ during the matter-dominated era, as it was shown in (2.72) and (2.176). This time dependence implies that $\xi_{\rm LN} \propto (1+z)^{-2}$ and thus, for higher redshifts, $\xi_{\rm LN} \to \xi_{\rm G}$ and the effects of spectral distortions get minimized.

Figure 6.17 shows the ratio between the cross-correlations of the possible combinations involving two tracers, with bias $b_1 = 1.0$ and $b_2 = 1.3$, whereas Figure 6.18 shows the cross-correlations for two tracers with bias $b_1 = 1.0$ and $b_3 = 1.6$.

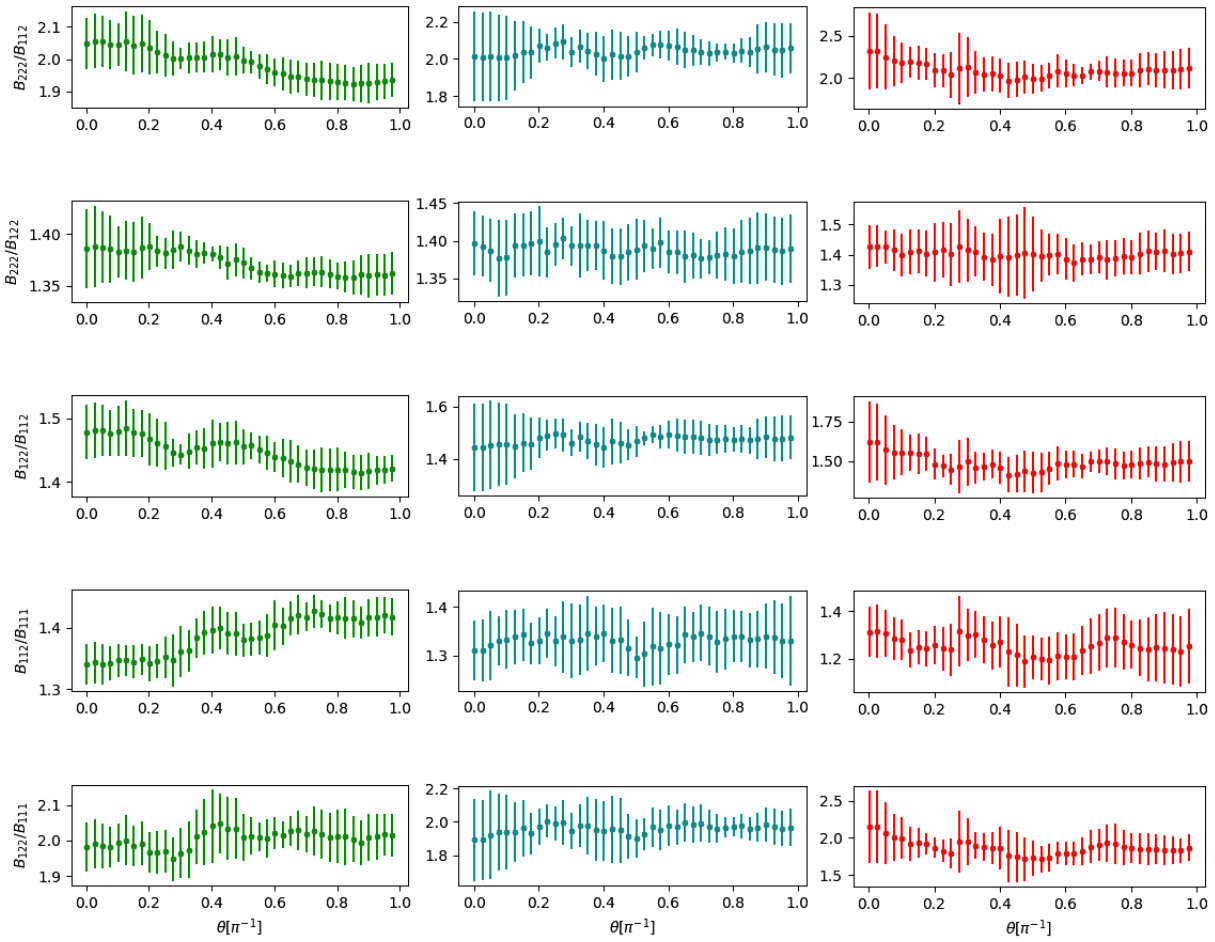

Figure 6.17: Ratio between the cross-correlations of the possible combinations involving two tracers with bias $b_1 = 1.0$ and $b_2 = 1.3$ at three different redshifts $z = 1$ (*left, green*), $z = 2.0$ (*middle, blue*) and $z = 3.0$ (*right, red*).

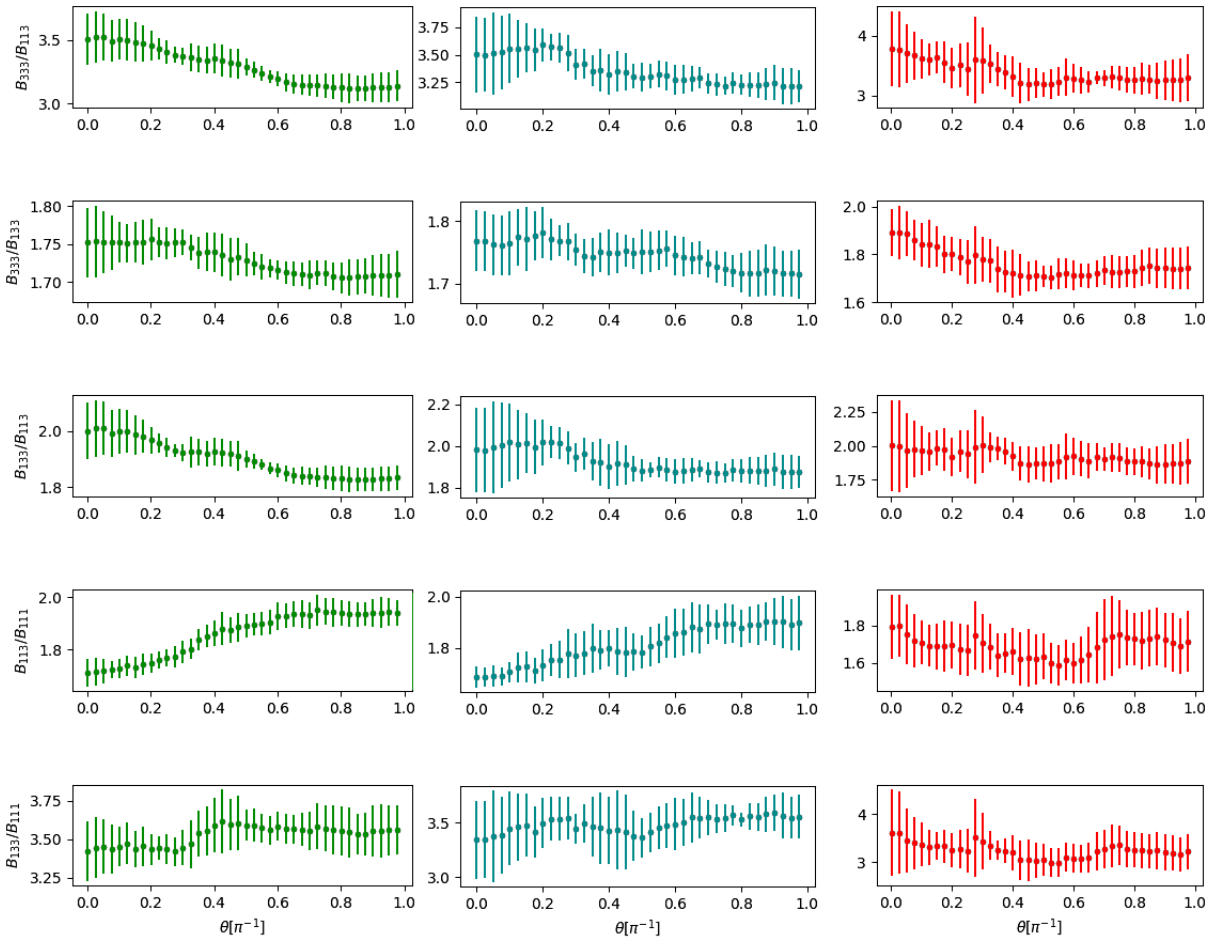

Figure 6.18: Ratio between the cross-correlations of the possible combinations involving two tracers with bias $b_1 = 1.0$ and $b_3 = 1.6$ at three different redshifts $z = 1$ (*left, green*), $z = 2.0$ (*middle, blue*) and $z = 3.0$ (*right, red*).

In Figures 6.19, 6.20 and 6.23 it is shown the relative errors for several ratios of the cross-correlation bispectrum addressed in Figures 6.17 and 6.18. It is possible to see, in light of this, that the bigger the difference between the tracers' biases, the bigger the improvement obtained on the bispectra sample variance.

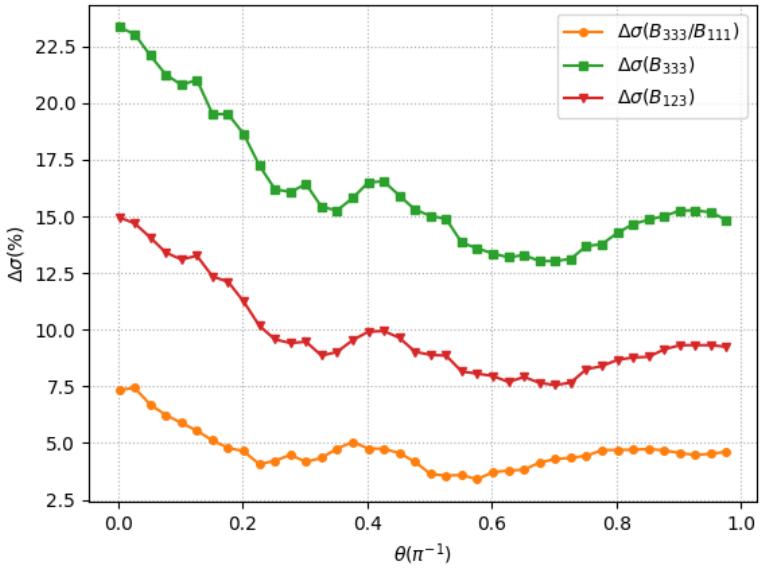

Figure 6.19: Relative percentual error $\Delta\sigma$ of the ratio of bispectra samples for the tracers of previous analysis (Figures 6.15 and 6.16) with bias $b_1 = 1.0$, $b_2 = 1.3$ and $b_3 = 1.6$.

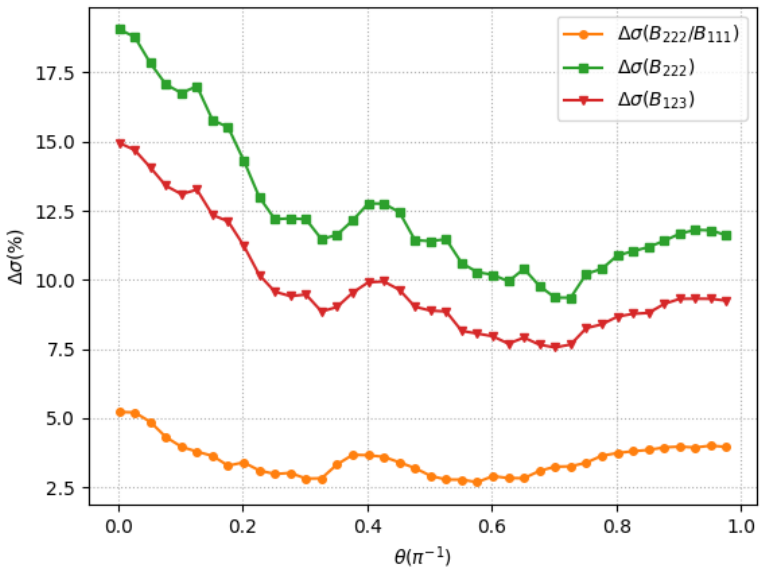

Figure 6.20: Relative percentual error $\Delta\sigma$ of the ratio of bispectra samples for the tracers of previous analysis (Figures 6.15 and 6.16) with bias $b_1 = 1.0$, $b_2 = 1.3$ and $b_3 = 1.6$.

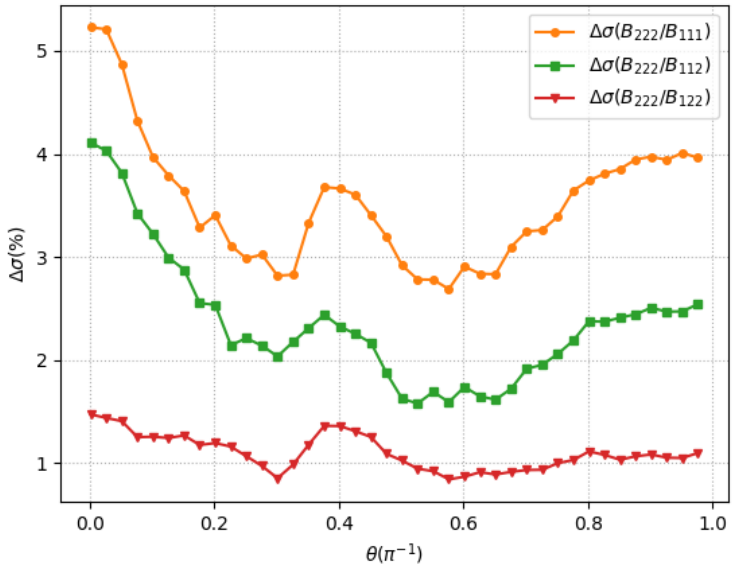

Figure 6.21: Relative percentual error $\Delta\sigma$ of the ratio of bispectra samples, as shown in Figure 6.16, for two tracers with bias $b_1 = 1.0$ and $b_2 = 1.3$.

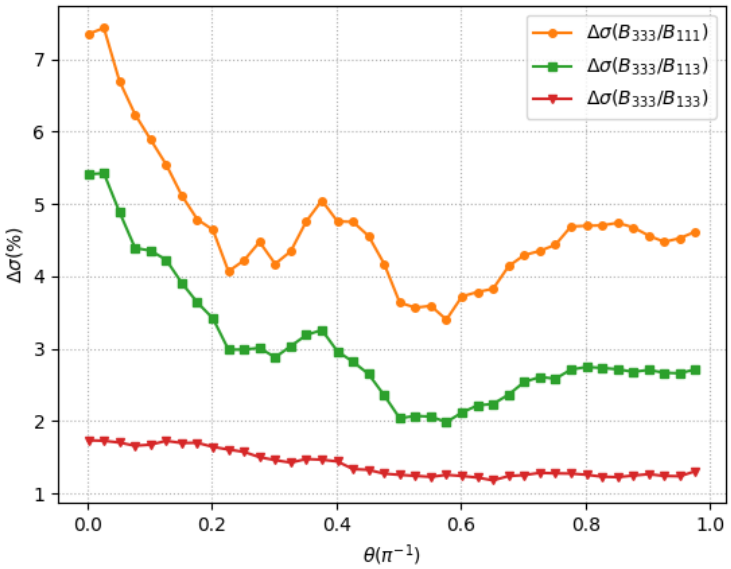

Figure 6.22: Relative percentual error $\Delta\sigma$ of the ratio of bispectra samples, as shown in Figure 6.16, for two tracers with bias $b_1 = 1.0$ and $b_3 = 1.6$.

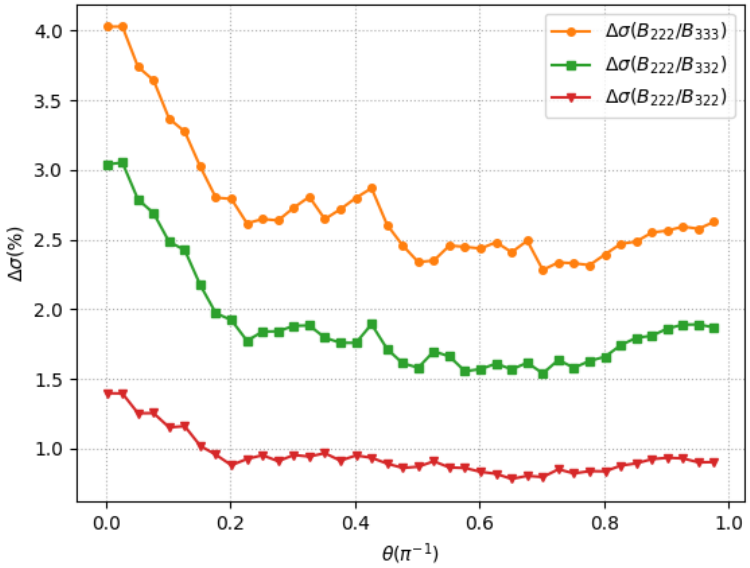

Figure 6.23: Relative percentual error $\Delta\sigma$ of the ratio of bispectra samples, as shown in Figure 6.16, for two tracers with bias $b_2 = 1.3$ and $b_3 = 1.6$.

Chapter 7

Conclusions and Final Remarks

In the past decade, an enormous amount of data supporting or falsifying theories developed to explain the Universe was collected. Luckily for the active cosmologists, the forthcoming years will bring much more information to keep research as promising as it was. From future galaxy surveys, in particular, we might get an outstanding turn on the Physics known today: from tests of Einstein's gravity to the very beginnings of the Universe.

This golden age in Cosmology motivated this master's dissertation, which aimed to present in a consistent and pedagogical fashion the project entitled *Primordial non-Gaussianities: Theory and Prospects for Observations*. Far from being a self-contained and finished study, here we present the final remarks of this two years process and our outlook for the future of this scientific branch, as it was possible to conclude from what has been developed and learned so far.

On the theory side, we saw how from a simplistic Newtonian description of fluids the non-relativistic matter collapses to give rise to the structures, such as galaxies and clusters of galaxies, and how the full relativistic treatment of the process of structure formation provides a more accurate way to comprehend the large-scale structures seen in the Universe. It was also studied how a period of inflation solves the issues of the standard Big Bang cosmology in an exquisite manner not only fulled with mathematical beauty but with observables that are being continuously tested [100, 101]. Despite the remarkable success and acceptance of inflation, proposed alternatives to this scenario must receive the same careful look, passing through rigorous observational tests.

With future [38, 45, 58] and ongoing [114] surveys, the hope is to reach competitive measurements with the CMB through the LSS. In Table 7.1 it is summarized the expected

potentials of some planned surveys that intend to start operating until 2020.

	LSST	**DESI**	**Euclid**	**SKA (P2)**
Survey type	Photometric	Spectroscopic	Photo + Spec	21 cm
Base	Ground	Ground	Space	Ground
Redshift	$z < 3$	$z < 1.4$ $z_{\mathrm{Ly}\alpha} = 2 - 3.5$	$z < 3$	$0.18 < z < 1.84$
Survey area (deg^2)	20k	14k	15k	30k
Number of objects	$\sim 10^9$ (WL)	$\sim 10^7$ gals. $\sim 10^5$ quasars	$\sim 10^7$ redshifts $\sim 10^9$ photo-z	$\sim 10^9$ gals.
Galaxy clustering	✓	✓	✓	✓
Weak lensing	✓		✓	✓
RSD		✓	✓	✓
Multi-tracer	✓	✓	✓	✓

Table 7.1: Main features of the most pinup surveys. Based on Table 2 of [9]. SKA phase-2 (P2) data was extracted from [22].

On the observational side, in this work we saw how a handful of tracers of large-scale structure possessing different biases[1] allows us to significantly reduce the errors on both the power-spectrum, as it is widely discussed in the literature, and bispectrum measurements, the latter being a very useful observable to probe early Universe theories. We would like to emphasize that multi-tracer analysis with the bispectrum is not an ordinary subject in the literature: as far as we could found, only Yamauchi and collaborators [132] have addressed this subject up to now.

We saw in Figures 6.21, 6.22 and 6.23 that the bigger the difference between the tracers' biases, the bigger the improvement obtained on the bispectra sample variance.

Since the work presented here is an ongoing project, there is still much to do: in order to make a link between theory and observations, there are real data already available [115] waiting for us to apply the tools so far developed, such as the FFT bispectrum estimator. Besides, there are also "real life" issues, such as redshift space distortions, which need to be added to the analysis so that we can properly constrain non-Gaussian physics, thereby increasing the accuracy of the measurements. Understanding this issues is a key component to fulfill our hopes of competing with CMB data.

A difficult matter is related to the non-vanishing bispectrum generated by gravity, which contributes on small scales. Hence, when considering surveys which maps scales that go from

[1] Notice that all surveys mentioned on Table 7.1 will provide multi-tracer maps.

the mildly to the non-linear regime, this intrinsic gravitational bispectrum that mix the primordial signal we are trying to measure must be eliminated.

Ways to separate primordial bispectrum signals from gravitational contributions are going to be further studied with N-body simulations such as those obtained with the codes `GADGET` [119] and the 2LPT initial conditions generator [34], which also account for pNGs [109].

One task we did not have time to accomplish was the implementation of non-Gaussianities in the multi-tracer code. This is something that would be interesting to do in order to parametrize the bispectrum in terms of different shapes and, therefore, constrain the many types of f_{NL} studied. This would also allow us to compare the results of the multi-tracer code with the constraints obtained from real and N-body simulation data, which put in test the basic aspects of the code.

Finally, there are estimators which optimize the information one can extract from a survey, in the presence of shot-noise and cosmic variance, for the case of the power-spectrum of a single [46] and multiple [96] tracers of the LSS. However, for the bispectrum and higher-correlations, e.g. trispectrum, there are no such optimal estimators. To develop these estimators for statistics beyond the power-spectrum is interesting once the multi-tracer technique provides a powerful way to compete with CMB measurements.

Bibliography

[1] The 2dF Galaxy Redshift Survey: http://www.2dfgrs.net/

[2] Abazajian, K. N., et al. “Inflation Physics from the Cosmic Microwave Background and Large Scale Structure”. Astroparticle Physics, v. 63, p. 55-65, 2015. [arXiv:1309.5381]

[3] Abramo, L. R., Leonard, K. E. “Why multi-tracer surveys beat cosmic variance”. Monthly Notices of the Royal Astronomical Society, v. 432, n. 1, p. 318-326, 2013. [arXiv:1302.5444]

[4] Abramo, L. R., Secco, L. F., Loureiro, A. “Fourier analysis of multi-tracer cosmological surveys”. Monthly Notices of the Royal Astronomical Society, v. 455, n. 4, p. 3871-3889, 2015. [arXiv:1505.04106]

[5] Acquaviva, V., et al. “Gauge-invariant second-order perturbations and non-Gaussianity from inflation”. Nuclear Physics B, v. 667, n. 1-2, p. 119-148, 2003.

[6] Arnowitt, R. S., Deser, S., Misner, C. W. “The dynamics of general relativity”. In: *Gravitation: An Introduction to Current Research*, Witten, L. (Ed.), p. 227-264, New York: John Wiley & Sons, 1962.

[7] Aitchison, J., Brown, J. A. C. “The Lognormal Distribution, with Special Reference to Its Use in Economics”. Cambridge: Cambridge University Press, Monographs, 1957.

[8] Alpher, R. A., Bethe, H. A., Gamow, G. “The Origin of Chemical Elements”. Physical Review, v. 73, n. 7, p. 803-804, 1948.

[9] Alvarez, M. et al. “Testing inflation with large scale structure: connecting hopes with reality”. arXiv preprint *arXiv:1412.4671*, 2014.

[10] Amendola, L., Tsujikawa, S. “Dark energy: theory and observations”. Cambridge: Cambridge University Press, 1. ed., 2010.

[11] Arfken, G. “Mathematical Methods for Physicists”. San Diego: Academic Press, 3. ed., 1985.

[12] Babich, D., Creminelli, P., Zaldarriaga, M. “The shape of non-Gaussianities”. Journal of Cosmology and Astroparticle Physics, v. 2004, n. 8, p. 009, 2004. [arXiv:astro-ph/0405356]

[13] Babu, G. J., Feigelson, E. D. “Spatial point processes in astronomy”. Journal of statistical planning and inference, v. 50, n. 3, p. 311-326, 1996.

[14] Bardeen, J. M. “Gauge-invariant cosmological perturbations”. Physical Review D, v. 22, n. 8, p. 1882-1905, 1980.

[15] Bartolo, N. et al. “Non-Gaussianity from inflation: theory and observations”. Physics Reports, v. 402, n. 3-4, p. 103-266, 2004. [arXiv:astro-ph/0406398]

[16] Baumann, D. “Cosmology: Part III Mathematical Tripos”.

[17] Baumann, D. “Primordial Non-Gaussianity”.

[18] Bernardeau, F., et al. “Large-scale structure of the Universe and cosmological perturbation theory”. Physics Reports, v. 367, p. 1-248, 2002. [arXiv:astro-ph/0112551]

[19] Bouchet, F. R. “Introductory overview of Eulerian and Lagrangian perturbation theories”. In: *Dark matter in the Universe: Proceedings of the CXXXII International School of Physics “Enrico Fermi”*, Bonometto, S., Primack, J. R., Provenzale, A. (Eds.), v. 132, p. 565-599, Amsterdam: IOS Press, 1996.

[20] Brout, R., Englert, F., Gunzig, E. “The creation of the Universe as a Quantum phenomenon”. Annals of Physics, v. 115, p. 78-106, 1978.

[21] Buchert, T. “Lagrangian Perturbation Approach to the Formation of Large-Scale Structure”. In: *Dark matter in the Universe: Proceedings of the CXXXII International School of Physics “Enrico Fermi”*, Bonometto, S., Primack, J. R., Provenzale, A. (Eds.), v. 132, p. 565-599, Amsterdam: IOS Press, 1996.

[22] Bull, P., et al. “Measuring baryon acoustic oscillations with future SKA surveys”. arXiv preprint *arXiv:1501.04088*, 2015.

[23] Byrnes, C. T. “Lecture Notes on Non-Gaussianity”. In: *The Cosmic Microwave Background: Proceedings of the II José Plínio Baptista School of Cosmology*, Fabris, J. C., Piattella, O., Rodrigues, D. C., Velten, H. E. S., Zimdahl, W. (Eds.), v. 45, p. 135-165, Springer International Publishing, 2016.

[24] Carroll, S. M. “Spacetime and Geometry: An Introduction to General Relativity”. San Francisco: Addison Wesley, 1. ed., 2004.

[25] Caticha, N. “Probabilidades”. Lecture notes for the undergraduate course *Probabilidade* given at the Institute of Physics of the University of Sao Paulo (IFUSP), 2016.

[26] Cattani, M. S. D. “Elementos de Mecânica dos Fluidos”. São Paulo: Blücher, 2. ed., 2013.

[27] Chen, X. “Primordial Non-Gaussianity from Inflation Models”. Advances in Astronomy, 2010. [arXiv:1002.1416]

[28] Coles, P. “Models of Nonlinear Clustering. I. - Interesting Distribution Functions”. In: *Dark matter in the Universe: Proceedings of the CXXXII International School of Physics “Enrico Fermi”*, Bonometto, S., Primack, J. R., Provenzale, A. (Eds.), v. 132, p. 239-253, Amsterdam: IOS Press, 1996.

[29] Coles, P. “Models of Nonlinear Clustering II - Applications of the Truncated Zel’dovich Approximation”. In: *Dark matter in the Universe: Proceedings of the CXXXII International School of Physics “Enrico Fermi”*, Bonometto, S., Primack, J. R., Provenzale, A. (Eds.), v. 132, p. 629-644., Amsterdam: IOS Press, 1996.

[30] Coles, P., Jones, B. “A lognormal model for the cosmological mass distribution”. Monthly Notices of the Royal Astronomical Society, v. 248, n. 1, p. 1-13, 1991.

[31] Collis, W. B., White, P. R., Hammond, J.K. “High-Order Spectra: The Bispectrum and Trispectrum”. Mechanical Systems and Signal Processing, v. 12, n. 3, p. 375-394, 1998.

[32] Cooray, A., Sheth, R. “Halo models of large scale structure”. Physics Reports, v. 372, n. 1, p. 1-129, 2002.

[33] Creminelli, P., et al. “Limits on non-Gaussianities from WMAP data”. Journal of Cosmology and Astroparticle Physics, 2006(05), 004, 2006. [arXiv:astro-ph/0509029]

[34] Crocce, M., Pueblas, S., Scoccimarro, R. “Transients from initial conditions in cosmological simulations”. Monthly Notices of the Royal Astronomical Society, v. 373, n.1, p. 369-381, 2006. [arXiv:astro-ph/0606505]

[35] Dalal, N. et al. “Imprints of primordial non-Gaussianities on large-scale structure: Scale-dependent bias and abundance of virialized objects”. Physical Review D, v. 77, n. 12, 2008. [arXiv:0710.4560]

[36] Desjacques, V., Seljak, U. “Primordial non-Gaussianity from the large-scale structure”. Classical and Quantum Gravity, v. 27, n. 12, 2010. [arXiv:1006.4763]

[37] Dewdney, P., et al. “SKA1 system baseline V2 description”. SKA Organization, 2015.

[38] DESI Collaboration. “The DESI Experiment Part I: Science,Targeting, and Survey Design”. arXiv e-print *arXiv:1611.00036*, 2016.

[39] Durrer, R. “The Cosmic Microwave Background”. Cambridge: Cambridge University Press, 1. ed., 2008.

[40] Efstathiou, G. “Cosmological Perturbations”. In: *Physics of the Early Universe: Proceedings of the Thirty-Sixth Scottish Universities Summer School in Physics*, Peacock, J. A., Heavens, A. F., Davies, A. T. (Eds), v. 36, p. 361-463, Melksham: Edinburgh University Press, 1990.

[41] Einstein, A. “The foundation of the general theory of relativity”. In: *The Principle of Relativity: a collection of original memoirs on the special and general theory of relativity*, Lorentz, H. A., Einstein, A., Minkowski, H., Weyl, H. Dover, 1952.

[42] Einstein, A., De Sitter, W. “On the relation between the expansion and the mean density of the universe”. Proceedings of the National Academy of Sciences, v. 18, n. 3, p. 213-214, 1932.

[43] Eisenstein, D., et al. “Cosmology from a Redshift Survey of 200 Million Galaxies.” astro2010: The Astronomy and Astrophysics Decadal Survey, v. 2010, 2009.

[44] Ellis, G. F. R., Bruni, M. “Covariant and gauge-invariant approach to cosmological density fluctuations’. Physical Review D, v. 40, n. 6, p. 1804-1818, 1989.

[45] Euclid Consortium: https://www.euclid-ec.org/

[46] Feldman, H. A., Kaiser, N., Peacock, J. A. "Power-spectrum analysis of three-dimensional redshift surveys". The Astrophysical Journal, v. 426, n. 1, p. 23-37, 1994. [arXiv:astro-ph/9304022]

[47] Fergusson, J. R., Shellard, E. P. S. "Shape of primordial non-Gaussianity and the CMB bispectrum". Physical Review D, v. 80, n.4, p. 043510-043536, 2009. [arXiv:0812.3413]

[48] Ford, L. H. "Inflation driven by a vector field". Physical Review D, v. 40, n. 4, p. 967-972, 1989.

[49] Fry, J. N. "The galaxy correlation hierarchy in perturbation theory". The Astrophysical Journal, v. 279, n.2 , p. 499-510, 1984.

[50] Fry, J. N., Gaztañaga, E. "Biasing and hierarchical statistics in large-scale structure". The Astrophysical Journal, v. 413, n. 2, p. 447-452, 1993.

[51] Giovannini, M. "A Primer on the Physics of the Cosmic Microwave Background". Singapore: World Scientific, 2008.

[52] Gliner, E. "Algebraic properties of the energy-momentum tensor and vacuum-like states of matter". Soviet Physics JETP, v. 22, n. 2, p. 378-382, 1966.

[53] Guth, A. H. "Inflationary universe: A possible solution to the horizon and flatness problems". Physical Review D, v. 23, n. 2, p. 347-356, 1981.

[54] Hawking, S. W. "Perturbations of an expanding universe". The Astrophysical Journal, v. 145, p. 544-554, 1966.

[55] Hubble, E. "A relation between distance and radial velocity among extra-galactic nebulae". Proceedings of the National Academy of Sciences, v. 15, i. 3, p. 168-173, 1929.

[56] Hubble, E. "The distribution of extra-galactic nebulae". The Astrophysical Journal, v. 79, p. 8-83, 1934.

[57] Ito, A., Soda, J. "Primordial gravitational waves induced by magnetic fields in an ekpyrotic scenario". Physics Letters B, v. 771, p. 415-420, 2017. [arXiv:1607.07062]

[58] Ivezic, Z., et al. "LSST: from science drivers to reference design and anticipated data products". arXiv preprint *arXiv:0805.2366*, 2008.

[59] Jain, B., Bertschinger, E. "Second Order Power Spectrum and Nonlinear Evolution at High Redshift". The Astrophysical Journal, v. 431, p. 495-505, 1994.

[60] Jeong, D. "Cosmology with high ($z > 1$) redshift galaxy surveys". PhD Thesis, The University of Texas at Austin, 2010.

[61] Kaiser, N. "On the spatial correlations of Abell clusters". The Astrophysical Journal, v. 284, p. L9-L12, 1984.

[62] Karagiannis, D. et al. "Constraining Primordial non-Gaussianity with Bispectrum and Power Spectum from Upcoming Optical and Radio Surveys". arXiv preprint *arXiv:1801.09280*, 2018.

[63] Kazarian, P. F. "On the tensor field inflation in the GR homogeneous cosmological model". arXiv preprint *arXiv:gr-qc/0005033*, 2000.

[64] Keldysh, L. "Diagram technique for nonequilibrium processes". Journal of Experimental and Theoretical Physics, v. 20, n. 4, p. 1018-1026, 1964.

[65] Khoury, J., et al. "The ekpyrotic universe: colliding branes and the origin of the hot big bang". Physical Review D, v. 64, p. 123522, 2001. [arXiv:hep-th/0103239]

[66] Koh, S. "Vector field and inflation". In: *International Journal of Modern Physics: Conference Series*, v. 1, p. 120-125, World Scientific Publishing Company, 2011.

[67] Komatsu, E. "The Pursuit of Non-Gaussian Fluctuations in the Cosmic Microwave Background". PhD Thesis, Tohoku University, *arXiv:astro-ph/0206039*, 2001.

[68] Landau, L. D., Lifshitz, E. M. "Fluid Mechanics", *Course of Theoretical Physics*, v. 6, Pergamon-Press, 2. ed., 1987.

[69] Lewis, A., Challinor, A., Lasenby, A. "Efficient computation of CMB anisotropies in closed FRW models". Astrophysical Journal, v. 538, p. 473-476, 2000. [arXiv:astro-ph/9911177]

[70] Large Synoptic Survey Telescope: https://www.lsst.org/

[71] Lewis, A. "The real shape of non-Gaussianities". Journal of Cosmology and Astroparticle Physics, 2011(010), 026, 2011. [arXiv:1107.5431]

[72] Liddle, A. R., Lyth, D. H. “Cosmological Inflation and Large-Scale Structure”. New York: Cambridge University Press, 2000.

[73] Liddle, A. “An Introduction to Modern Cosmology”. Chichester: John Wiley & Sons, 2003.

[74] Liguori, M., et al. “Primordial Non-Gaussianity and Bispectrum Measurements in the Cosmic Microwave Background and Large-Scale Structure”. Advances in Astronomy, 2010. [arXiv:1001.4707]

[75] Linde, A. “Particle Physics and Inflationary Cosmology”. Contemporary Concepts in Physics, v. 5, Chur: Harwood Academic Publishers, 1990.

[76] Liu, J., Wang, Y., Zhou, S. “Inflation with massive vector fields”. Journal of Cosmology and Astroparticle Physics, 2015(08), 033, 2015. [arXiv:1502.05138]

[77] Lumley, J. L. “Eulerian and Lagrangian descriptions in fluid mechanics”. National Committee for Fluid Mechanics Films (film notes), n. 21621. Education Development Center, 1969.

[78] Maldacena, J. “Non-Gaussian features of primordial fluctuations in single field inflationary models”. Journal of High Energy Physics, v. 7, n. 5, p. 233-264, 2003. [arXiv:astro-ph/0210603]

[79] Magalhães, M. N. “Probabilidade e Variáveis Aleatórias”. São Paulo: Edusp, 3. ed., 2013.

[80] Martínez, V. J. “Is the Universe Fractal?”. Science, v. 284, p. 445-446, 1999.

[81] Martínez, V. J., Saar, E. “Statistics of the galaxy distribution”. Boca Raton: Chapman & Hall/CRC Press, 1. ed., 2002.

[82] Mukhanov, V. “Quantum theory of gauge-invariant cosmological perturbations”. Journal of Experimental and Theoretical Physics, v. 67, n. 7, p. 1297-1302, 1988.

[83] Mukhanov, V., Feldman, H., Brandenberger, R. “Theory of Cosmological Perturbations”. Physics Reports, v. 215, n. 5-6, p. 203-333, 1992.

[84] Mukhanov, V. “Physical Foundations of Cosmology”. Cambridge: Cambridge University Press, 2005

[85] Mukhanov, V., Winitzki, S. “Introduction to Quantum Effects in Gravity”. Cambridge: Cambridge University Press, 2007.

[86] Olson, D. W. “Density perturbations in cosmological models”. Physical Review D, v. 14, i. 2, p. 327-331, 1976.

[87] Olver, F. W. J. “Bessel Functions of Integer Order”. In: *Handbook of Mathematical Functions with Formulas, Graphs, and Mathematical Tables*. Abramowitz, M., Stegun, I. (Eds.). New York: Dover Publications, 1972.

[88] Padmanabhan, T., “Structure formation in the universe”. Cambridge: Cambridge University Press, 1993.

[89] Papoulis, A., Pillai, S. U. “Probability, Random Variables, and Stochastic Processes”. New York: McGraw-Hill, 4. ed, 2002.

[90] Paterson, A. R. “A First Course in Fluid Dynamics”. New York: Cambridge University Press, 1983.

[91] Peacock, J. A. “Statistics of Cosmological Density Fields”. In: *New Insights into the Universe: Proceedings of a Summer School Held in València, Spain*, Martínez, V. J., Portilla, M. Sáez, D. (Eds.), v. 40, p. 1-64, Berlin: Springer-Verlag, 1992.

[92] Peacock, J. A. “Cosmological Physics”. Cambridge: Cambridge University Press, 1999.

[93] Peacock, J. A., et al. “A measurement of the cosmological mass density from clustering in the 2dF Galaxy Redshift Survey”. Nature, v. 410, p. 169-173, 2001. [arXiv:astro-ph/0103143]

[94] Peebles, P. J. E. “The Large-Scale Structure of the Universe”. New Jersey: Princeton University Press, 1. ed., 1980.

[95] Penzias, A. A., Wilson, R. W. “A Measurement Of Excess Antenna Temperature At 4080 Mc/s”. Astrophysical Journal Letters, v. 142, p. 419–421, 1965.

[96] Percival, W. J., Verde, L., Peacock, J. A. “Fourier analysis of luminosity-dependent galaxy clustering”. Monthly Notices of the Royal Astronomical Society, v. 347, i. 2, p. 645-653, 2004. [arXiv:astro-ph/0306511]

[97] Peter, P., Uzan, J.-P. “Primordial Cosmology”. New York: Oxford University Press, 1. ed., 2013.

[98] Planck Collaboration XVI. “Planck 2013 results. XVI. Cosmological parameters”. Astronomy & Astrophysics, v. 571, i. A16, 2014. [arXiv:1303.5076]

[99] Planck Collaboration XVII. “Planck 2015 results. XIII. Cosmological parameters”. Astronomy & Astrophysics, v. 594, i. A13, 2016. [arXiv:1502.01589]

[100] Planck Collaboration XVII. “Planck 2015 results. XVII. Constraints on primordial non-Gaussianity”. Astronomy & Astrophysics, v. 594, i. A17, 2016. [arXiv:1502.01592]

[101] Planck Collaboration XX. “Planck 2015 results. XX. Constraints on Inflation”. Astronomy & Astrophysics, v. 594, i. A20, 2016. [arXiv:1502.02114]

[102] Sakurai, J. J., Napolitano, J. J. “Modern Quantum Mechanics”. Boston: Addison-Wesley, 2. ed., 2011.

[103] Sasaki, M. “Gauge-invariant scalar perturbations in the new inflationary universe”. Progress of theoretical physics, v. 70, n. 2, p. 394-411, 1983.

[104] Saslaw, W. C., Hamilton, A. J. S. “Thermodynamics and galaxy clustering: nonlinear theory of high order correlations”. The Astrophysical Journal, v. 276, p. 13-25, 1984.

[105] Scialom, D. “Inflation with a complex scalar field”. arXiv preprint *arXiv:gr-qc/9609020*, 1996.

[106] Schwinger, J. “The special canonical group”. Proceedings of the National Academy of Sciences, v. 46, i. 10, p.1401-1415, 1960.

[107] Schwinger, J. “Brownian motion of a quantum oscillator”. Journal of Mathematical Physics, v. 2, p. 407–432, 1961.

[108] Scoccimarro, R. “The Bispectrum: From Theory to Observations”. The Astrophysical Journal, v. 544, n. 2, p. 597-615, 2000.

[109] Scoccimarro, R., et al. “Large-scale bias and efficient generation of initial conditions for nonlocal primordial non-Gaussianity”. Physical Review D, v. 85, n. 8, p. 083002, 2012. [arXiv:1108.5512]

[110] Seljak, U. “Extracting primordial non-gaussianity without cosmic variance”. Physical Review Letters, v. 102, n. 2, 2009. [arXiv:0807.1770]

[111] Senatore, L., Smith, K. M., Zaldarriaga, M. “Non-Gaussianities in single field inflation and their optimal limits from the WMAP 5-year data”. Journal of Cosmology and Astroparticle Physics, v. 2010, n. 1, p. 028, 2010. [arXiv:0905.3746]

[112] Shapley, H. “A study of 7900 external galaxies”. Proceedings of the National Academy of Sciences, v. 21, n. 11, p. 587-592, 1935.

[113] Sheth, R. K., Tormen, G. “Large-scale bias and the peak background split”. Monthly Notices of the Royal Astronomical Society, v. 308, n. 1, p. 119-126, 1999. [arXiv:astro-ph/9901122]

[114] Sloan Digital Sky Survey: http://www.sdss.org/

[115] Sloan Digital Sky Survey (Data Release 14): https://www.sdss.org/dr14/

[116] Slosar, A. et al. “Constraints of local primordial non-Gaussianity from large-scale structure”. Journal of Cosmology and Astroparticle Physics, v. 2008, n. 08, p. 031, 2008. [arXiv:0805.3580]

[117] Smith, S. “The Scientist and Engineer’s Guide to Digital Signal Processing”. San Diego: California Technical Publishing, 1. ed., 1997.

[118] Square Kilometre Array: https://www.skatelescope.org/

[119] Springel, V. “The cosmological simulation code GADGET-2”. Monthly Notices of the Royal Astronomical Society, v. 364, i. 4, p. 1105-1134. [arXiv:astro-ph/0505010]

[120] Starobinsky, A. A. “Spectrum of relic gravitational radiation and the early state of the Universe”. Soviet Journal of Experimental and Theoretical Physics Letters, v. 30, p. 682-685, 1979.

[121] Sudarsky, D. “Quantum Origin of Cosmological Structure and Dynamical Reduction Theories”. In: *The Philosophy of Cosmology*, Chamcham, K. Silk, J., Barrow, J. D., Saunders, S. (Eds.), p. 330-355, Cambridge: Cambridge University Press, 2017.

[122] Sullivan, M. “Type Ia supernovae and cosmology”. In: *Lectures on Cosmology: Accelerated Expansion of the Universe*, Wolschin, W. (Ed.), Lecture Notes in Physics, v. 800, p. 59-97, Berlin Heidelberg: Springer, 2010.

[123] The Supernova Cosmology Project: http://supernova.lbl.gov/union/

[124] Tegmark, M., Zaldarriaga, M. “Separating the early universe from the late universe: cosmological parameter estimation beyond the black box”. Physical Review D, v. 66, n. 10, p. 103508, 2002. [arXiv:astro-ph/0207047]

[125] Tegmark, M., et al. “Cosmological constraints from the SDSS luminous red galaxies”. Physical Review D, v. 74, n. 12, p. 123507, 2006. [arXiv:astro-ph/0608632]

[126] Tellarini, M., Ross, A. J., Tasinato, G., Wands, D. “Galaxy bispectrum, primordial non-Gaussianity and redshift space distortions”. Journal of Cosmology and Astroparticle Physics, v. 2016, n. 6, p. 014, 2016. [arXiv:1603.06814]

[127] Tong, Y. L. “The Multivariate Normal Distribution”. New York: Springer-Verlag, 1. ed., 1990.

[128] Wands, D. “Multiple Field Inflation”. In: *Inflationary Cosmology*, Lemoine, M., Martin, J., Peter, P. (Eds.), p. 275-304, Berlin Heidelberg: Springer, 2008.

[129] Watkinson, C. A., Majumdar, S., Pritchard, J. R., Mondal, R. “A fast estimator for the bispectrum and beyond - A practical method for measuring non-Gaussianity in 21-cm maps”. Monthly Notices of the Royal Astronomical Society, v. 472, n. 2, p. 2436-2446, 2017. [arXiv:1705.06284]

[130] Weinberg, S. “Quantum contributions to cosmological correlations”. Physical Review D, v. 72, n. 4, 2005. [arXiv:hep-th/0506236]

[131] Weinberg, S. “Lectures on Quantum Mechanics”. Cambridge: Cambridge University Press, 1. ed. 2015.

[132] Yamauchi, D., Yokoyama, S., Takahashi, K. “Multitracer technique for galaxy bispectrum - An application to constraints on non-local primordial non-Gaussianities”. Physical Review D, v. 95, n. 6, 2017. [arXiv:1611.03590]

[133] Zel'dovich, Y. B. "Gravitational Instability: An Approximate Theory for Large Density Perturbations". Astronomy & Astrophysics, v. 5, p. 84-89, 1970.

Appendix A

Correlation Functions in Cosmology

For practical purposes, the cosmological density distribution in the Universe may be treated as a random field. Not only due to this random nature, which comes from the initial conditions set by some primordial universe theory, the fact that galaxy surveys map a huge number of objects enforces us to analyze the data statistically. The most used tools in statistics are the mean and variance of the distribution characterizing the studied quantities. In general, for processes with zero-mean, it is used the auto-correlation or its Fourier counterpart, the power-spectrum. In order to extract properties that goes beyond Gaussianity in some data set, we need to invoke higher-order statistics. Hence, in this appendix the technique of higher-order spectra (sometimes referred as polyspectra) and their Fourier counterparts, the N-point correlation functions, are presented.

A.1 N-point correlation functions

When confronting the analysis of data sets in science, we automatically invoke a statistical approach. In our case, when studying the distribution of galaxies (i.e., the count of objects in some volume V), the first quantity we would like to know is the mean density $\bar{\rho}$ of these objects in that volume.

As studied in Chapter 5, Hubble found that it is not the distribution of the galaxy count N which obeyed a Gaussian distribution, but its logarithm, $\log N$ [56]. This points out to the clustered nature of the matter distribution in the Universe, once it is subjected to gravitational instability that leads to its eventual collapse (Figure A.1). Therefore, one might ask "how the galaxies are clustered"? Or, perhaps, a more mathematical question: "how can one distinguish among different distributions"? That is, since galaxies are randomly distributed in the Universe, observations should tell us which statistical distribution is behind the galaxy field.

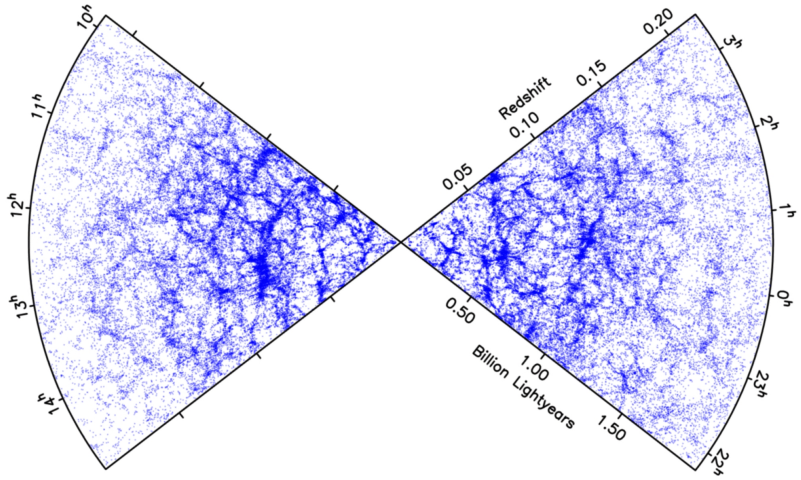

Figure A.1: 2dF Galaxy Redshift Survey map showing the galaxy distribution of 62559 galaxies. The survey measured over 2.2×10^5 good-quality galaxy spectra. Notice that the galaxies are not uniformly distributed in the sky, but instead they clustered according to some theory. The positions of the galaxies, on the other hand, are randomly distributed. Extracted from [1].

One way of answering these questions is by looking not only at the mean or the variance, but at the higher-order moments of the distribution of galaxies. Another possibility is to look at the N-point correlation functions of the random field $\delta(x)$, $\langle \delta(x_1) \dots \delta(x_n) \rangle$, which is the variance for the case of $x_1 = x_2$ in the two-point correlation function, $\langle \delta(x_1)\delta(x_2) \rangle$, the skewness when $x_1 = x_2 = x_3$ in the three-point correlation function, $\langle \delta(x_1)\delta(x_2)\delta(x_3) \rangle$, and the kurtosis when $x_1 = x_2 = x_3 = x_4$ in the four-point correlation function $\langle \delta(x_1)\delta(x_2)\delta(x_3)\delta(x_4) \rangle$.

For Gaussian processes, which follow the distribution given by

$$P(x|\mu, \sigma) = \frac{1}{\sqrt{2\pi\sigma^2}} e^{-\frac{(x-\mu)^2}{2\sigma^2}}, \tag{A.1}$$

it is well known that the second-order moment completely describes them, since higher moments adds no new information. This can be seen by considering the case of a random process $X \sim \mathcal{N}(\mu = 0, \sigma^2)$[1]. All of the odd moments vanish since the Gaussian distribution with $\mu = 0$ is an even function. By differentiating $p = 2k$ times the integral

$$\int_{-\infty}^{\infty} e^{-\frac{x^2}{2\sigma^2}} dx = \sqrt{2\pi\sigma^2}, \tag{A.2}$$

we obtain

$$\int_{-\infty}^{\infty} x^p e^{-\frac{x^2}{2\sigma^2}} = \sigma^p (p-1)!!. \tag{A.3}$$

[1]The notation $X \sim \mathcal{N}(\mu, \sigma^2)$ simply means that the random variable X follows a normal distribution with mean μ and variance σ^2.

Thus,

$$\langle x^p \rangle = \begin{cases} 0 & p = 2k+1 \\ \sigma^p (p-1)!! & p = 2k \end{cases}. \tag{A.4}$$

Writing it explicitly, $\langle x \rangle = 0$, $\langle x^2 \rangle = \sigma^2$, $\langle x^3 \rangle = 0$, $\langle x^4 \rangle = 3\sigma^4$, and so on.

This fact about Gaussian fields motivates the search for statistical tools capable of differentiating the moments of the distributions, once it is known that for pure Gaussian processes one expects to have identically zero odd moments and all others depending on the variance σ^2 [31].

A.1.1 Two-point correlation function

The previous discussion focused on the moments of distributions. We can go further and ask how different points of some distribution, say $X = X(x_1)$ and $Y = X(x_2)$, are correlated.

The covariance of two variables X and Y with a joint probability distribution $P(x, y|I)$[2] is defined by

$$\begin{aligned} \mathrm{Cov}(X, Y) &\equiv \langle (X - \langle X \rangle)(Y - \langle Y \rangle) \rangle \\ &= \langle XY \rangle - \langle X \rangle \langle Y \rangle, \end{aligned} \tag{A.5}$$

and the correlation function is

$$\xi_{XY} \equiv \langle XY \rangle. \tag{A.6}$$

Making contact with Cosmology, consider the density contrast $\delta(\mathbf{x})$ describing the perturbations of matter, which can be described, for example, by a Gaussian (or log-normal) distribution. The two-point correlation function becomes

$$\xi(\mathbf{x}_1, \mathbf{x}_2) = \langle \delta(\mathbf{x}_1) \delta(\mathbf{x}_2) \rangle, \tag{A.7}$$

and describes how the perturbations at different points in space are correlated.

Since we assume the Universe is homogeneous, the cosmological two-point correlation function becomes

$$\xi(\mathbf{r}) = \xi(\mathbf{x}_2 - \mathbf{x}_1) = \langle \delta(\mathbf{x}_1) \delta(\mathbf{x}_2) \rangle. \tag{A.8}$$

[2] We use I to codify the information one assumes that it's true to describe the variables X and Y. For details about this notation we address the reader to reference [25].

A.1.2 Three and four-point correlation functions

Following the definition of the two-point correlation function, the three and four-point functions are defined respectively as

$$\zeta(\mathbf{x}_1, \mathbf{x}_2, \mathbf{x}_3) \equiv \langle \delta(\mathbf{x}_1)\delta(\mathbf{x}_2)\delta(\mathbf{x}_3) \rangle \tag{A.9}$$

and

$$\eta(\mathbf{x}_1, \mathbf{x}_2, \mathbf{x}_3, \mathbf{x}_4) \equiv \langle \delta(\mathbf{x}_1)\delta(\mathbf{x}_2)\delta(\mathbf{x}_3)\delta(\mathbf{x}_4) \rangle. \tag{A.10}$$

A.2 The power-spectrum

By definition, the power-spectrum is the Fourier transform of the two-point correlation function:

$$P(\mathbf{k}) = \int \xi(\mathbf{x}) e^{-i\mathbf{k}\cdot\mathbf{x}} d^3x \tag{A.11}$$

or

$$\langle \delta(\mathbf{k}_1)\delta(\mathbf{k}_2) \rangle \equiv P(k_1)\delta^D(\mathbf{k}_1 + \mathbf{k}_2), \tag{A.12}$$

where $\delta^D(\mathbf{k})$ is the Dirac delta function. Hence,

$$\xi(\mathbf{x}) = \int P(\mathbf{k}) e^{i\mathbf{k}\cdot\mathbf{x}} \frac{d^3k}{(2\pi)^3}. \tag{A.13}$$

For the case of and isotropic Universe, the power-spectrum depends only on the modulus $|\mathbf{k}|$ and it is possible to write $\mathbf{k} \cdot \mathbf{x} = kx\cos\theta$, leading to

$$P(k) = 4\pi \int_0^\infty x^2 \xi(\mathbf{x}) \frac{\sin(kx)}{kx} dx, \tag{A.14}$$

once we switch to spherical coordinates to perform the change of variables

$$u = \cos\theta \Rightarrow du = -\sin\theta d\theta. \tag{A.15}$$

With the additional assumption of homogeneity, the modes of different wavevectors are uncorrelated. Hence, the only information that can extracted from the power-spectrum is the variance of each mode [71].

In Figure A.2 it is shown the matter power-spectrum as measured by different probes. As expected from what was learned in Chapter 2, for large-scales (small k) the power-spectrum grows with $\sim k$ and decreases as $\sim k^{-3}$ at small scales (large k).

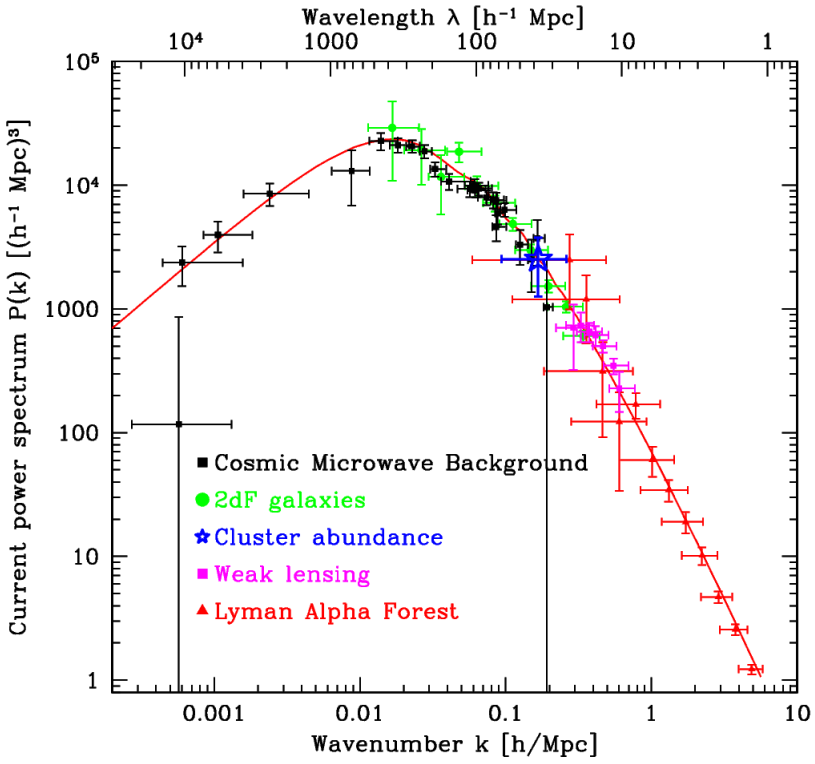

Figure A.2: Measures of the linear matter power-spectrum $P(k)$ with different probes. Extracted from [124].

A.3 The bispectrum

Similarly to the power-spectrum, the bispectrum may be defined as the Fourier transform of the three-point correlation function:

$$\langle \delta(\mathbf{k}_1)\delta(\mathbf{k}_2)\delta(\mathbf{k}_3)\rangle \equiv (2\pi)^3 B(\mathbf{k}_1,\mathbf{k}_2,\mathbf{k}_3)\delta^D(\mathbf{k}_1+\mathbf{k}_2+\mathbf{k}_3). \tag{A.16}$$

Unlike the power-spectrum, for the case of a non-vanishing bispectrum, different wavevectors are correlated: once you measure $\delta(\mathbf{k}_1)$ and $\delta(\mathbf{k}_2)$, then the bispectrum gives us the most likely $\delta(\mathbf{k}_3)$ [71].

A.4 The trispectrum

Once again, the trispectrum is defined as the Fourier transform of the four-point correlation function:

$$\langle \delta(\mathbf{k}_1)\delta(\mathbf{k}_2)\delta(\mathbf{k}_3)\delta(\mathbf{k}_4)\rangle \equiv (2\pi)^3 T(\mathbf{k}_1,\mathbf{k}_2,\mathbf{k}_3,\mathbf{k}_4)\delta^D(\mathbf{k}_1+\mathbf{k}_2+\mathbf{k}_3+\mathbf{k}_4). \tag{A.17}$$

A.5 The polyspectra

In general, for the N-point correlation functions, the polyspectra is defined as

$$\langle \delta(\mathbf{k}_1) \dots \delta(\mathbf{k}_p) \rangle \equiv (2\pi)^3 \mathscr{P}(\mathbf{k}_1, \dots, \mathbf{k}_p) \delta^D(\mathbf{k}_1 + \dots + \mathbf{k}_p) \tag{A.18}$$

or, in terms of the N-dimensional Fourier transform,

$$\mathscr{P}(\mathbf{k}_1, \dots, \mathbf{k}_p) = \prod_{n=1}^{p} \int \xi(\mathbf{x}_1, \dots, \mathbf{x}_p) e^{-i\mathbf{k}_n \cdot \mathbf{x}_n} d^3x. \tag{A.19}$$

A note on continuity: in the above definitions we were dealing with a continuous random variable described by some continuous probability density function. This is going to be associated with the fluctuations in the matter density field, generated by some process such as inflation and/or structure formation. However, the observables available are in the form of count of objects in the sky, which are given by integer numbers. Therefore, one must treat the above definitions for the case of discrete distributions. This subtlety is addressed in section §5.2.1.